Vrije Universiteit Brussel
FACULTY OF ENGINEERING

Bruface
Brussels Faculty of Engineering

Experimental study and modelling of the clamp load reduction of the roll restrictor bolts

Vincent Verhasselt

Promoter: prof. dr. ir. Marc Van Overmeire

Supervisor: ir. Eric-Jan Scharlee

Thesis submitted in partial fulfillment of the requirements for the Master:

Master of Science in Electro-Mechanical Engineering: Mechatronics-Constructions

Academic year 2012-2013

Abstract

Vincent Verhasselt, 2012-2013

Master of Science in Electro-Mechanical Engineering: Mechatronics-Constructions

Experimental study and modelling of the clamp load reduction of the roll restrictor bolts

keywords: bolted connections, loosening mechanisms, engine mounts

All tests in my master thesis were performed at *Ford Lommel Proving Ground*, which is a testing facility of *Ford of Europe*. The topic of my thesis is situated in the Ford product reliability development department and has been studied for the last 40 years by mechanical engineers.

We will try to find a solution for engine mount bolts of Ford passenger cars which sometimes get loose in durability tests. From a literature study, we will try to find all different failure mechanisms or causes of this failure.

To find the failure mechanism that occurs, we will first measure the clamp load in real time by glueing strain gauges on these bolts. We will monitor this clamp load together with the forces and accelerations acting on this engine mount. A last parameter that might influence the loosening of the bolts is the relative displacement between the engine mount and the transmission on which it is bolted. When the clamped component is able to move, this could cause both rotational and non-rotational movement.

A design of experiments will provide us with the most significant parameters that cause high forces on the engine mounts. We will also evaluate the severity of all different test tracks in terms of forces on the engine mount.

With ultrasonic sensors, we will measure the evolution of the pretension force during a complete reliability test. Also the change in torque of the bolts will be measured and linked to the pretension force. We will also use these ultrasonic sensors to evaluate the accuracy of the measurements with a torque wrench, used after durability tests.

In chapter 5 we will try to link the evolution in long reliability tests to the measurements in real time. This might enable us to predict the evolution of the pretension force of engine mount bolts for a different powertrain.

Finally, a selection of possible solutions for the failure mechanism will be tested and evaluated. We will use three kinds of washers, threadlocker, increase the torque of the bolts and finally remove the anti-corrosion coating of the clamped component.

We will find that the coating on the clamped component will cause the loosening effect. It is hard to model this effect. A removal of the coating should eliminate the problem completely.

Samenvatting

Vincent Verhasselt, 2012-2013

Master of Science in Electro-Mechanical Engineering: Mechatronics-Constructions

Experimentele studie en modellering van voorspanningsreductie van roll restrictor bouten

kernwoorden: boutverbindingen, loskomende mechanismes, motor steunen

Alle testen in deze masterscriptie zijn uitgevoerd bij *Ford Lommel Proving Ground*, een testcentrum van *Ford of Europe*. Het onderwerp van mijn afstudeerwerk situeert zich in het domein van betrouwbaarheidstesten bij Ford.

We proberen een oplossing te vinden voor het soms loskomen van boutverbindingen van de motorsteunen bij personenwagens van Ford in duurzaamheidstesten. Vanuit een literatuurstudie gaan we alle mogelijke falingsmechanismen proberen te identificeren.

Om de falingsmechanismen te vinden die optreden bij de motorsteunen, gaan we de klemkracht van de bouten meten met behulp van rekstrookjes. Ook meten we de krachten en acceleraties van deze motorsteun gedurende de testen. Als laatste parameter zullen we eveneens de relatieve verplaatsing meten tussen de motorsteun en de versnellingsbak waarop deze steun bevestigd is. Als deze motorsteun zich kan verplaatsen ondanks vastgeschroefd te zijn op de versnellingsbak, kan rotationeel of niet-rotationeel loskomen optreden.

Een *design of experiments* zal ons een betere kijk geven op parameters die tijdens de duurzaamheidstesten hoge krachten veroorzaken op de motorsteunen. Ook zullen we de verschillende *testevents* op basis van die krachten vergelijken en rangschikken.

Met ultrasone sensoren kunnen we de evolutie van de voorspanning van de bouten meten gedurende een volledige duurzaamheidstest. Ook het bijhorende aanhaalmoment van de bouten wordt gemeten en gerelateerd aan de voorspanning. Deze sensoren laten ons bovendien toe de nauwkeurigheid van de gemeten aanhaalmomenten na duurzaamheidstesten te bepalen.

In hoofdstuk 5 zullen we de metingen in *real time* koppelen aan de evolutie van de klemkracht. Vervolgens zullen we een voorspelling maken van de evolutie van de voorspanning van motorsteunbouten voor een ander type motor.

Ten slotte gaan we een selectie van mogelijke oplossingen uitproberen. Het effect van drie verschillende rondsels, vloeibaar borgmiddel, een verhoging van het aanhaalmoment en het verwijderen van de coating van de component zullen geëvalueerd worden.

We zullen besluiten dat de coating van de geklemde component de oorzaak is van het loskomen van de bouten. Dit effect is moeilijk te modelleren. De coating lokaal verwijderen lost echter het probleem volledig op.

Description sommaire

Vincent Verhasselt, 2012-2013

Master of Science in Electro-Mechanical Engineering: Mechatronics-Constructions

Étude expérimentale et modelage de la réduction de précontrainte des boulons de limiteurs de roulis

Mots-clés: jonctions de boulons, mécanismes de défaillance, appuis de moteur

Tous les tests pour ce mémoire de Master ont été exécutés chez *Ford Lommel Proving Ground*, un centre de recherche de *Ford of Europe*. Le sujet de ce mémoire se situe dans le domaine des essais de fiabilité chez Ford.

Nous essaierons de trouver une solution pour le détachement imprévu de certaines jonctions de boulons des appuis de moteur en ce qui concerne les voitures de Ford pendant les tests de durabilité. À l'aide d'une étude bibliographique, nous essaierons d'identifier tous les mécanismes de défaillance.

Afin de trouver ces mécanismes de défaillance, nous mesurons la force de serrage des boulons à l'aide de jauges de contrainte. En outre, nous mesurons les forces et les accélérations de ces appuis de moteur au cours des tests. En tant que dernier paramètre, nous mesurons également le déplacement relatif entre les appuis de moteur et la boîte de vitesses à laquelle ces appuis sont fixés. Si les appuis de moteur peuvent se déplacer malgré le fait qu'ils sont fixés, un détachement rotationnel ou non-rotationnel peut se manifester.

Un *design of experiments* nous fournira une meilleure vue aux paramètres qui produisent des forces majeures sur les appuis de moteur. De plus, nous comparerons et nous classerons les différents *test events* en relation avec ces forces.

Nous pouvons, avec des capteurs ultrasoniques, mesurer l'évolution de la précontrainte des boulons pendant un test complet de la durabilité. Le moment de serrage des boulons est aussi mesuré et mis en rapport avec la précontrainte. Les capteurs nous permettent également de déterminer l'exactitude des moments de serrage mesurés après les tests de durabilité.

Dans le chapitre 5, nous relierons les mesures en temps réel à l'évolution de la force de serrage. Ensuite, nous ferons une prévision de l'évolution de la précontrainte des boulons des appuis de moteur d'un autre type de moteur.

En somme, nous mettrons à l'essai une sélection des solutions éventuelles. L'effet de trois rondelles différentes, du frein filet liquide, d'une augmentation du moment de serrage et de l'enlèvement du *coating* du composant seront évalués.

Nous trouverons que le *coating* du composant provoquera le détachement des boulons. Il est difficile de modéliser cet effet. L'enlèvement du *coating* du composant devrait éliminer complètement le problème.

Note of thanks

In the first place, I want to thank my supervisor at Ford Lommel Proving Ground, ir. Eric-Jan Scharlee. He gave me the opportunity to write my master thesis at Ford Lommel Proving Ground. He was always very helpful organizing tests and bringing me in contact with the competent specialists.
I had great colleagues: ing. Bert Van Meir, ing. Bart Van Gorp and ing. Simon Mooney who helped me with practical issues, instrumentation and measurements.
The head of the instrumentation team at Ford Lommel, Frank Van Den Boer helped me a lot with choosing the right sensors and developing practically the test setup.
I also want to thank these specialists working at Ford: ir. Matt Sykes (application specialist), ir. Peter Guenther (test method specialist) and ir. Salauddeen Azimuddeen (component engineer) who gave me the right data of previous tests and helped me to find the right methods.
Special thanks goes to Frans Boulpaep of the VUB for performing tensile tests for me.
Finally, I am grateful to my VUB supervisor, professor dr. ir. Marc Van Overmeire for all the support and advice on my master thesis.

Table of contents

List of figures

List of tables

List of symbols and abbreviations

ABS	Anti-lock Braking system
Pascar	Accelerated durability test used by Ford Motor Company
GTDI	Gasoline Turbocharged Direct Injection
MDL	Maximal Durability Load
DTL	Durability Test Load.
IB5	Five-speed transmission of a Ford Fiesta
ST	Sport Technologies
NVH	Noise Vibrations and Harshness
R	Electrical resistance (Ohm)
ρ	Specific electrical resistance, or resistivity (Ohm meter)
l	Length (m)
A	Cross section (m^2)
ΔR_{Gage}	Resistance change due to strain (Ohm)
R_{gage}	Initial resistance of the strain gauge (Ohm)
ε	Strain
σ	Stress (Pa)
E	Young modulus (Pa)
C	Capacitance between the plates of a capacitor (Farad)
ε_0	Vacuum permittivity (Farad per meter)
K	Dielectric constant of the gap between the plates of a capacitor
S	Surface of the plates of a capacitor (m^2)
d	Distance between the plates of a capacitor (m)
LC	Load Cell
LP	Load Probe
FF	Force Factor

Chapter 0: Problem statement

In the past five years, engine mount bolts sometimes get loose in durability tests. The problem can vary between a torque drop below the minimal allowable torque, to a complete loosening. The problem can occur for each model and each type of engine, although the occurrence increases for more powerful engines.

When the torque of the bolts has dropped, it does not necessarily means than the bolt has rotated in the loosening direction. In the past, bolted connections have been observed that have lost more than 50% of the initial torque without any rotation. A fracture of the bolts or visible damage has never been detected. The engine mount at which the problem occurs the most is the transmission roll restrictor.

In this master thesis, we will investigate on the loosening of the bolts of this engine mount in six chapters.

The first chapter will give information about the testing facility: Ford Lommel Proving Ground. We will situate the topic of this thesis in the company and go more into detail about the most used test events for the investigation. Finally, the powertrain layout will be explained and the problems to be addressed in this thesis will be explained.

The second chapter will handle all possible failure mechanisms described in literature that might be applicable for this kind of problem. Most of these mechanisms are verified in laboratories and the most important parameters that influence the mechanism are well-known. When we perform tests at a test track, we cannot control all these parameters. We will need to develop ourselves methods to measure which failure mechanism occurs.

In the third chapter, we will try to measure in real time a few parameters during the test events. First, we will explain the used sensors and measurement method, because some of these sensors are not yet used for this kind of problem. A ranking of severity of the events will be made a design of experiments will make clear which parameters influence this severity. The real time results will enable us to select a few loosening mechanisms that are still possible. To know which one of these mechanisms is causing the problem, we will perform measurements during a full durability test in the next chapter.

In the fourth chapter, the long term measurements will enable us to tell with certainty which failure mechanisms are working at the joint. We will measure the evolution of the pretension force of the bolts through a full durability cycle. This will give us a clear view on how the relation between the torque of a bolt and the pretension force of that bolt changes. It will also enable us to determine how accurate the commonly used methods are and how it can be possible that the joint fails completely. The final phase of the failure will involve a second failure mechanism that we also will investigate.

In the fifth chapter, we will try to make a link between chapter three and four. Does the failure mechanism follow a certain pattern? If so, we should be able to measure the initial conditions of this pattern which would enable us to predict the further evolution of the failure. Are we able to measure some parameters of the engine mounts from different powertrains in real time and use this information to predict theoretically the evolution of the failure during a full durability test? If not, which further measurements or research should be performed to be able to? We will deal with these questions in chapter 5.

In the final chapter, we will try to measure the influence of a few solutions that reduce the cause of the failure mechanism. If one can take away the cause of the failure mechanism, it is not any more of interest to try to model or predict the failure. We will try out the possible solutions that are available at Ford Lommel Proving Ground which are: three types of washers, threadlocker, a torque increase and removing the coating on the clamped component. The most important statement we want to make clear is the measurement method we used. It should be of great interest for future design of engine mounts to use the same measurement method because it enables measuring the cause of the loosening mechanism directly. The method we used, can measure the cause of the loosening mechanism in only one day. Finally we will also mention the economic feasibility of these possible solutions in mass production.

Chapter 1: Ford Lommel Proving Ground

Ford Lommel Proving Ground is the test centre of the European part of Ford Motor Company. The engineers and professional drivers test cars on public roads as well as on the 83km long test track. This track contains a lot of special roads to test durability, performance and vehicle dynamics.

I was working within the Customer Correlation team, a part of the durability department. The durability department is responsible signing off all vehicle systems, including chassis, powertrain, body and suspension. There are two main durability tests for passenger cars: Pascar 1 and 2.

The Pascar 1 test focuses on the durability of the suspension, chassis and body. We try to cause the same damage to the chassis and suspension in 5000 km as 90 percentile of the end users will do in 240,000 km or in 10 years. The Pascar 2 test takes about 40,000 km and is more focused on the drivetrain and the brakes.

To test the durability in such an accelerated way, we need to apply higher loads and increase the frequency. One should always take caution during accelerated tests: if the loads become too high, some components might fail while we never detect failures from our customers. One should always respect the physics of failure. The determination of the loads during the durability tests is one of the main tasks of the customer correlation engineer. For the transmission roll restrictor however, the loads applied in the accelerated tests are limited to the maximal loads that might occur when the car is used by the customer on public roads.

1.1 Important test tracks

To improve the readability of this thesis, it might be interesting to explain some durability test tracks to which will be referred.

The Cobblestones slalom is very rough surface: it is made out of river stones placed into a concrete surface. We slalom the car ten times on this surface to test the suspension mainly in the transverse direction. Other components such as the engine mountings will be exposed to a lot of vibrations. A figure of the Cobblestone event can be found in Appendix Figure B 1.

The traction control event consists of a very slippery surface on which we accelerate “wide open throttle”. The traction control system will try to prevent the wheel spin as much as possible by reducing the engine power and actuating the brakes. This actuation is similar to the threshold braking technique used by the ABS. This causes a shock on the drive train each

time the brakes are actuated. A figure of the traction control event can be found in Appendix Figure B 2.

The Chatterbumps event contains 3 parts: the acceleration, constant speed and braking part. A Chatterbump is a concrete surface that alternates between two different heights. We first perform an acceleration on this surface. Each time the front wheels drive over a Chatterbump, wheel spin is provoked which results in shocks on the drivetrain. The following Chatterbumps are driven at constant speed and do not cause high loads on the engine mountings. During the Chatterbumps braking, the ABS system interferes most of the time and the shocks in the longitudinal direction of the car cause high loads on the engine mountings. A figure of the Chatterbumps event can be found in Appendix Figure B 3.

The Chuckholes lane contains a variety of potholes and bumps, which are driven at constant speed. This event tests mainly the suspension and shock absorbers. It is certainly not made to test the engine mounting. A figure of the Chuckholes lane can be found in Appendix Figure B 4.

1.2 The powertrain

In this master thesis, we will refer a lot to the powertrain of a car and its mountings. Most European Ford passenger cars are front wheel driven. This powertrain configuration creates much space inside the car.

We will give a short overview of the powertrain layout of a Ford Fiesta.

On the right side in the engine bay, we find the engine in a transverse direction. On the left side of the engine bay, we find the gearbox. Both are connected by the clutch in between. To fix this powertrain in space, we need a minimum of three mountings. The first is the engine mount. This mount mainly carries the weight of the powertrain, together with the second mount: the gearbox mount. Apart from the static load, these mounts are also designed to carry the pitch and yaw of the powertrain. The third mount is the transmission roll restrictor. This engine mount supports only the roll of the engine. For a Ford Fiesta, the transmission roll restrictor is designed to resist 30kN of longitudinal force (roll of the engine) and only 3kN in the transverse direction (yaw moment). Because the differential is included in the gearbox, all wheel torques are transmitted directly to the powertrain. So during severe accelerations, we can expect large forces on the transmission roll restrictor. The transmission roll restrictor is connected to the subframe, which is a removable chassis part.

The subframe makes the assembly of the car easier: the suspension and steering parts can be pre-assembled onto the subframe. During the final assembly of the car, one only needs to fix the subframe to the chassis of the car.

The subframe also enlarges the cascade of failures during extreme test events.

Extreme test events are used in the Performance department. The main purpose of this test is to evaluate the strength and safety of the car. For example: if one drives too fast through a large pothole, first the suspension should deform, secondly the subframe and in a final stage the chassis. A chassis failure is mostly not repairable, while the subframe and suspension parts are relatively cheap to replace. [1]

Appendix Figure B 5 gives a clear overview of the powertrain layout. Appendix Figure B 6 is a picture of the powertrain of a Ford Fiesta, seen from below the car.

1.3 The transmission roll restrictor

All the measurements will be performed with the customer correlation car, i.e. a Ford Fiesta with a 1.6 120hp Sigma engine and a five-speed manual transmission. This car is generally used for comparing different events or road surfaces.

A picture of its roll restrictor with the applied torqueing procedure is shown below.

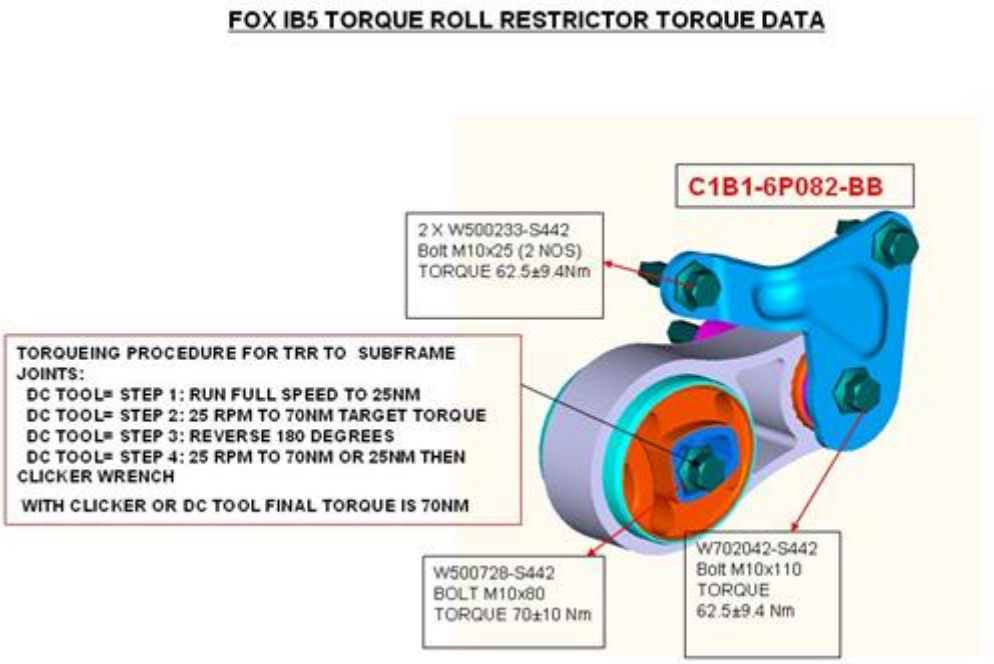

Figure 1: Transmission roll restrictor and torqueing procedure

Note that W500728 and W702042 have the 10.9 quality standard and W500233 has the 8.8 quality standard.

Remember that the 8.8 quality standard means a yield strength of 8x8x10= 640MPa and a tensile strength of 8x100= 800MPa. In the same way, the 10.9 quality standard means a yield strength of 10x9x10= 900MPa and a tensile strength of 10x100= 1000MPa.

The W500728 bolt clamps the big rubber bush on the subframe. The inside of the rubber bush is made out of aluminium, as the roll restrictor itself. The subframe is made out of steel and is e-coated. Also the roll restrictor bracket, the blue part of the roll restrictor in the drawing above, is a steel part with a 20 to 40 µm thick e-coating. E-coating is nowadays a standard procedure to protect components against corrosion. The part is submerged in a paint bath. By charging the component positively and the paint bath negatively, the paint is electrostatically attracted onto the component.

E-coating is a very good protective layer, but it has a few drawbacks.

First, the friction coefficient between the e-coated part and the bolt head is not always the same. This means that if we torque these bolts in mass production, the minimal pretension force cannot always be guaranteed. In the past, the engineers in Dunton performed experiments on the influence of the finish of the bolt to get a more constant friction coefficient. The test results showed that the S-442 finish was the best solution for this problem.

Secondly, the e-coating causes a larger initial loss of clamp load because it provokes more the Brinelling, or static embedding of the bolt. This will be explained further. To reduce this problem, we now use a three step torqueing procedure: a machine torques the bolts to one third of the design torque and that slowly torques the bolt to the nominal torque. In the second step, the bolt is rotated in the loosening direction for 180 degrees. In the third step, the bolt is again torqued to the nominal torque. Eventually a man with a clicker torque wrench checks the torque of the bolts. The three step torqueing procedure has the effect that a bolt at the same torque delivers a higher pretension force than a bolt torqued with a single step torqueing procedure. This is due to the fact that the reverse rotation of the bolt in the second step removes a bit the coating on the engine mount and the head of the bolt, resulting in a lower friction coefficient. The torqueing procedure is always applied in mass production, but the prescribed fastening speed cannot be achieved with the torque wrenches we use at Ford Lommel Proving Ground.

1.4 Loosening of the roll restrictor bolts

In the past five years, test engineers of Ford Lommel more and more have had to deal with engine mount problems, especially the transmission roll restrictor. As the engine torque increases in modern cars, this engine mount has to cope with higher forces and vibrations.

The problems that occur is the loosening of the engine mount bolts, failure of the rubber bushes or, less often, rupture of the transmission roll restrictor. The rubber bushes have already been studied by two students from HAN (Hogeschool van Arnhem en Nijmegen), so we will concentrate on the bolted connections of the roll restrictor. It is very important to note that the loosening of the bolts has never caused a broken bolt. In the worst case a bolt falls out of the assembly. This can cause broken drive shafts or breaking the gearbox housing.

The loosening problem occurs in all passenger cars and can occur for every powertrain. The loosening of can be a rotation of the paint mark on the bolts head, but sometimes they measure torque drop without rotation of the bolt head. In the worst case a bolt can completely rotate loose and fall out.

Measuring the on-torque is one of the three ways to measure the torque of a bolt. The on-torque is the torque measured when the bolt starts to rotate in the fastening direction. The loosening torque is the peak torque measured while slowly loosening the bolt. The back-to-mark-torque is the torque needed to rotate the bolt back to its original position. For engine mounts, the failure criterion used by Ford is based on the measured on-torque. After the Pascar 1 test, technicians always torque these bolts to 50% of the nominal torque (Ford system requirement). When the bolts rotate below this torque, the residual torque is reported as an issue. When the residual torque is above 50% of the minimal torque, they will not measure the on-torque because this measurement increases slightly the torque of the bolt. After the Pascar 2 test, the residual on-torque is measured for all engine mount bolts. When the residual torque is less than 50% of the minimal torque, the residual torque is also reported as an issue.

The loosening problem is more likely to happen with more powerful cars, especially the sporty derivatives such as the currently developed Ford Focus ST. The application engineers in Dunton have performed measurements in the past, which show that the use of hydromounts on the gearbox side increases the forces on the roll restrictor. The hydromounts used on some Ford passenger cars are passive dampers, which is probably why they are less stiff at higher frequencies. Also durability tests in wet conditions result in higher roll restrictor forces because the stick-slip effect becomes worse. Stick-slip happens during acceleration or during braking. We use the term stick-slip when the grip of the tyre alternates between the grip (stick) and sliding or wheel spin (slip). This causes heavy low frequent vibrations in the powertrain. Stick-slip is mostly provoked by the Chatterbumps event, but in everyday use, it can also occur when a wide open throttle acceleration is performed on a uneven surface such a rail road crossing.

When you deal with important bolted connections, most handbooks advise you to use spring or locking washer. But most premium car manufacturers often use a threadlocker (Loctite) for all powertrain and suspension bolts. These solutions are more expensive, so it might be interesting to measure the effect on the failure mechanism of the bolts. With this information, it should be easier to evaluate these solutions in terms of cost and effectiveness.

Chapter 2: Failure mechanisms, a literature study

Before explaining the different mechanisms of failure described in literature, it is important to note that all the bolts of the transmission roll restrictor of a Ford Fiesta with an five-speed manual gearbox are designed to take transverse forces. In design books such as *Machinenelemente* by Roloff/Matek [2], it is stated that for this kind of connections, the bolts are designed to clamp the components hard together, so that the static friction between the two components takes the full external transverse force. The bolts should see no effect of the external forces.

In spite of this theoretical statement, we will still consider the possibility of the external varying loads causing the loss of pretension or yielding the bolts owing to a too high external axial force.

2.1 Loss of pretension

The loss of pretension causes the thread and head surface to lose its capability to prevent the bolt from getting loose, i.e. with a zero axial force on the thread and head, the tangential friction force must also be zero. This effect will result in a bolt rotating in an accelerated way: the more the bolt gets loose, the more the bolt will lose its pretension, the faster it will loosen. Eventually, the bolt will become completely loose or even fall out of the assembly. We have never noticed broken or severely damaged bolts. [2]

2.2 Yielding the bolt

Too high external forces could cause the bolt to yield. This means that the bolt would be permanently extended, which is equal to a permanent drop of clamp load. A second cause for yielding the bolt might be an overestimated friction coefficient. When the actual friction coefficient is lower than expected, one will achieve higher pretension forces when the same torque is applied. When this force is near the yield limit of the bolts, any external force on the bolts could cause a permanent elongation of the bolt, so a permanent drop in pretension force. [2] [3] [4]

2.3 Fatigue

A third reason might be a fatigue issue. Due to cyclic loading, a bolt can lose its stiffness in the axial direction. The main criterion on which you can distinguish a fatigue failure to the other mentioned mechanisms is the number of cycles before failure. In fatigue testing machines, the number of cycles is mostly in a minimal order of magnitude of 10^7 for stresses of 100MPa, while other mechanisms are in the order of 10^3 cycles. [5] [3] Loosening can occur in high cycle fatigue by a crack at the first root of a bolt, leading to permanent elongation and loss of clamp load. [6] [7] This effect depends mostly on tightening conditions such as the clamp length and the thread length. The way the bending moments are distributed in the bolt will determine the loosening fatigue.

2.4 Self-loosening due to relative motion on thread flanks and contact surfaces

This mechanism, mostly described by Gerhard H. Junker, states that a bolt can lose its capability of self-locking due to external forces. The external forces can both be axial or transverse. In axial loading of a bolted connection, the bolt itself will shrink due to the Poisson's effect and the female thread will widen open due to the radial component of the reaction force, caused by pitch angle of the thread. This will cause a small motion at the thread surface. [8] A figure of this Poisson shrinkage due to axial loading can be found in Appendix Figure B 7.

In the transverse case, the external loading can cause a small motion at the thread surface or even between the head of the bolt and the clamped members.

The effect of a small motion can cause the loosening by the following principle: when sliding over each other, one can no longer expect the static friction coefficient. The dynamic friction coefficient is typically lower than the static one, which enables forces normally below the static friction now to result in motion. Compare with opening a bottle of whiskey: when you pull the cork with a low force, the bottle will not open. By rotating the cork, a low pulling force will be sufficient to open the bottle.

This principle will act on the level of the thread surface and in transverse loading it can cause the complete loosening of the bolt. In axial loosening, the complete loosening cannot be reached.

2.5 Non-rotational loss of pretension: embedding

Embedding is the effect of locally yielding the surface. [9] There are two kinds of embedding: static and dynamic embedding. Static embedding is also known as the Brinelling effect. Due to surface imperfections and the surface roughness, the actual contact surface is always smaller than the theoretical one. This happens at the interface between the component and the head of the bolt, as well as on the thread surface. This will lead to stress concentrations which will cause a local surface yielding. When the bolted connection is cyclically loaded, this local surface yielding will end after a couple of cycles. Static embedding is normally not problematic for small bolts, i.e. M12 or smaller.

Dynamic embedding occurs when the bolt performs a marginal motion under loading. Due to sliding of the bolt head on the component, the surface of the component can yield locally. The coating of the component and mechanical strength properties of the bolt head and of the clamped component material are important parameters.

In common cases, dynamic embedding can lead to a pretension loss until the Junker effect occurs.

2.6 Conclusion

There are many ways a bolted connection can fail. The first two mechanisms, the loss of pretension and yielding of the bolt should only be possible due to off-design loads. This should be easy to detect when we measure the clamp load in real time during the durability test. The third failure mechanism, fatigue fracture, is related to the material failure of the bolt. This failure should be easily detected by looking at failure reports of the last five years of different cars.

The last two failure mechanisms are specifically for bolts. The detection of this failure type requires both real time measurements and long term tests.

In chapter three, we will try to measure the clamp load, roll restrictor forces and accelerations together with the relative displacement of the roll restrictor on the gearbox during a Pascar 1 cycle.

In chapter four, we will try to measure the clamp load evolution during a Pascar 1 test.

With the results of the evolution during a full test and the knowledge of what happens during one cycle, we should be able to link both measurements in a model that could predict the evolution of the clamp load during Pascar 1. Moreover we will try to find the easiest technique to measure the input parameters of this model.

Chapter 3: Real time Tests

When we are dealing with the failure of a bolted connection, we need to know the loads acting on the component. These loads have already been measured in the past: nominal loads in durability tests are around 10kN on the roll restrictor. The component is designed to fail at loads above 30kN. The abuse test for the transmission roll restrictor is declutching as fast as possible when reverse gear is engaged and the engine rotates at maximum rpm. At the abuse load, the roll restrictor might slip on the gearbox or subframe and the rubber components might be damaged but the component may not break. With the aim of improved durability design of the component, it might be interesting to measure and model the loading of the roll restrictor as a function of some major parameters: weather conditions, test mass installed in the car, severity of the event, engine torque…

This could help us in establishing the spectrum of loads on the component during a Pascar 1 test. If we can find the failure mechanism and how it is related to the forces on the component, we might be able to evaluate the survival of the connection during the test.

To determine which kind of failure mechanism occurs, it should be very interesting to know what is happening with the clamp load during durability tests. Do we lose pretension or are we reach the yield limit of the bolts? Does fatigue occur or not? Are the criteria of rotational or non-rotational loosening fulfilled? To answer this last question, one should also be able to measure the relative displacement between the component and the gearbox.

3.1 Real time sensors

3.1.1 Real time clamp load measurements

To be able to measure the clamp load in the bolts real time, there are two commonly used techniques: by means of a load cell or by glueing strain gauges onto the bolts. At the roll restrictor engine mount, the use of a load cell is not preferred because the only possibility to place a load cell is between the component and the bolt head. Apart from a lack of space, this technique would also include a change of clamp length of the bolts and a change of friction between the component and the bolt head.

A bolt instrumented with strain gauges is much more interesting due to the unchanged dimensions and friction surfaces of the bolts. A strain gauge is able to measure in real time the elongation of the material on which it is glued by using Pouillet's law:

$$R = \rho \frac{l}{A} \qquad (1)$$

R, ρ, l and A are respectively the resistance, conductivity, length and cross section of the conductive wire in the strain gauge.

A strain gauge is actually a wire that is oriented in such a way that the elongation we want to measure causes an elongation of a very thin wire. [10] Poisson's effect will also cause a reduction of the cross section. These two effects will cause an increase of the resistance of the strain gauge. Because the wire needs to be very thin, the current through the strain gauge must be limited. A too high current would also heat up the wire, which would cause a change in conductivity and thickness of the wire material.

The strain sensitivity of a strain gauge, also called K-factor, is given by the following formula:

$$K = \frac{\Delta R_{Gage} / R_{gage}}{\Delta l / l} = \frac{\Delta R_{Gage} / R_{gage}}{\varepsilon} \qquad (2)$$

With ΔR_{Gage} being the resistance change due to strain, R_{gage} the initial resistance of the strain gauge and ε the strain.

In practice the resistance change has a magnitude of a few milli Ohm.

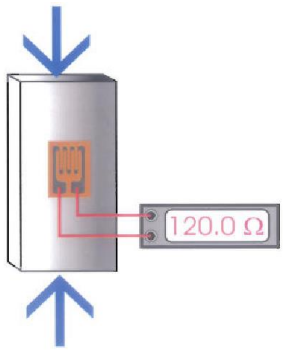

Figure 2: Strain gauge principle [10]

This is why we always use a strain gauge in a Wheatstone bridge to amplify the output signal of the strain gauge. If you use a Wheatstone bridge with strain gauges instead of the resistances in the bridge, you can compensate temperature and bending effects. This is called a full bridge. The temperature effects are compensated by the fact that all strain gauges in the bridge will experience the same influence of the temperature; so this will not change the output of the bridge. When the component bends, one side will be in tension and the opposite side will be in pressure. The bending effects can be compensated by gluing the strain gauges on opposite sides of the component in a way described in Figure 3.

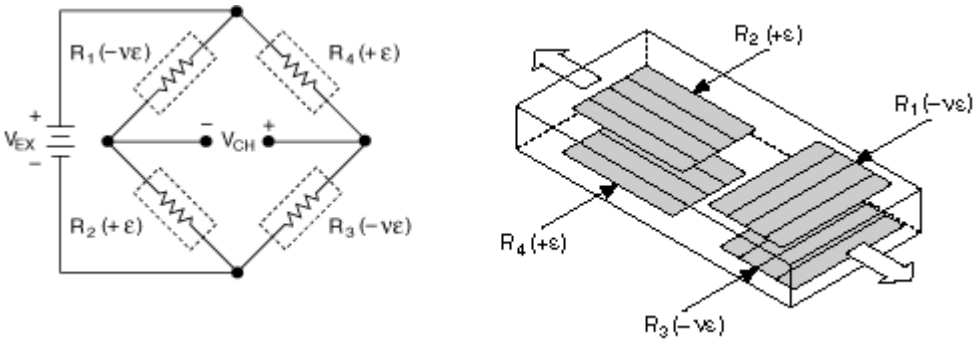

Figure 3: Configuration of strain gauges so that only the axial load is measured

Source: http://zone.ni.com/reference/en-XX/help/370466V-01/measfunds/full3/

A short overview of the limitations of strain gauges is listed below:

- Creep: creep is defined as a change of the output signal of the strain gauge during a constant load and constant environmental parameters. This negative influence makes the strain gauges less useful for measuring the clamp load over long periods, for example 20 minutes. Creep is not caused by the strain gauge itself, but by the glue between the strain gauge and the component. One can distinguish positive and negative creep, which is visualised in Figure 4. In essence, creep is not a significant issue while most software programs, such as N-Code Glyphworks, can compensate the effect.

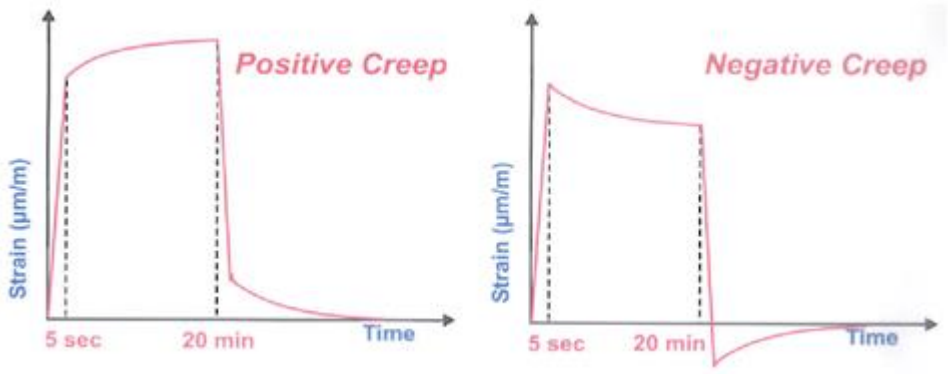

Figure 4: Positive and negative creep [10]

- Temperature influences: the temperature has two main effects on the strain gauge. It changes the K-factor due to a change in conductivity and it can also cause a zero shift. Both effects can be reduced by using an inactive strain gauge for temperature compensation in a pseudo quarter bridge. This is a half bridge in which only one strain gauge is oriented in the direction of the elongation and the second strain gauge is turned 90 degrees to this direction and will not measure any elongation, but will face the same temperature changes. In a full bridge, temperature is automatically compensated.

- Free space: when strain gauges are glued onto bolts, there should be in the first place a flat surface with a recommended surface roughness between 1.5µm and 3µm for normal strain measurements. This might be a problem when the bolts axis has a full thread. So the diameter of the hole in which the bolt must fit, should be large enough such that the strain gauges are not touched when the bolt is torqued. There should also be an untouched path where you can place the wires of the strain gauges. Finally, the bolt diameter should be large enough to glue a full bridge.

When instrumenting the Ford Fiesta roll restrictor bolts with strain gauges, the main problem is the free space problem described above. We needed to machine the bolts as described in **Fout! Verwijzingsbron niet gevonden.**. A picture of a finished bolt can be found in Appendix Figure B 9.

For the M10x80 bolt and the M10x25 bolt, the diameter was locally reduced to a diameter lower than the strength diameter prescribed in literature. Therefore, a tensile test was performed at the VUB to find the yield limit of these machined bolts.

Both bolts failed elastically (cup shape) in the machined area.

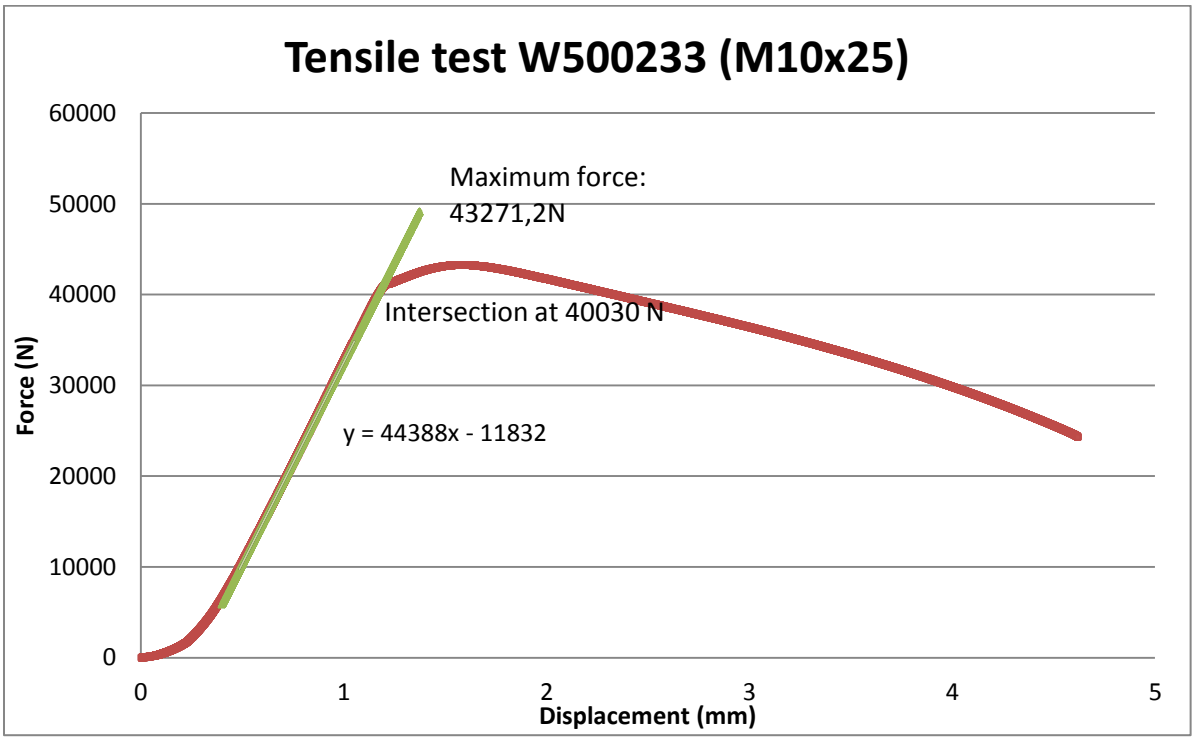

Figure 5: Tensile test results of the W500233

The W500233 M10x25 bolt with dog point, shown in Appendix Figure B 9, has a yield strength of 40kN and a tensile strength of 43,2kN. The green line is the 0.2% line parallel with the linear part of the red curve. The intersection is assumed as yield strength.

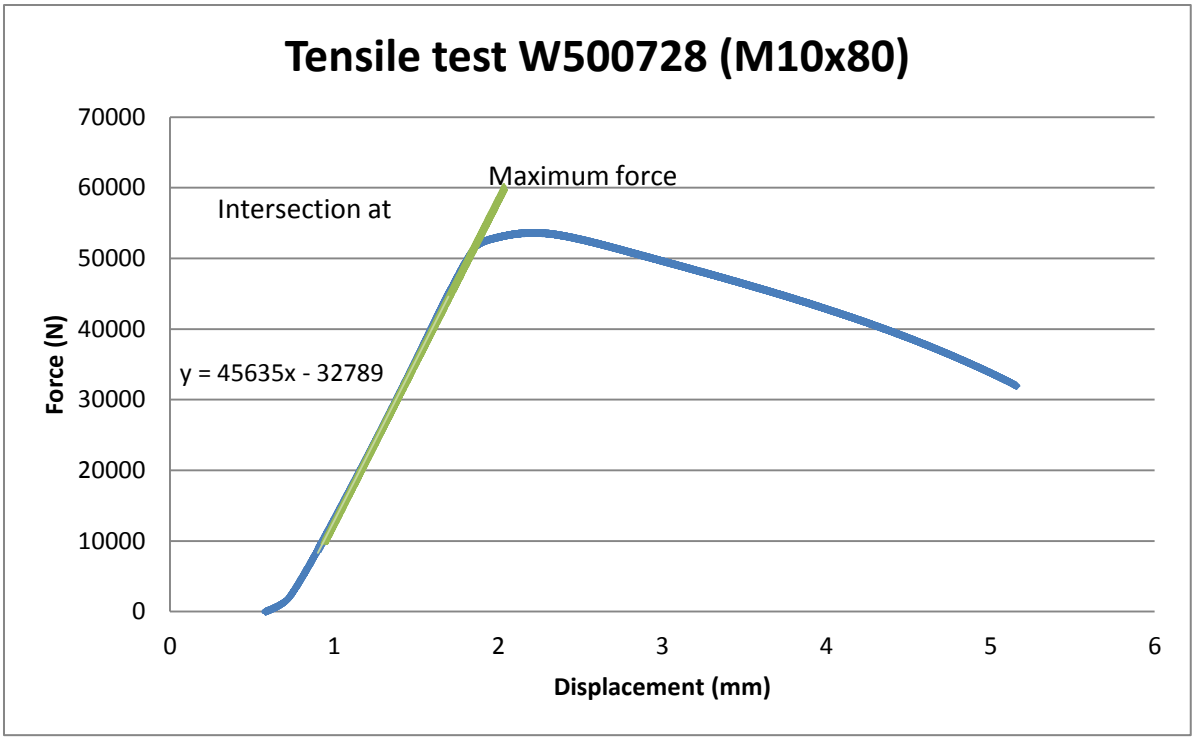

Figure 6: Tensile test results of the W500728

The W500728 M10x80 has a yield strength of 50,4kN and a tensile strength of 53,6kN.

These values are still much higher than the maximum clamp load that can occur at nominal torque according to the graph underneath.

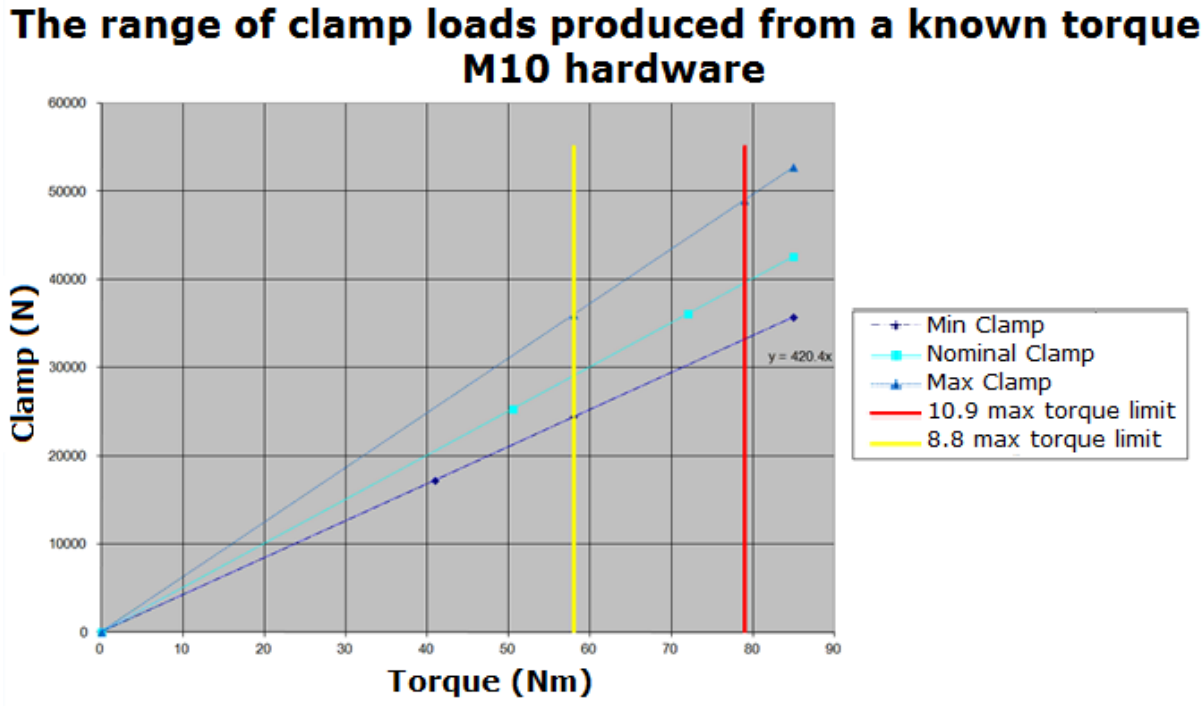

Figure 7: Clamp load versus torque graph used by Dunton design engineers

Because the bolts are too small to glue a full strain gauges bridge, we used a pseudo half bridge. We used the smallest strain gauges available at Ford Lommel:

Micro Measurements type EA-06-062TV-350.

This means that we cannot exclude bending effects. So the next three cases will be indistinguishable. A picture of the different cases which are indistinguishable can be found in Appendix Figure B 10.

Because the head of the bolts was not perfectly perpendicular to the longitudinal axis of the bolts, they bent during calibration according to the position in the tensile test machine. This leads to an offset value according to the position of the bolt in the machine. The K-factor of the strain gauges was not influenced by this bending effect, so the bolts can be used only for changes in clamp load, not for an absolute estimation.

To have an estimation of the error made by this method, we performed 10 tensile tests with the bolt rotated about 35 degrees between each test.

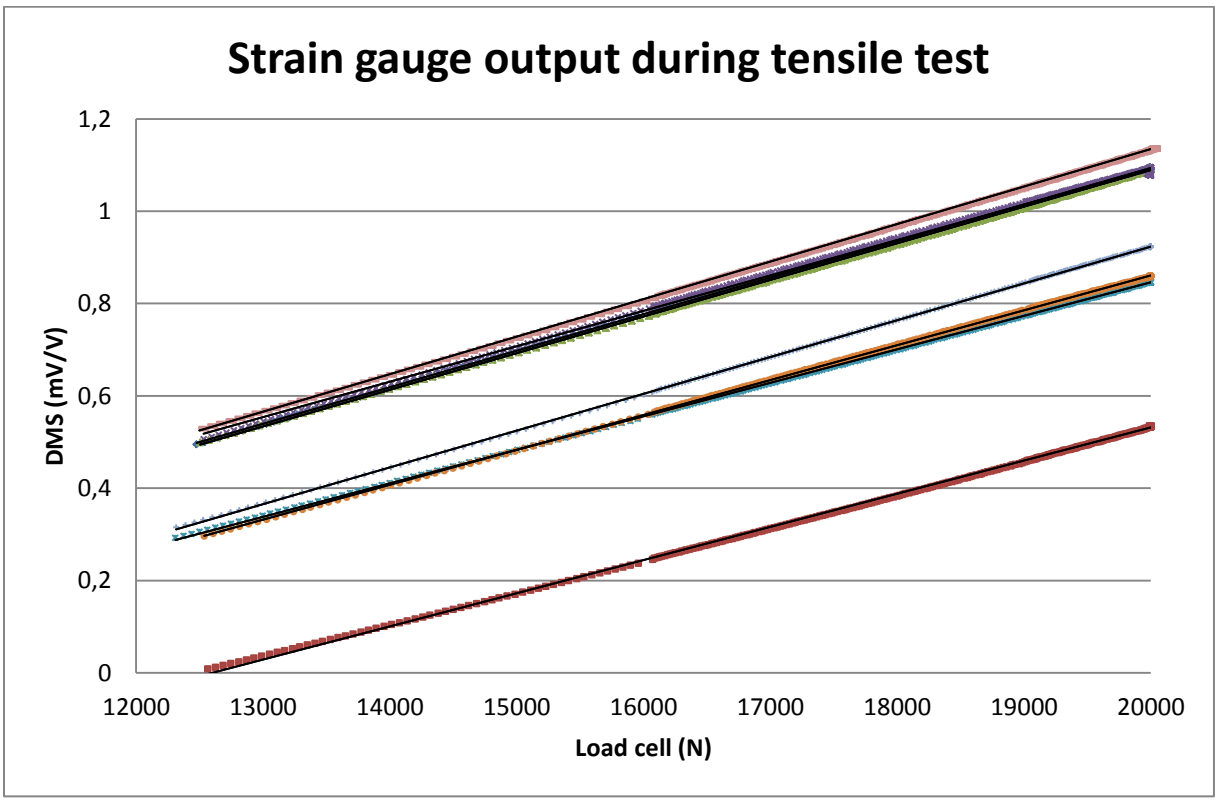

Figure 8: Strain gauge output measured in tensile test each time in a new position

The mean slope of the curves is 7,70102e^{-5} mV/VN and the standard deviation is 3,26039e^{-6} mV/VN. So we can state that the 95% confidence interval on the slope is $\pm$8% of the value of the slope.

3.1.2 Measuring the real time force acting on the roll restrictor

To measure the axial force acting on the transmission roll restrictor, the most commonly used sensor is a full bridge of strain gauges. Measuring the axial force acting on the roll restrictor of a car has already been done many times before by the Road Load Data team. My colleague Bart Van Gorp provided me with the instructions and scheme that can be found in Appendix Figure B 11.

My roll restrictor was instrumented according to this scheme with the prescribed strain gauges: Micro Measurements type EA-06-125AC-350.

The roll restrictor was calibrated by the instrumentation team in Lommel up to 15kN with a total uncertainty of 1.1%. The total uncertainty is the root sum square of the maximal non-linearity and the maximal hysteresis.

3.1.3 Measuring the relative displacement between the roll restrictor and the gearbox

The mechanism of loosening of the bolts described by Junker [8] is caused by a small relative displacement at the level of the thread. We were not able to find the order of magnitude of this marginal displacement. We took the radial clearance of 0.23mm between bolt and nut, measured with a normal calliper on an M10 pitch 1.5 bolt, as a maximum displacement of a bolt under tension. To measure such a displacement we need a very accurate sensor. At the instrumentation unit in Lommel, we have only two types of real time sensors available.

The first type of sensor is a sliding resistance. These sensors are cheap but not so easy to connect, because they need a good fixation on the component. The accuracy is sufficient: up to 10 microns. At Ford Lommel we have the SLS 095, a hybrid linear potentiometer position sensor constructed by Penny & Giles. A picture of this sliding resistance can be found in Appendix Figure B 12.

The second type of sensor is a non-contact capacitive sensor. The working mechanism of this sensor is explained in Appendix Figure B 13.

The capacitive sensor is basically made out of two isolated circular conductors, A and B in Appendix Figure B 13.

The outside electrode is connected to the ground and the inside electrode is connected with an oscillator. When an object closes in front of the sensor, an electrostatic coupling between electrode A and the object and from the object to electrode B exists. The current of this RC network is measured and is correlated to the distance between the sensor and the object.

This can be demonstrated by the equation of the capacitance between two plates:

$$C = \frac{\varepsilon_0 K S}{d} \tag{3}$$

C is the capacitance between the plates, ε_0 the vacuum permittivity, K the dielectric constant of the gap, S the surface of the plates and d the distance between the plates. [11] [12]

This relation shows us that the capacitance depends on the distance we want to measure, but also on the physical properties of the medium and the object. It also limits the capability of measuring the absolute distance between the gearbox and the roll restrictor on a driving vehicle, because the temperature of the gearbox is not constant. Also the humidity and temperature of the air cannot be assumed constant.

When measuring during short Pascar 1 events, these issues are not a problem. The big advantage of this type of sensor is the high accuracy of 2.5 microns. The sensor is also very small which makes it easy to place. [13]

The main disadvantages of this type of sensor are the price of about 1,000 euros per sensor and the fact that they are very easy to damage. The sensor is also not water resistant: even a small drop of water on the two electrodes changes drastically the permittivity and dielectric constant of the gap. This means that we cannot drive events such as the gravel road or the traction control event, but also any other event which includes speeds above 80km/h on a wet track because of the spray of the front tires.

Nevertheless, we tried to use this sensor because of the high accuracy. The instrumentation team in Lommel calibrated a Capacitec HPT-150E-V-N2-80-2.5 sensor which can measure up to 2.5 microns with a total uncertainty of only 0.42%.

Note that this sensor can be used on conducting materials as on non-conducting materials.

We could place only one capacitive sensor at the gearbox side of the transmission roll restrictor at the back of the bracket. A picture of the installed sensor at the back of the roll restrictor bracket can be found in Appendix Figure B 14.

The sensor was placed within the calibrated distance range, which can be seen in the close-up picture in Appendix Figure B 15.

3.1.4 Measuring the real time accelerations at the gearbox side of the roll restrictor

The Road Load Data team always measure the tri-axial acceleration at the three engine mounts. They also normally place a accelerometer on the chassis near each engine mount. These data are necessary to measure the damping ratio of the engine vibrations to the body of the car. Because we had two channels left on my data logger, we placed two accelerometers

on the gearbox side of the roll restrictor. These accelerations are mainly to visualise the movement of the engine mount during Pascar 1 events. More specifically: it makes it possible to get an idea of the direction of the loading. When one measures high forces with the strain gauges on bolts of the roll restrictor together with high Z-accelerations (axial direction to the bolts) and low X-accelerations (transverse direction to the bolts), the forces acting on the bolts are due to much yaw of the engine. This could be problematic because the roll restrictor is designed only for 3kN in this direction. Vice versa, when one measures high accelerations in the X-direction and low accelerations in the Z-direction, it is likely that the forces in the bolts are caused by forces in this X-direction. This is what is assumed in the design of the component.

We used the same accelerometers as applied by the Road Load Data team:

Silicon Design 2210-100

This accelerometer can measure accelerations up to 100g with a non-linearity of maximum 1% of the scale.

3.1.5 Data acquisition system for real time measurements

To log these real time sensors, we used a Dewe-43 V from Dewetron. A picture of this data acquisition system can be found in Appendix Figure B 16.

This acquisition system has 8 analogue channels and also a CAN-bus logger. This is very interesting because you get all the vehicle information such as engine rpm, vehicle speed, brake and clutch pedal switch, throttle position and even ABS requests. The Dewe-43 V is merely an amplifier. The actual logging of the signals is handled by a connected laptop with the corresponding DeweSoft software. This means that the capacity of storable data is 300GB. This is why we logged all channels at the maximum sampling frequency of 5 kHz. The people of the Road Load Data team usually log at 80Hz because they are commonly interested in the highest peak loads and their frequency to calculate the fatigue of components. Since we are interested in what is happening at these peak loads, we used the maximum sampling frequency available.

3.2 Design of experiments investigation of the roll restrictor bolts

When testing the engine mounts, it is important to know the effect of some expected influences on the durability tests. When the Road Load Data team perform measurements on forces or accelerations of engine mounts, they always drive all the Pascar 1 events multiple times in different conditions: Durability Test Load vs. Maximum Durability Load and dry conditions vs. wet weather conditions.

We will perform a two level full factorial DOE investigation with the test load, weather conditions and event severity as input parameters. Event severity will consist out of two levels: a medium event and the most severe event in term of roll restrictor forces.

To choose these two levels, we drove all the durability events while measuring the force on the roll restrictor equipped with strain gauges. In the next chart, the highest peak force during the event is plotted for each event passage. The Road Load Data team usually drive each event three times, but the Chatterbumps event is driven ten times because this event has a low repeatability. The traction control event is clearly the most severe event. Unfortunately it makes a lot of water spray underneath the car, which can easily disturb the sensors installed on the roll restrictor. The Chatterbumps event is the second most severe: roll restrictor forces above 7kN were measured. This event does not include any water, which makes the choice of the Chatterbumps as a high level input manifest.

To choose the low level event, we look at the middle of the graph. The three passages of the Chuckholes Lane are concentrated together at this point, which makes it suitable for the low level input.

At Ford Lommel, we use statistical Minitab software to perform a design of experiments. We first define all the input levels and the type of test. The software then proposes the tests that need to be driven with random sequence. We were not fully able to drive all the tests with random sequence, as we have no control of the weather conditions.

The tests were performed with the customer correlation car: a Ford Fiesta 1.6 Sigma four cylinder engine with 120hp and a maximum torque of 155Nm.

Appendix Figure B 17 gives an overview of the severity of all events.

The table below contains the input parameters of each test, together with the maximum measured peak force at the roll restrictor.

Table 1: DOE test conditions and measured roll restrictor force of a Fiesta 1.6 Sigma

Ford Fiesta 1,6 Sigma 120hp 155Nm			
weather	load	event	force (N)
WET	DTL	Chatterbumps	7036
WET	DTL	Chuckholes lane	3093
WET	MDL	Chatterbumps	7786
WET	MDL	Chuckholes lane	2986
DRY	MDL	Chatterbumps	9237
DRY	MDL	Chuckholes lane	3113
DRY	DTL	Chatterbumps	5689
DRY	DTL	Chuckholes lane	2752

MDL means Maximal Durability Load and DTL means Durability Test Load.

Note that the highest peak forces occur during the Chatterbumps braking.

A few weeks later, a colleague of Road Load Data had to drive all durability events with a Ford Fiesta ST 1.6 GTDI that produces 180hp and 240Nm. He gave me the data shown in the next table.

Table 2: DOE test conditions and measured roll restrictor force of a Fiesta ST 1.6 GTDI

Ford Fiesta ST 1,6 GTDI 180hp 240Nm			
weather	load	event	force (N)
WET	DTL	Chatterbumps	13690
WET	DTL	Chuckholes lane	4304
WET	MDL	Chatterbumps	9914
WET	MDL	Chuckholes lane	4160
DRY	MDL	Chatterbumps	7296
DRY	MDL	Chuckholes lane	3983
DRY	DTL	Chatterbumps	7085
DRY	DTL	Chuckholes lane	3876

Note that the highest peak forces occur during the Chatterbumps acceleration.

This enables me to add another input parameter: engine type.

After entering all test results in Minitab, the program shows us the effect of all combinations of the inputs. Some of them are significant, others are not. One should remove the least significant combination of the highest order and perform another analysis. This procedure will be repeated until all combinations of the inputs are significant. [14]

With the above test data, we obtained the following results after the first analysis.

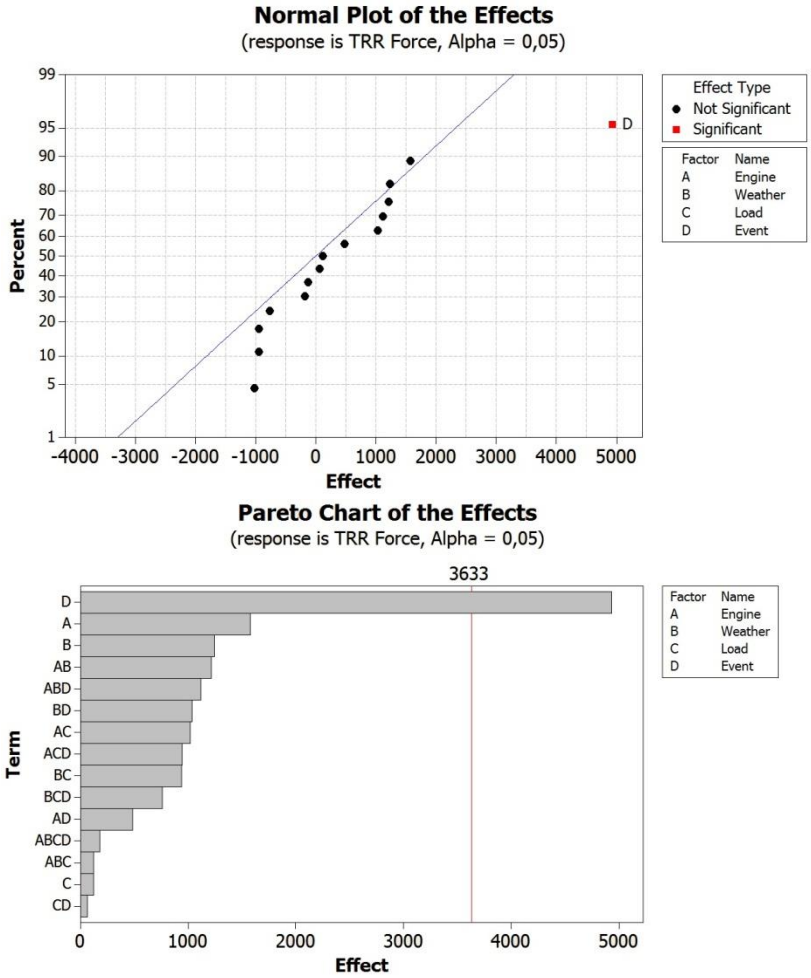

Figure 9: DOE analysis results after the first iteration with four inputs

The omission of the insignificant combinations led to the transfer function in which only the type of event matters. [15]

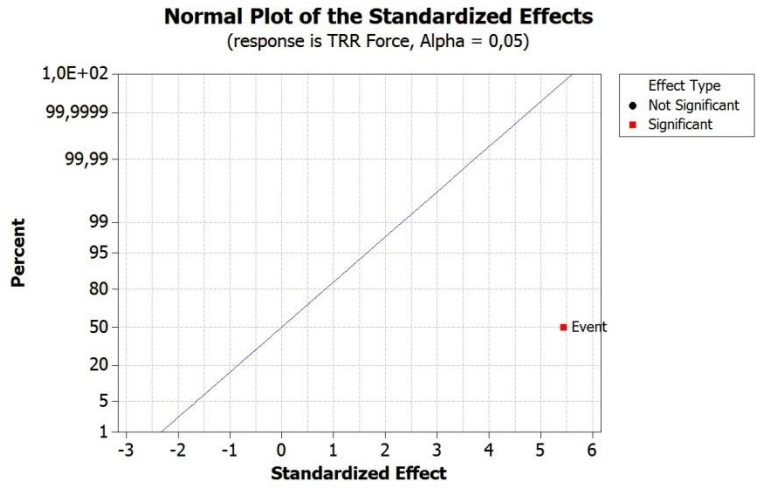

Figure 10: DOE analysis after omission of all insignificant combinations

The obtained transfer function is:

$$TRR\ force = 2466N * type\ event + 6000N$$

The type event variable can be no more than two values: -1 for a light event and +1 for a severe event.

The result obtained is quite obvious and could have been predicted without this analysis. It should be more interesting to perform such an analysis for the Chatterbumps event exclusively. This event has a low repeatability, so it would be interesting to know which parameters influence the event the most. In Minitab, it is possible to use a 'number of replicates for corner points'. This means that you have results of the same test under the same conditions. Since we have already driven the Chatterbumps event ten times, the use of this function will enhance the accuracy of the analysis. After performing the iterative analysis, the next results are obtained.

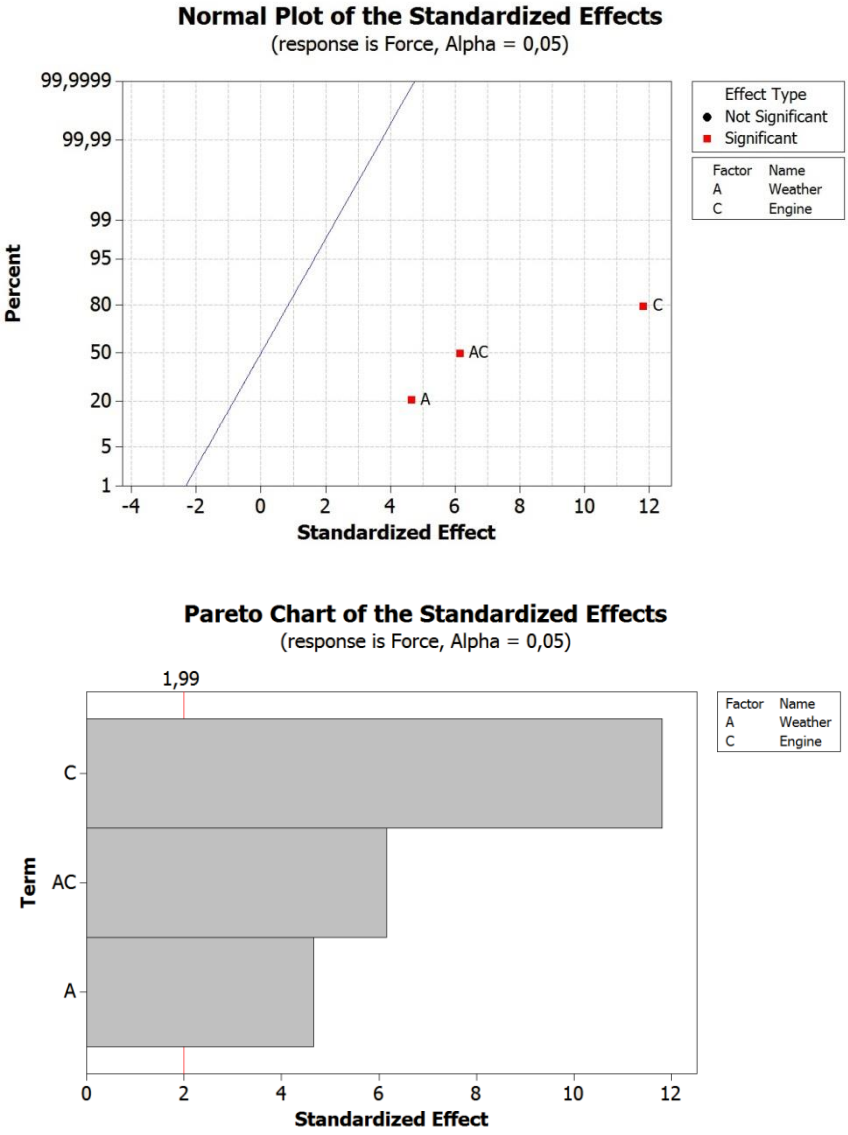

Figure 11: DOE analysis results of the Chatterbumps event

The corresponding transfer function is the following:

$$TRR\ force = 687N * weather + 1743N * engine + 907N * weather * engine + 6570N$$

The weather parameter assumes the value -1 in dry conditions and +1 if the track is wet. The engine parameter is -1 for the Sigma engine (120hp and 155Nm torque) and assumes the value +1 for the 1.6 GTDI engine (180hp and 240Nm torque). Note that the type of engine cannot simply be interpolated for another type of engine. This one parameter is the combination of several parameters such as power and torque characteristic, Eigen modes, weight of the engine, transmission, differential, etc.

It is remarkable that the load of the car is of no importance for the roll restrictor forces during the Chatterbumps event.

3.3 Finding the applicable loosening mechanism

When measuring the combination of bending force and axial forces with a strain gauges pseudo half bride during all the durability events, we never detect a loss of pretension. Note that we only measure the change of the force, not the absolute value. This absolute value of the pretension is measured with the ultrasonic sensors discussed later. The highest measured force on top of the static pretension does not approach the yield limit of the bolts, measured by tensile tests performed at the VUB. This results in the exclusion of the first two failure mechanisms: loss of pretension and yielding the bolt. After the durability tests with ultrasonic bolts, we always measured the clamp load when the bolts were disassembled from the car. If the bolts should have been elongated permanently, the measured value should significantly differ from zero. But this was never the case, as one can read in chapter 4.

This brings us to the fatigue question. Fatigue is the failure that occurs after cyclic loading below the yield strength. The failure is partially brittle, partially ductile. A fatigue rupture of a bolt mostly takes place at the root of the first thread, due to the stress concentration of the diameter change. A stress concentration mostly causes the initiation of a fatigue failure. Starting from this stress concentration, the crack propagates into the material. Each load cycle, the material yields a bit further, creating a specific fracture surface called beach marks. When the diameter is reduced too much, a brittle rupture causes the failure.

We looked at all the reported bolt failures of the last five years, but none of them reported a broken bolt.

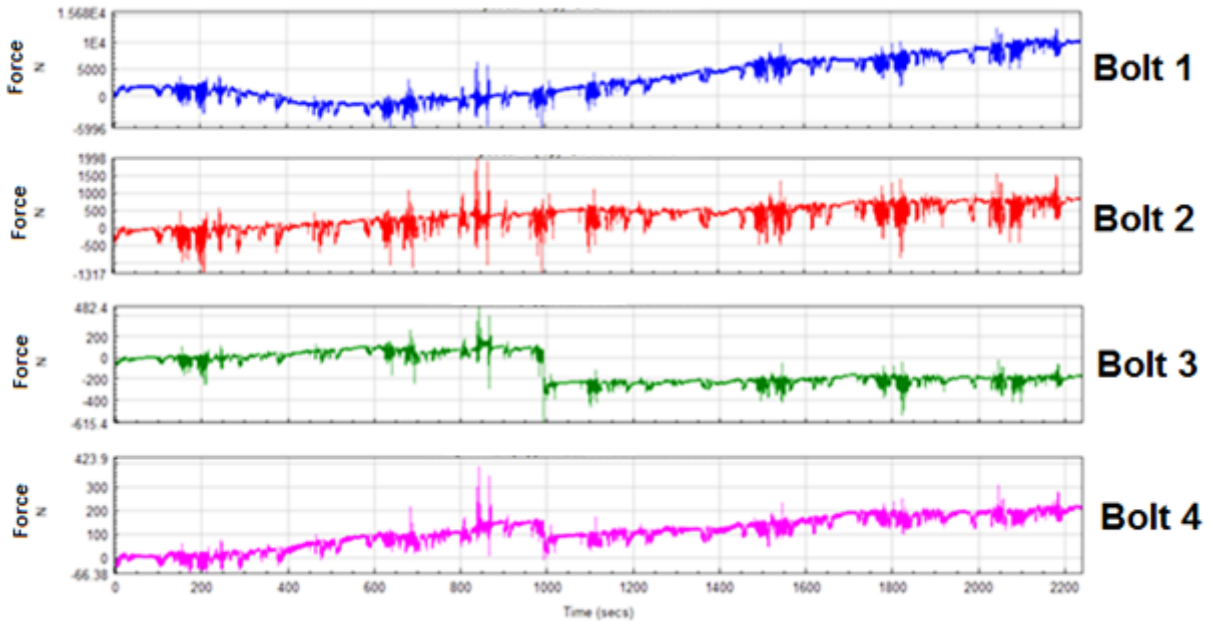

Figure 12: Forces measured with strain gauges on the bolts during a Pascar 1 cycle

The total evolution of the clamp load during a Pascar 1 cycle is not correct as mentioned before, but sudden changes in clamp load are not influenced by effects such as creep of the strain gauges. Such a permanent change in clamp load can be spotted in bolt 3 and 4 at 1000 seconds. This effect will be investigated later in this chapter.

The Road Load Data team always samples at 512Hz and use a low pass filter of 80Hz. This 80Hz has a traditional origin: when the Road Load Data Team first started to measure forces on chassis and body parts, the available technology at that time only allowed to measure 50 channels at 80Hz. To stay comparable with all previous measurements, they kept this frequency for chassis and body forces. For other measurements such as NVH, much higher frequencies are measured.

When we look at the frequency spectrum of the forces measured in the subframe bolt, we notice that this low pass filter is appropriate.

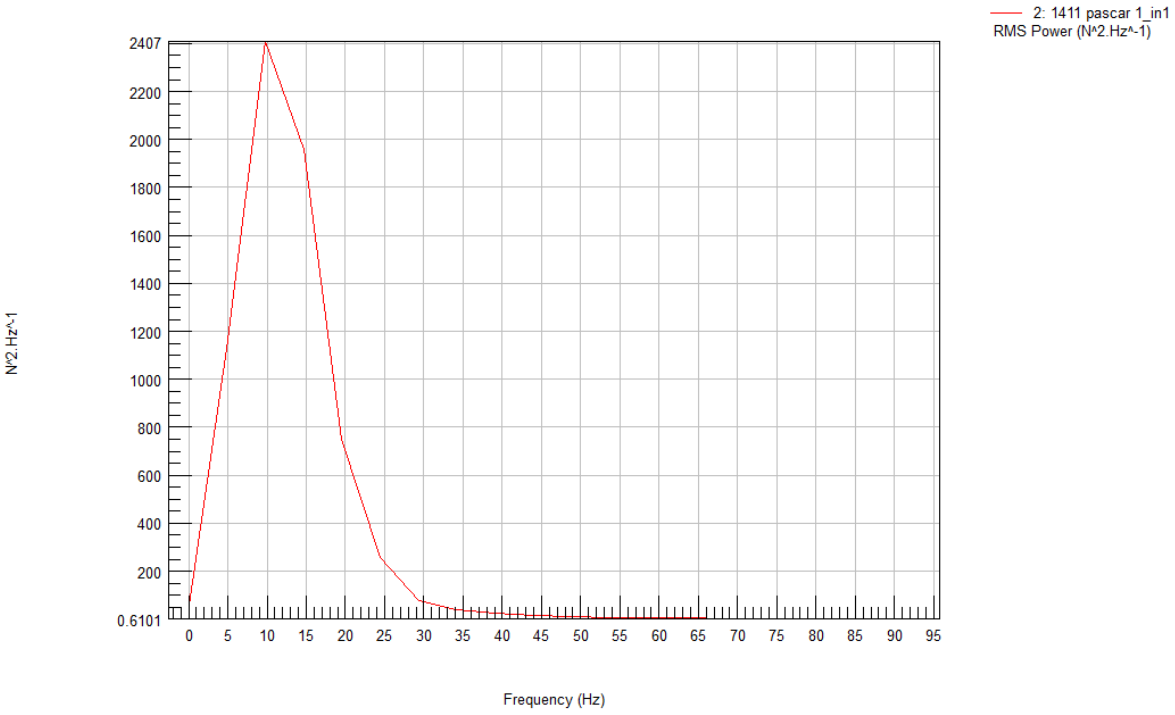

Figure 13: Fourier spectrum of the measured forces of the sub frame bolt during a full Pascar 1 cycle

Looking at the accelerometers placed on the roll restrictor bracket during the severe Chatterbumps event, we observe that the accelerations in the longitudinal direction of the car are significantly larger in magnitude than in the transverse direction. This is consistent with the low axial forces measured with the strain gauges on the bolts.

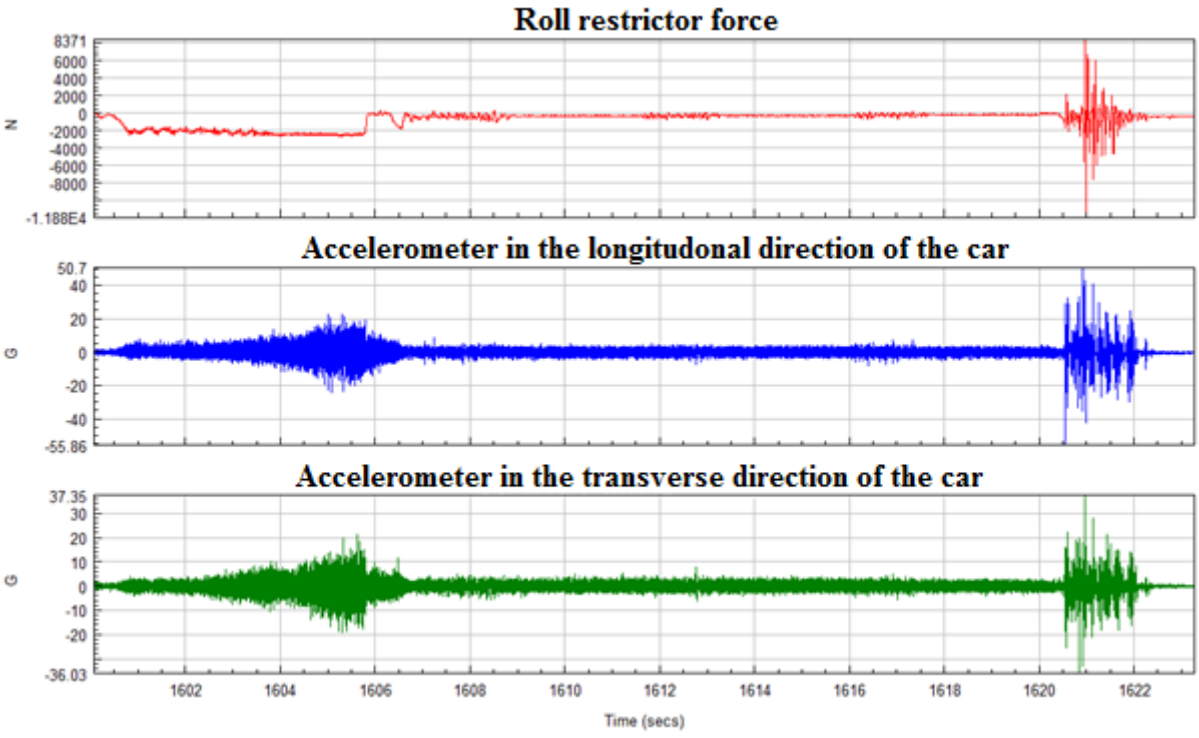

Figure 14: Roll restrictor force and two accelerometers during the Chatterbumps event

The last installed sensor on the roll restrictor measures the relative displacement between the roll restrictor bracket and the gearbox. One should not expect large displacements as the bracket is bolted onto the gearbox with three M10 bolts. The axial forces on the roll restrictor are thus somehow spread over these bolts. We are only able to measure the displacement at one of these bolts, without the knowledge of the contribution to the force on the roll restrictor. As the sensor is placed about 1mm away from the gearbox onto the bracket, we will measure the combination of two displacements: the strain of roll restrictor bracket and the relative movement of the bracket onto the gearbox. The direction of this movement is indicated on Appendix Figure B 18.

Note that there is a third displacement: the movement of the holder of the sensor. As the weight of the sensor is very low and the holder is made from steel with a thickness of 3mm, we will neglect this contribution.

The sudden change in clamp load is shown below. During the Chatterbumps braking, high forces occur together with relatively large displacements. The strain gauges on the bolt itself measure a different force before and after the event. As it is only a half bridge, we can only conclude that the bolt is in a different stress situation because of the Chatterbumps braking.

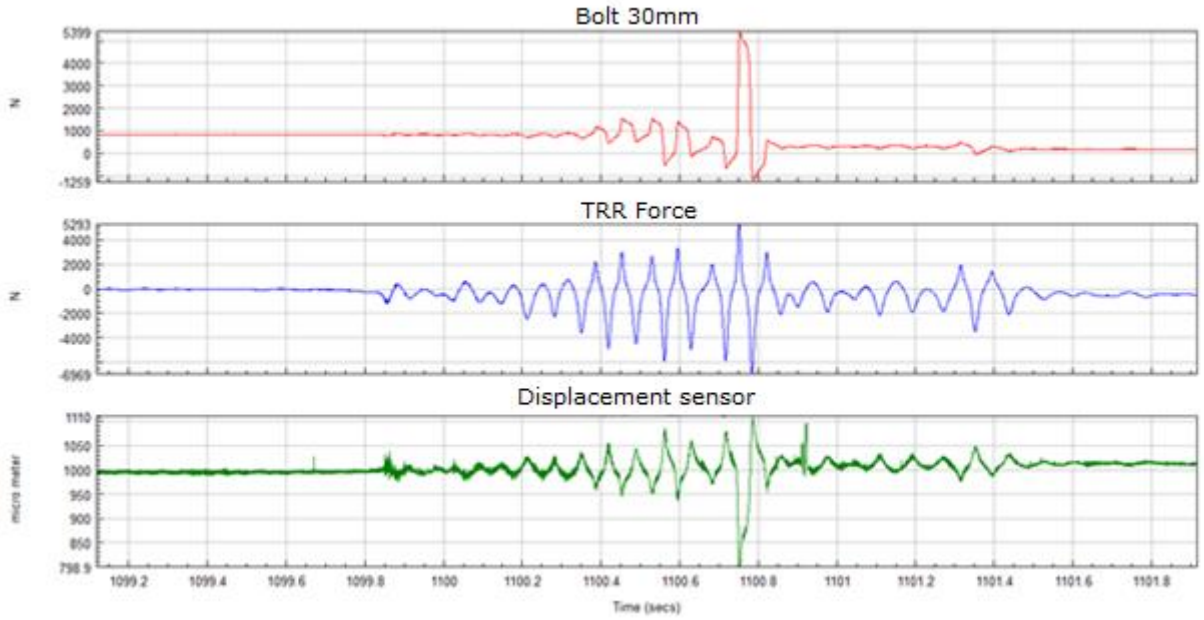

Figure 15: Forces and displacement measured of the same W500233 bolt together with the roll restrictor force during Chatterbumps braking, dry track and MDL

Figure 16 shows the relative displacement measured by this capacitive sensor in function of the axial forces on the roll restrictor during the severe Chatterbumps braking event.

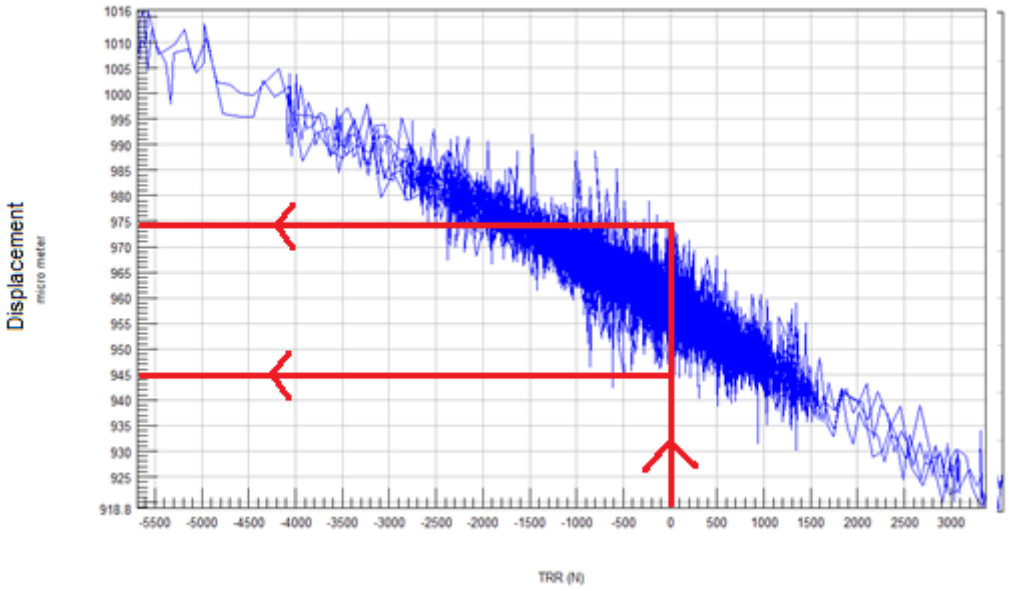

Figure 16: Displacement versus roll restrictor forces, dry track, DTL

With the durability test load, we never spotted visible non-linear effects at a zero roll restrictor force. Only a difference of 30 micrometres can be seen.

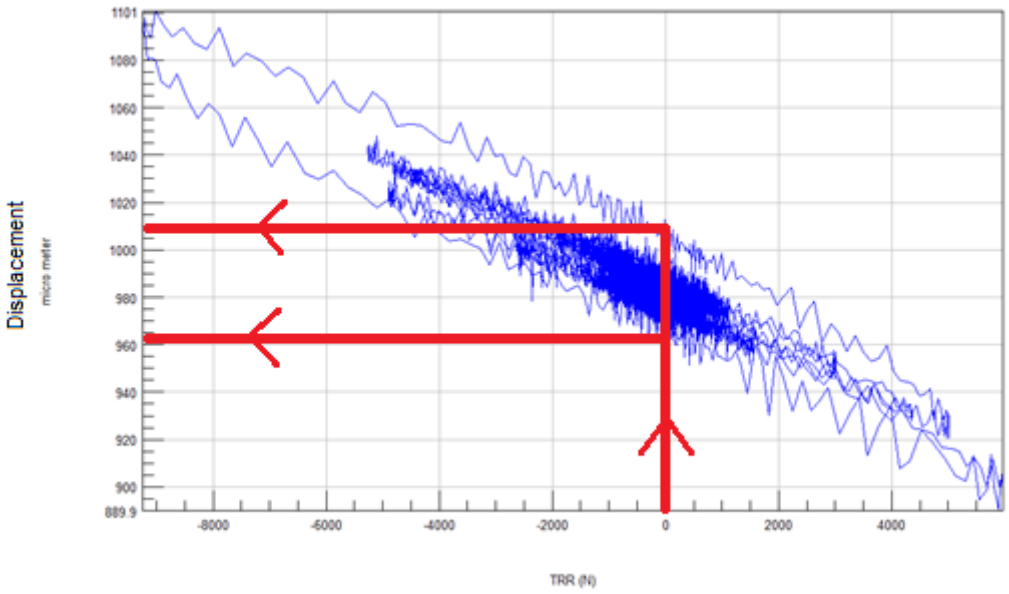

Figure 17: Displacement versus the roll restrictor force during the Chatterbumps event, dry track, MDL

When the car is loaded with the maximum durability load, we see that there is a non-linear effect at high roll restrictor forces. To interpret these results, we first consider the strain of the roll restrictor bracket. As a force acts on the bracket, there will be a strain of the bracket. The bracket of the roll restrictor is made out of 4.6 mm thick steel plate, so yielding of this bracket is out of the question.

Below the yield strength of steel, the strain is given by the Hooke's law:

$$\varepsilon = \frac{\sigma}{E} \tag{4}$$

So the relation between the strain and the stress is linear. This means that the non-linear displacement occurring at higher roll restrictor forces must be due to a movement of the roll restrictor onto the gearbox.

The sudden change of stress situation of the bolt together with the relative displacement between the roll restrictor and the gearbox, show that the bolt performs a small displacement at high roll restrictor forces. According to literature, this effect would cause Junker's loosening and/or embedding. Because these two mechanisms are almost undetectable in a small number of cycles, we should perform tests on the long term.

To determine the influence between the clamp load and the relative displacement between the roll restrictor and the gearbox, we repeat the above tests with the bolts torqued at a lower torque. Note that the torque is linear with the pretension force. We can clearly observe that if we reduce the torque in steps of 10Nm, the relative displacement between the roll restrictor and the gearbox increases.

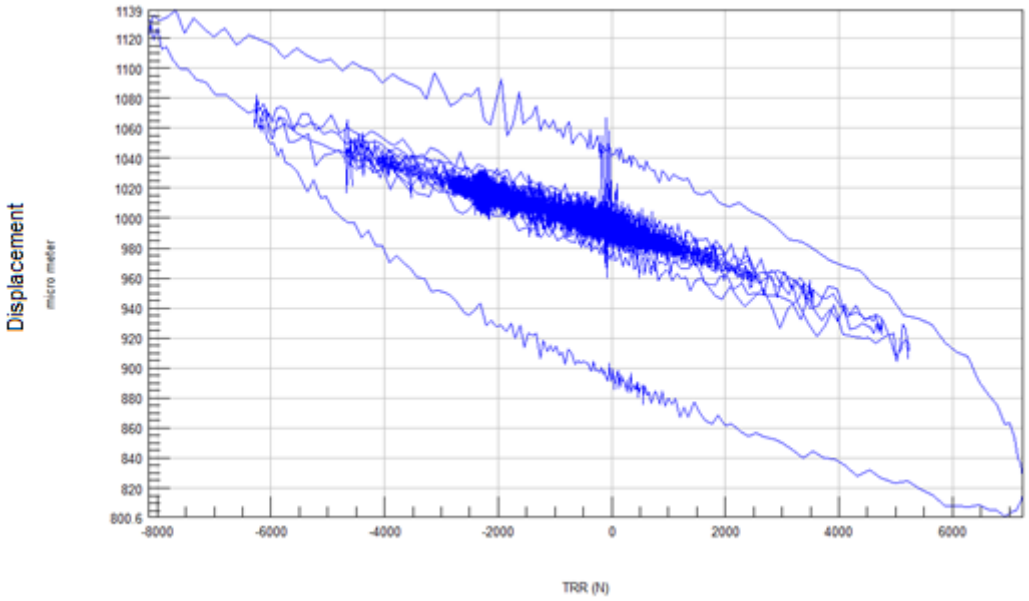

Figure 18: Displacement versus the roll restrictor forces, dry track and DTL. 10Nm below nominal torque

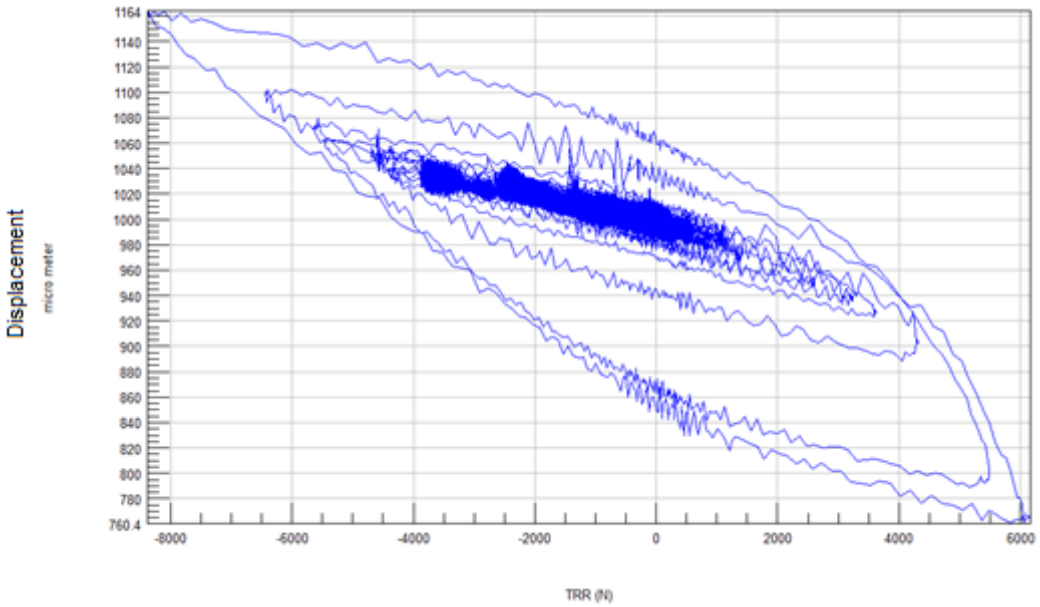

Figure 19: Displacement versus the roll restrictor forces, dry track and DTL. 20Nm below nominal torque

The Chatterbumps event has a low repeatability, so one should be careful when comparing different passages of the event under different bolt torque. We chose three passages of the event at which similar maximum roll restrictor forces occur between 8kN and 9kN.

The relation between the displacement difference at no-load of the roll restrictor and the torque of the front W500233 bolt is shown in Figure 20.

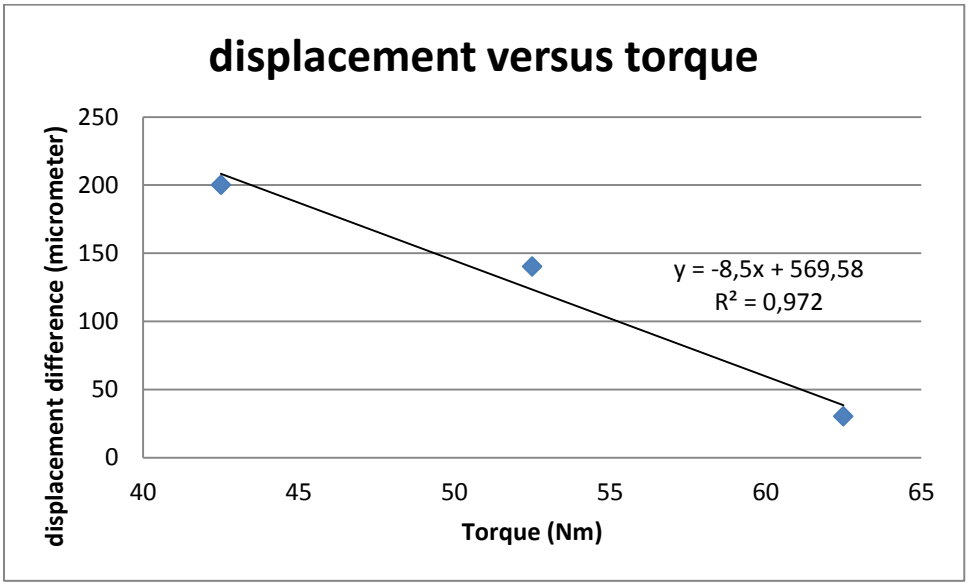

Figure 20: Difference in displacement at no-load on the roll restrictor measured at different torques on the bolts

The relation in this range looks very linear, but it is important to remember that at some lower torque the displacement will be limited. We decided not to reduce the torque more than 20Nm, because of the increased risk of fracturing the gearbox case or breaking the expensive capacitive sensor.

Out of the literature study, we know that relative displacements on the thread surface and between the bolt head and the component can cause two types of failure mechanisms: non-rotational and rotational loosening.

The non-rotational loosening, or embedding effect, is mainly influenced by the thickness of the paint on the component. Due to the movement of the bolt, the paint slowly creeps underneath the bolt head which reduces the thickness of the clamped part and so a reduction of the pretension force.

Rotational loosening, described by Junker, is the effect in which the movement causes the change from static friction to dynamic friction. When this dynamic friction is too low to prevent the bolt from rotating in the loosening direction, the bolt can lose all its pretension force.

3.4 Conclusion

With the data of the real time measurements, we can conclude that the bolts never lose the pretension force. The dynamic forces in the bolts are small relative to the pretension force of the bolts. The yield limit of the bolts is never reached. When we look at the type of failure, a fracture of the bolts is never reported in the last five years which can exclude fatigue. Remarkable is the relative displacement between the roll restrictor and the gearbox. This can cause rotational or non-rotational loosening. To decide which type of loosening occurs, we need to perform some test on the long term: do the bolts immediately start to rotate or do we lose pretension force without rotation? More general, at which level of pretension force do the bolts start to rotate?

Chapter 4: Long term tests

To decide which failure mechanism occurs due to the movement found in chapter 3, we need to perform a series of tests during Pascar 1. First we will try to monitor the evolution of the pretension force during a Pascar 1 test. Secondly we will examine rotational loosening. Finally, we will investigate the most frequently used technique at Ford Lommel: the measurement of the on-torque. It should be interesting to know the accuracy of this technique and to know how the relation to the pretension force changes during durability tests.

4.1 Long term sensors

As stated earlier, measuring the clamp load on the long term, for example one month, cannot be done by the use of strain gauges. In the Ford John Andrews Entwicklungszentrum in Merkenich, Germany, the engineers of the bolt lab use ultrasonic waves to measure the clamp load of a bolt. The machine used is an LP3000 from Intellifast from Speyer, Germany. A picture of the loadcell readout and LP3000 can be found in Appendix Figure B 19.

4.1.1 Principle of ultrasonic measurement technique

The ultrasonic technique is a very accurate but expensive technique to measure the clamp load of the bolts. There is no need to modify the friction surfaces of the bolts or change the diameter of the bolts, as was the case with the strain gauges. Only the surface on the head of the bolt and the surface on the other side of the bolt need to be grinded until they are perfectly parallel. A piezoelectric sensor/actuator is glued on the head of the bolt. We excite the piezoelectric material with a current so that it causes an ultrasonic longitudinal wave in the bolt. This signal travels with the speed of sound, depending on the bolt material. The wave is reflected on the parallel surface on the other side of the bolt, and once returned to the piezoelectric material, the ultrasonic wave is converted into an electric signal that can be measured by the load probe which can be seen in Figure 22.

If the bolt is elongated by a tensile force, the ultrasonic signal will travel longer; we say that the ‘time of flight’ has increased. During the calibration, we link the change in time of flight to a clamp load. The manufacturer of the load probe claims to achieve a total error below 3% of the measured value.

There are two main influences that contribute to errors. The speed of sound in the material is temperature dependent and when the bolt is bent by the load, the ultrasonic waves will not reflect the same as before. The temperature effect is compensated by the load probe through measuring the temperature of the bolt. We assume that the temperature is equal over the entire

bolt. For example, we cannot perform measurements on bolts that are mounted in a hot gearbox. [16]

The reflected signal is transformed in the load probe by an algorithm made by the manufacturer. This makes it much easier to spot the change in time of flight. But when the echo changes due to bending, this change is exaggerated by the algorithm and can cause severe errors. When the bolt is bended, the grinded surface on the head of the bolt is no longer parallel to the surface on the other side. One should always check when measuring the time of flight if the transformed echo is not changed with respect to the original echo measured at no-load. An example of this effect is shown in Figure 21. The blue signal is the actual reflection of the ultrasonic waves. The red signal is the transformed signal. The machine measures the change in time of flight by observing the shift of the negative red peak. In the right figure, one can see that there are suddenly three peaks instead of one. This is due to bending effects.

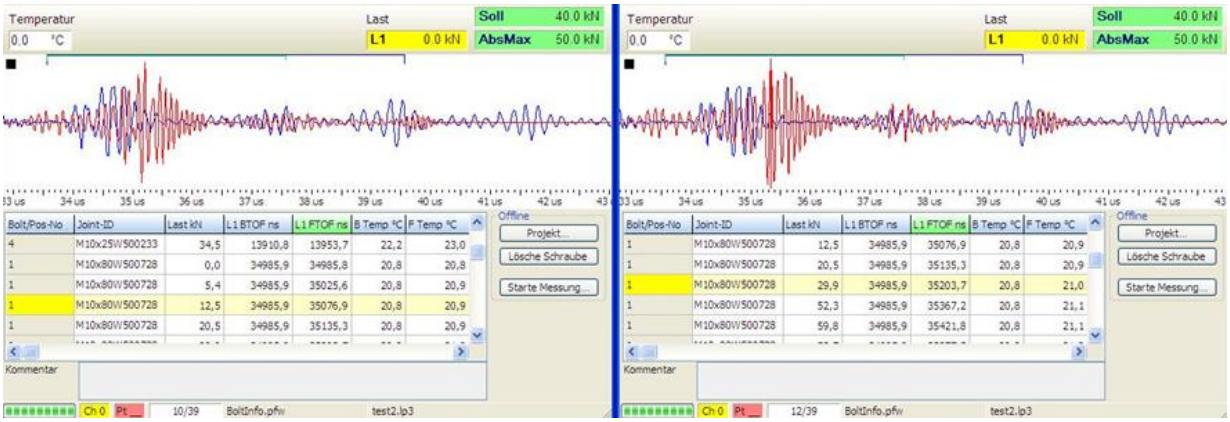

Figure 21: Example of the echo received with the load probe

4.1.2 Calibration of the ultrasonic bolts

Because the load probe measures only a difference in time of flight, we need to calibrate the bolts using a load cell in order to find the force factor that relates the change in time of flight to the clamp load.

Before the calibration, we measure the total length of the machined bolts. This enables us to estimate the time of flight of the ultrasonic signal.

$$TOF_{theoretical} = \frac{2 * total\ length\ in\ mm}{0{,}6026\ {}^{mm}/_{ns}} + 1323{,}3ns \qquad (5)$$

The denominator of the first term is the speed of sound in steel. The second term is a characteristic time delay of the sensor and machine. This theoretical value is a help for finding the first echo, but manual adaptation of this value is always necessary.

Secondly, the parameters of the algorithm should be adapted until the algorithm transforms the original echo signal into a signal with one isolated negative peak. The time shift of this peak will be used as change in time of flight of the whole signal.

An initial force factor should be chosen. Experience of the user can be a high advantage for the choice, as an initially chosen force factor close to the correct force factor can make iterations unnecessary.

We now torque a bolt in a calibrated load cell to 25kN in steps of 5kN. Note that we place a steel bush between the load cell and the bolt to the designed clamp length. At each torque step we measure the pretension force with the load cell (LC) and with the load probe (LP).

With these samples, the new force factor can be calculated using this formula:

$$FF_{new} = \frac{\sum LC_i}{\sum LP_i} * FF_{initial} \quad (6)$$

When the initial force factor differs a lot from the new force factor, it is advisable to perform an iteration of the calibration. For example: in the last calibration of the W500728 bolt, the force factor changed only 1.5%.

The next picture shows the bolt screwed into the load cell, through the steel bush. The red probe is a temperature sensor. We assume that the bolt and female thread are at the same temperature.

The probe on the right is the load probe that should be placed on the head of the bolt in such a way that the electrode is on top of the piezoelectric sensor. The probe is kept onto the bolt with integrated magnets.

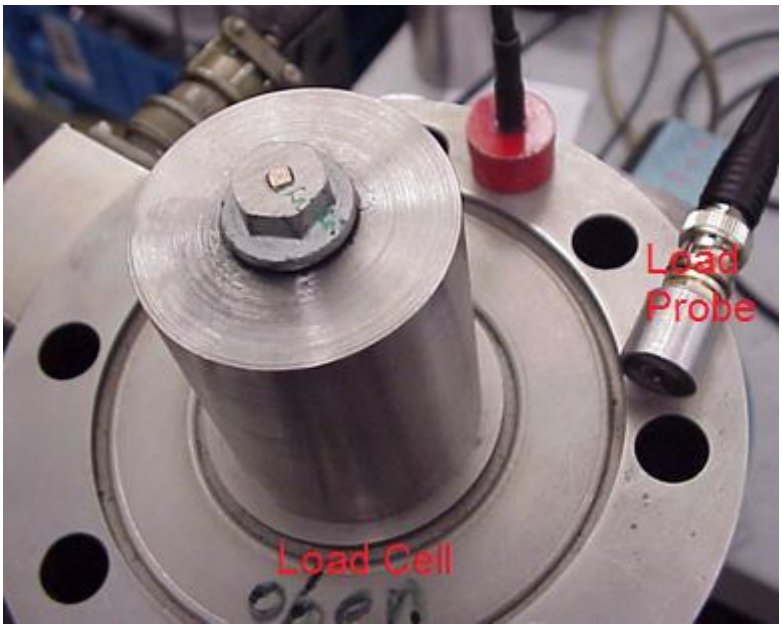

Figure 22: Calibration tools for the ultrasonic bolts

We perform a calibration on 5 bolts of the same type, taking the average force factor for all the other bolts of this type.

4.2 Ultrasonic technique

The ultrasonic technique is perfect to visualize the evolution of the pretension force during durability tests. An important issue during these tests is the protection against corrosion. We cannot use grease as protection because this might influence the friction coefficient on the thread surface for future testing. While both ends of the bolt are grinded parallel, the corrosion protective finish is removed. We used plastic caps on the bolt head and a protective coating of the type 'Galvatec' on the other end of the bolt.

Figure 23 show the evolution of the pretension force of the roll restrictor bolts during a Pascar 1 durability test. The Pascar 1 test was a bit modified to protect the ultrasonic sensors: all corrosion related events were not driven. The car used for this test was a Ford Fiesta with a 1.0 GTDI petrol engine with 100hp and a maximum torque of 170Nm.

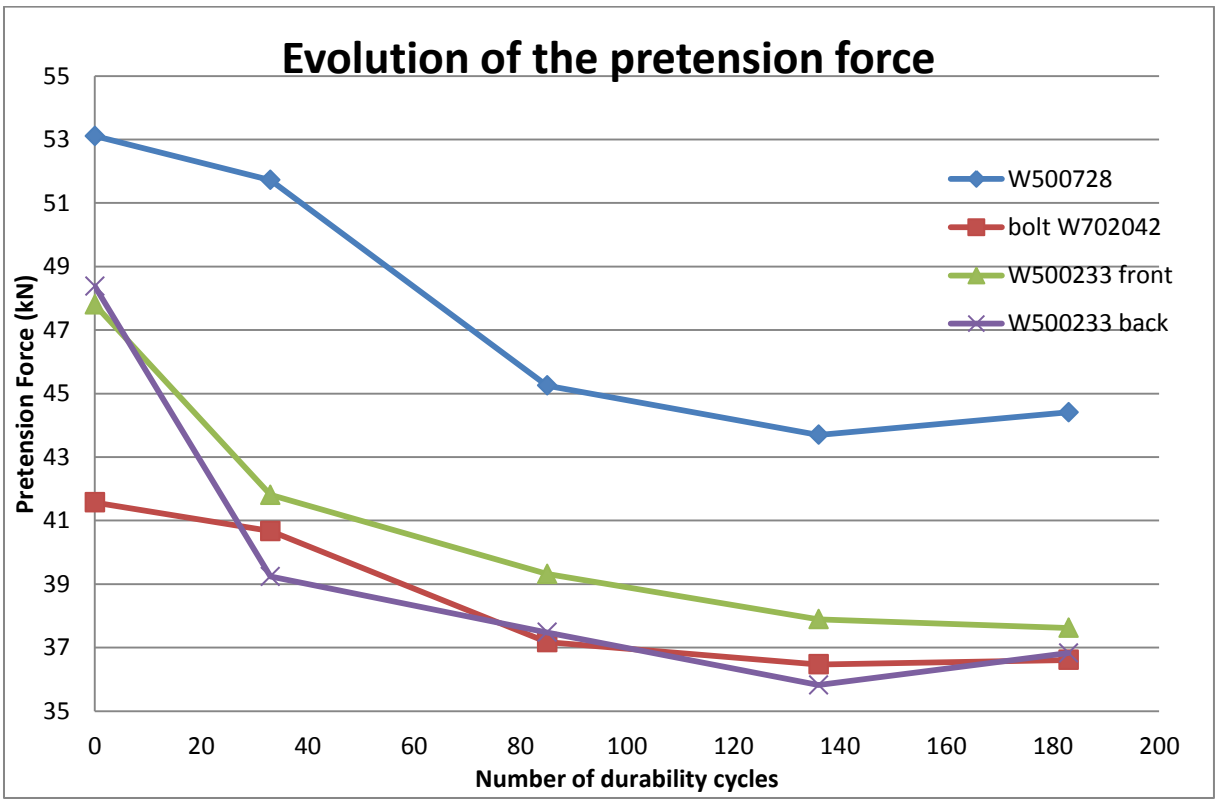

Figure 23: Evolution of the pretension force during a durability test

The first drop of pretension force, at cycle 33, is mainly due to the Brinelling effect. Brinelling is the local surface yielding of the bolt, female thread or component surface underneath the bolt head. The cause of this effect is mainly the imperfections of the surface

and thread. The contact surface will always contain a number of stress concentrations that will locally yield. The effect increases with the size of the bolts.

Note that the increase of pretension force for two bolts in the last measurement are not significant due to the machine error of 3% claimed by the manufacturer.

Since no paint marking on any of the bolts has moved during this test, the further loss of pretension must be caused by embedding. When the bolts are loosened, damage to the coating can be spotted on the roll restrictor and on the paint of the subframe. This is proven with the following picture.

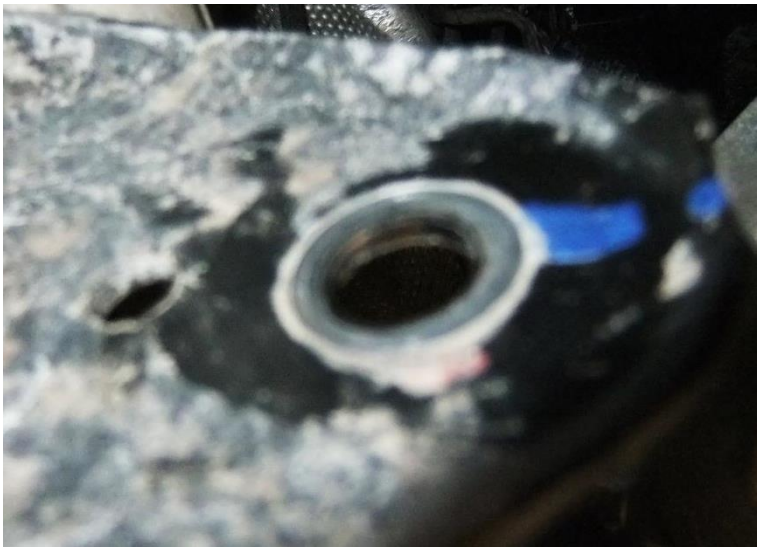

Figure 24: Subframe coating damaged by the head of bolt W500728

More pictures of the damaged coating can be found in Appendix Figure B 20 until Appendix Figure B 22.

In Appendix Figure B 22 we spot an indentation round the hole of the subframe bolt, W500728.

To check if all these visible embedding traces are actually responsible for the loss of pretension force, we measured the thickness of the component round the holes with a micrometre after the second step in the torqueing procedure. Because the surface is slightly damaged at this time, we measured the thickness on four places round each holes and calculated the average thickness. Also the thickness of the subframe round the holes of the W500728 bolt was measured. The component was installed on the Ford Fiesta with a 100hp Fox engine which performed a Pascar 1 durability test.

Afterwards the thickness of the component and subframe were measured with the same tools and the same procedure. The results of this test can be observed in the following table.

Table 3: Thickness of the component and subframe before and after a Pascar 1 test

	Average thickness before test (mm)	Average thickness after test (mm)	Difference (µm)
bolt 1 + subframe	62,8025	62,6225	-180
bolt 2	83,8075	83,735	-72,5
bolt 3	4,5375	4,5275	-10
bolt 4	4,53	4,52375	-6,25

Is this loss of thickness or embedding effect responsible for the measured loss in pretension force during this Pascar 1 test? This can be proven by the following calculations.

In a pre-stressed bolted connection, the tensile force of the bolt should always be equal to the compressive force of the clamped component. These forces are measured before and after the durability test with the ultrasonic sensors. If we measure the clamped cross section and the cross section of the bolt, we are able to calculate the stress in both the bolt and the component.

$$\sigma = \frac{F}{A} \tag{7}$$

Note that the cross section of the clamped component is always a rough estimation. The two W500233 bolts clamp a plate to the gearbox, but the stress in this plate is not uniform: the stress will be higher close to the bolt axis than for example at 5mm from the hole. For these two bolts, we estimated this surface by the circle covered by the head of the bolt. The W702042 and W500728 bolts hold the inside of the rubber bushes which are 62.8mm and 83.8mm long. For this situation it is more advisable to take the full cross section of the aluminium shaped cylinders.

By using the material properties, we are able to calculate the strain of the bolt and the clamped component.

$$\varepsilon = \frac{\sigma}{E} \tag{8}$$

As mentioned above, the clamped component for the W500233 bolt is a steel bracket, so E=210 GPa and the W500728 and W702042 bolts clamp an aluminium component, so E=69 GPa. The engineering strain is defined as follows:

$$\varepsilon = \frac{length\ under\ stress - original\ length}{original\ length} \tag{9}$$

The original clamp length of the bolts is known from the design specifications, so we can calculate the length under stress of the bolt. This length should be the same as the length of the clamped component. So we can easily adapt the formula of the engineering strain to calculate the original length of the component. We can calculate the same original length of the clamped component but starting from the pretension force measured after the durability test. The difference between these two original lengths of the clamped component should be the depth of embedding.

The results of these calculations are shown below.

Table 4: Measured and calculated embedding depth

	Measured loss of thickness (µm)	Calculated loss of thickness (µm)
bolt 1 + subframe	-180	-86,9
bolt 2	-72,5	-36,1
bolt 3	-10	-4,6
bolt 4	-6,25	-5

We have to mention that these theoretical bolt calculations are always very rough. Note that in this calculation, we have neglected the presence of the coating on the component or subframe. This coating has a much lower Young modulus and is hard to take into the calculations. But even with this "back of the envelope calculation", we are able to conclude that the loss of clamp length of the bolts is the main cause of the drop in pretension force. The calculated loss in clamp length, needed to have the loss of measured pretension force, is always smaller than the actual measured loss of clamp length. It is important to note that the two short W500233 bolts, i.e. bolt 3 and 4 in Table 4 are very sensitive to thickness changes: 10µm loss of clamp length causes 10kN loss in pretension force.

Since the bolts did not rotate, we can exclude rotational loosening in this test. The reported failures of the last five years at Ford Lommel Proving Ground show however that this failure mechanism can happen in a later phase of the durability testing, i.e. Pascar 2, or occurs sooner with more powerful cars. So an investigation of the rotational loosening mechanism should be worth the effort.

4.3 Rotational loosening

The loosening mechanism described by Junker states that during each small movement in the contact between the bolt and the component, the bolt rotates in the loosening direction. This rotation can be very small, i.e. a thousandth of a degree. To find out what the magnitude of rotation is near the nominal torque, we set up an experiment. First we torque all the bolts at 10Nm below the nominal torque and mark the position of the bolt head. Secondly we torque the bolts until the nominal torque. The comparison between the two positions of the head is made in Figure 25.

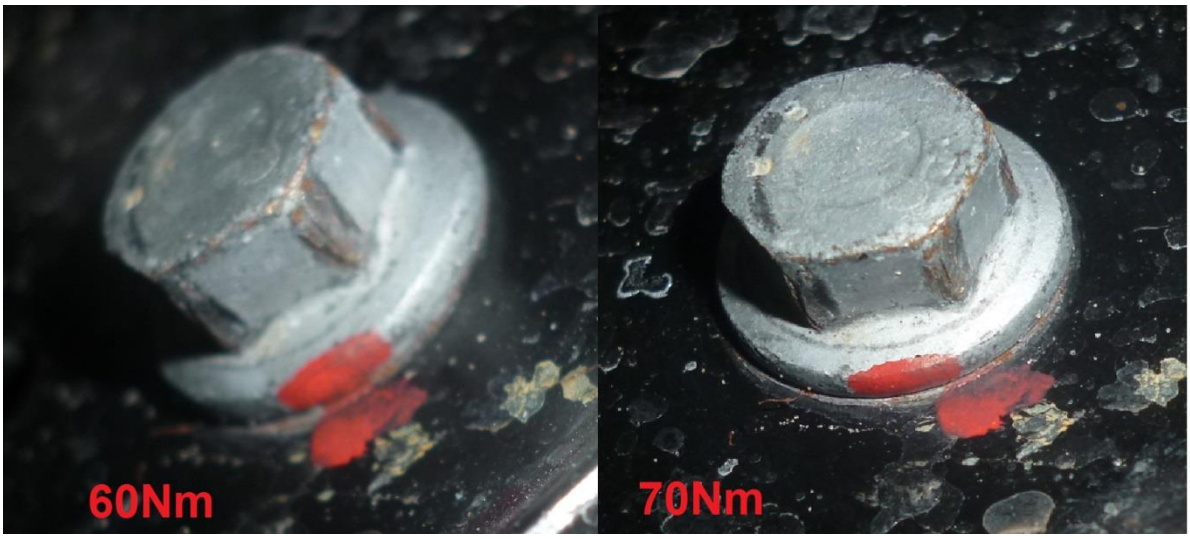

Figure 25: Angle of rotation between minimal and nominal torque

We can conclude that if the bolts loose 10Nm due to the mechanism described by Junker, we should be able to notice the loosening by looking at the paint mark. The durability engineers told me that in the past there have been bolted connections which have lost about 50% of the on-torque after durability test without rotating. The engineers at Ford Dunton Technical Centre have a Junker machine to compare different locking devices for fasteners. It is unfortunately not able to test the loosening effect of the roll restrictor bolts mounted in the component. Experience with this machine has shown that if the Junker loosening occurs, it is easy to spot the bolt rotating in the loosening direction.

With this knowledge we performed a test in which we first torque the bolts at the minimal allowable torque. Secondly we mark the position of the bolt. Because loosening increases with higher loads, we drive 100 times the traction control event. The traction control event is slightly heavier than the Chatterbumps event, but the event does not take so long to drive. Afterwards, we check the markings. If the bolt has not rotated, we decrease the torque of the bolts with 7Nm and start all over. This decrease of 7Nm was chosen in function of time available for this test. Before decreasing the torque, it might also be interesting to measure the on-torque of the bolts.

The tests will be performed with a Ford Fiesta 1.6 Sigma with an IB5 gearbox, the same used in all the previous tests.

The test results can be observed in the following table.

Table 5: Junker loosening test with marked bolts

Test	Torque applied on bolt (Nm)				Colour Marking	Test performed	result
Nr.	1	2	3	4			
1	49,2	42	42,2	42	red	100 x Traction control	no movement
2	43,1	34,7	35	35	gold	100 x Traction control	no movement
3	36,1	27,7	28	27,8	blue	100 x Traction control	no movement
4	30,2	20,9	21,9	21	green	100 x Traction control	no movement
5	23,6	15	15,4	14,9	yellow	100 x Traction control	no movement
6	15,2	7,6	8,2	8,6	red	11 x Traction control	rattle
	Nothing changed					14 x Traction control (25 times in total)	little movement
	Nothing changed					15 x Traction control (40 times in total)	large movement
	Measured on-torque					Test stopped	
	6,9	3,8	0	0			

In test nr. 6, we made pictures of movement and rotation of each bolt. These pictures can be found in Appendix Figure B 23 until Appendix Figure B 26.

We can conclude that the rotating described by Junker occurs within a range of 12% to 22% of the nominal torque. When this type of loosening occurs, the torque can drop very fast to zero. The measured on-torque after driving a hundred times the traction control event did not show a significant drop. Note that the 110mm long bolt, bolt 2, lost 3,8Nm of torque without rotating.

Because we performed this test in steps of torque losses, we are able to say that rotational loosening does not occur above 25% of the nominal torque (test number 5) when the loads on the roll restrictor are limited to 9kN. Note that a Fiesta ST can reach roll restrictor load above 13kN.

4.4 Measurement of the on-torque with a torque wrench

The residual torque of a bolt cannot be measured by the loosening torque because the friction force at the thread surface and between the head of the bolt and the component changes direction. This can simply be proven by the fact that the friction is always in the opposite direction of the movement. If one rotates the bolt in the other direction, the friction will also change direction.

This is why the technicians at Ford Lommel always measure the on-torque. The on-torque is the torque measured when the bolt starts to rotate in the fastening direction. To see how accurate this technique is, we performed the following experiment.

One person torques an M10 bolt in a nut with a washer in between till a torque between 30 and 60 Nm. A second person measures the on-torque without the knowledge of the original torque. This is repeated 15 times and the average error and standard deviation is calculated. The results of these tests are shown in the table below. [15]

Table 6: Test results with the torque wrench

Person	Experience	Average error (Nm)	Standard deviation (Nm)
Trainee	None	3,38	3,03
Myself	Hobby	2,53	1,71
Technician	Professional	-0,22	1,35

These results show that the error made by a professional person is very low, which proves that the on-torque measurements are very accurate.

Note that we should add the error made by the torque wrench. The torque wrenches used at Ford Lommel, ½ inch or 3/8 inch from Snap-On, are very accurate: if the bolt is torqued below 10° per second, the error for both torque wrenches is lower than 4% of the readout. Since we torque by hand, this is always the case.

We also measured the real time clamp load with the use of strain gauges described earlier in this thesis, while measuring the on-torque with a torque wrench. The average increase of the clamp load due to measuring the on-torque was 2.9kN. The table above indicates that a technician should do a lot better than me.

But there are problems that can occur sporadically and that should be treated differently. An example is shown in the next table.

Table 7: Torque change in limited number of driven events, during the same Pascar 1 test

	Bolt 1	Bolt 2	Bolt 3	Bolt 4
Initial torque (Nm)	70,8	62,1	62,8	62
On-torque after 100 Chatterbumps (Nm)	65,5	60,4	59,5	58,2
Difference (Nm)	-5,3	-1,7	-3,3	-3,8
Initial torque (Nm)	70,1	62	61,8	62
On-torque after 100 cobblestones (Nm)	73,1	65,2	65,2	78,3
Difference (Nm)	3	3,2	3,4	16,3

When looking at the results of the measured on-torque after 100 Cobblestones slaloms, one might infer that the bolt is tighter than before. This is not likely because bolt 4 has quality 8.8 which means that at 78Nm the stress in the bolt is near the tensile strength and already far above the yield strength. The occurring effect is the so called ‘stick-on-torque’: the friction between the head and the component has increased due to the anti-corrosion coating on the component. When rotating the bolt with a torque wrench in clockwise direction, the bolt resists highly against movement until the moment it snaps loose. At that moment the bolt

gives way, a short rotational movement causes a shock onto the torque wrench. The digital torque wrenches used at Ford Lommel show this high torque on the display. When we immediately measure the on-torque again, we measure a torque much lower than the one in the previous measurement, but still higher than the original on-torque, as we increased the torque. The occurrence of the stick-on effect is stochastic: it can occur at any bolt after short or long tests. The detection of the effect depends on the operator: one should notice the shock when the bolt snaps loose.

The stick-on effect can also occur after a heavy durability test such as Pascar 1. The following table contains such results.

Table 8: On-torque before and after the same Pascar 1 test

Torque (Nm)			
Bolt 1	Bolt 2	Bolt 3	Bolt 4
initial			
69,8	62,3	61,7	60,5
after test			
52,5	59,9	68,1	66,2
difference			
-17,3	-2,4	6,4	5,7

These measurements were performed by a trained technician. The stick-on effect was observed at bolt 3 and 4. This test was performed together with the ultrasonic sensors placed on these bolts. Knowing that the pretension force has dropped 10kN for bolt 3 and even 12kN for bolt 4, we can conclude that the results from the on-torque measurements are not correct. To evaluate the accuracy of the torque measured on bolt 1 and 2, we will look at the relation between the pretension force and the torque.

Table 9: Change of the relation between pretension force and torque during the same Pascar 1 test

	Pretension force/Torque (kN/Nm)			
	Bolt 1	Bolt 2	Bolt 3	Bolt 4
Initial	0,7608883	0,6672552	0,7747164	0,799669
After test	0,8459048	0,6111853	0,5524229	0,556344
Change (%)	11,173324	-8,403068	-28,69353	-30,4282

If the stick-on effect does not occur, the coefficient that relates the pretension force to the torque can differ up to ±10%. If the stick-on effect occurs, one should take into account that the torque of the bolt with the original pretension force/torque coefficient is 30% less. For example, if one measures 100Nm on-torque after a long test and the stick-on effect occurred, the torque that produces the same pretension force in the original conditions is only 70Nm. So I propose a revision the Ford requirement stating that we allow a 50% torque drop after Pascar 1 and 2. If we relate this requirement to the pretension force that actually guaranties the

connection, we should allow a torque drop of only 71.4% (=50%/0.7) if the stick-on effect occurs.

4.5 Conclusions

The long term measurements show that the loss of pretension force is due to non-rotational loosening or also called embedding effect. When the embedding continues to 25% of the nominal torque and loads on the roll restrictor are limited to 9kN, rotational loosening will occur and complete loosening of the bolts will follow very quickly.

The torque wrench and the technique of measuring the on-torque is very efficient, but care must be taken when the stick-on effect occurs. In the case of this stick-on effect, I would advise to use an adapted requirement of the allowable torque drop.

In the next chapter, we will relate the real time loads to the embedding effect and try to establish an estimation rule to predict the embedding effect.

Chapter 5: Estimation of the embedding effect

We know that the relative displacement between the roll restrictor and the gearbox causes the embedding effect. From the real time measurements, we can conclude that the relative movement only occurs above a certain force, depending on the pretension force. The ultrasonic measurements show us the evolution of the pretension force. Together with the real time results, we should be able to determine the relation between the number of movements and the corresponding loss of pretension. In this chapter, we will try to make the link between the real time results and the results obtained with the long term measurements.

5.1 Test conditions and assumptions

First we need to point out that only the evolution of the pretension force of the front W500233 bolt will be observed, since we were only able to measure the relative displacement of this bolt.

The first assumption deals with the relation between the evolution of the pretension force and the number of cycles. In the past, lab tests [17] on loss of pretension of bolted connections have shown that there is a linear relationship between the number of cyclic loading of the joint and the percentage of the remaining pretension force, when both quantities are plotted in a log-log graph. The relationship can be expressed by the following formula:

$$\log_{10} \frac{actual\ pretension\ force}{initial\ pretension\ force} = A + B \log_{10} number\ of\ cycles \qquad (10)$$

in which A and B are two constants that need to be determined experimentally. The definition of the number of cycles is heuristic: it can be the number of driven kilometres, number of load cycles, hours of operation… In our case, we can take the number of durability cycles. It is also possible to estimate how many times we have a relative displacement between the gearbox and the roll restrictor. However, this will only lead to different constants, but it makes the results more comparable with other powertrains.

In the previous two chapters we explained that the movement of the joint causes non-rotational loosening and finally rotational loosening. But this movement is characterised by various parameters of which we do not know the influence. The speed of the movement, the amplitude (hysteresis) of the movement, temperature, the amount of paint remaining on the contact surface, the remaining pretension force, dimensions of the bolts and the hole… The exact influence of these parameters cannot be tested on a car at the test track, because these parameters cannot be controlled. This should be examined under controlled circumstances in a laboratory. This complex tribology problem related to this movement is out of the scope of this master thesis. We will define a load cycle as the exceedance of the roll restrictor force at which the hysteresis might occur. The speed at which the load is applied and the amplitude of

the movement will be neglected. We will also assume that the pretension force does not change. One should expect that the roll restrictor force needed to have a displacement depends on the pretension force of the bolts. Due to the above assumption, we will not take this effect into account.

In the last assumption, we will state that the type of powertrain has no direct influence on the loosening effect. We have performed measurements with a Ford Fiesta 1.6 Sigma engine with 120hp and 155Nm engine torque. We will assume that a 1.6 GTDI engine used in the ST version of the same car has no other influence apart from the higher roll restrictor loads. So we assume that the eigenmodes, weight and inertia of the engine, damping characteristics and similar parameters do not influence the loosening effect. The only difference between both powertrains will be the number of movements during a durability cycle.

These assumptions will enable us to evaluate the roll restrictor bolts on all Ford Fiesta powertrains. Before using these results, one should verify if all assumptions are valid or not. The aim of the following estimations is to have an idea of the order of magnitude of the number of movements during a Pascar 1 durability test and the possible effect on the pretension force.

5.2 Estimation method

When we plot the long term results of bolt 3 achieved in the previous chapter, we obtain the following graph.

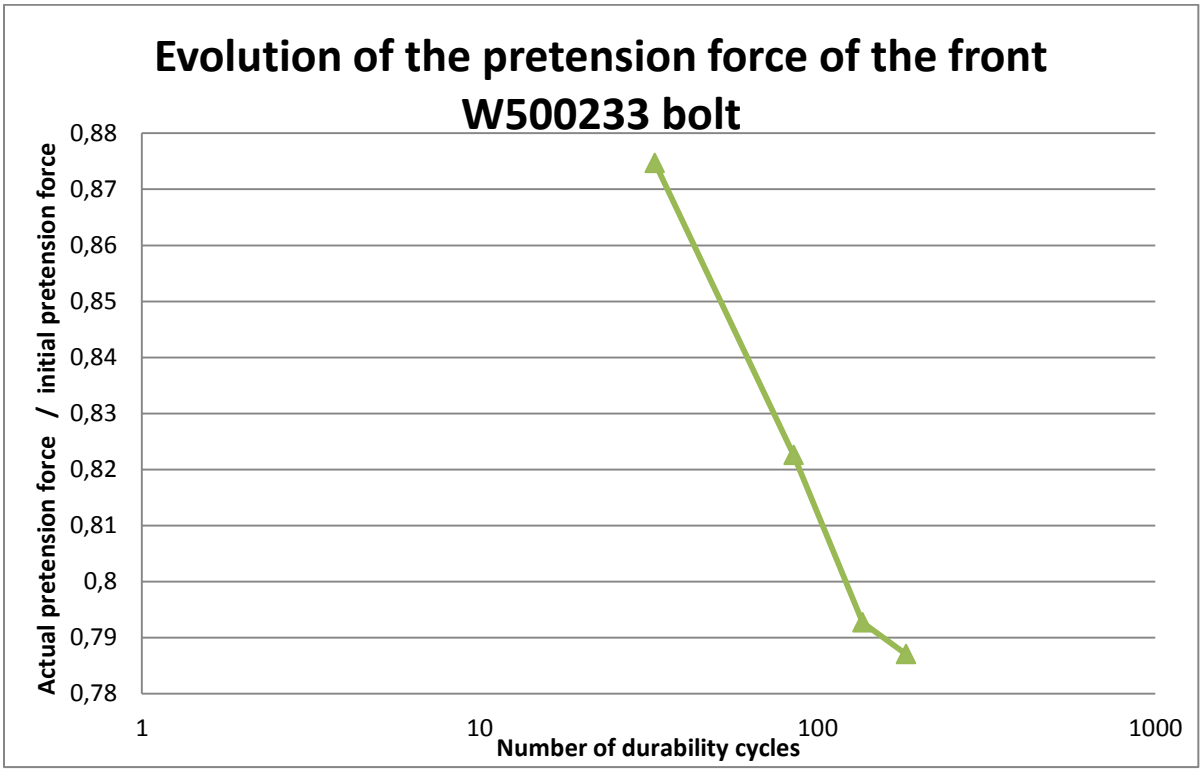

Figure 26: Log-log graph of the evolution of the front W500233 bolt in a Pascar 1 test

When we identify the A and B constants of the logarithmic expression, using the least squares method, we find the relation underneath.

$$\log_{10} \frac{actual\ pretension\ force}{initial\ pretension\ force} = 0.0029 - 0.0462 \,.\log_{10} \#\ durability\ cycles \qquad (11)$$

with residual $R^2 = 0.9828$

This equation however provides an estimation method only for a Ford Fiesta with a 1.6 Sigma 120hp engine. It would be more interesting to adapt the number of durability cycles to the number of movements during a complete Pascar 1 durability test.

The number of movements during a single Pascar 1 cycle is estimated by the following heuristic method. We multiply the events that cause forces exceeding the level at which movement occurs by the number of times we drive these events in a Pascar 1 cycle. We have measured all the Pascar 1 events several times in chapter 3. When we look back to Appendix Figure B 17, we see that the Cobblestones slalom and the Chatterbumps event cause roll restrictor forces above 4kN. For some events, such as the Chatterbumps event, this level is exceeded only a few times. In the case of the 1.6 Sigma engine, only 5 out of 10 passages

exceeded the 4kN force limit at which movement was spotted. We will multiply the above by 5/10.

When we calculate this sum for the Ford Fiesta 1.6 Sigma engine, we find 293 times a movement of the joint on the gearbox. This results in the following logarithmic equation:

$$\log_{10} \frac{actual\ pretension\ force}{initial\ pretension\ force} = 0.0032 - 0.0420 \,.\log_{10} \#\ movements \qquad (12)$$

with residual $R^2 = 0.9753$

Respecting all assumptions, we should be able to calculate the same number of load cycles for a Ford Fiesta with a 1.6 GTDI ST engine. There is however an important remark to make. The Chatterbumps braking is about the same for a 1.6 Sigma and a 1.6 GTDI engine, but the Chatterbumps acceleration causes a much higher force on the roll restrictor for the 1.6 GTDI. When we look back at the real time roll restrictor force during the Chatterbumps braking, we mostly spot one single peak above 4kN. But when we look at the Chatterbumps acceleration in wet conditions with a Ford Fiesta 1.6 GTDI ST, we notice multiple peaks.

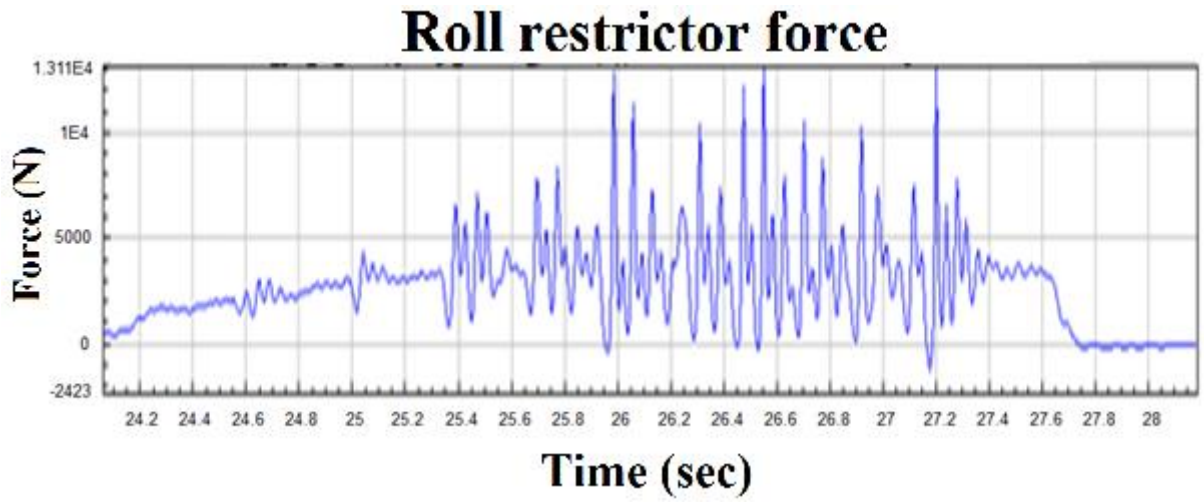

Figure 27: Roll restrictor force during Chatterbumps acceleration with a Ford Fiesta ST in wet conditions

It is very hard to decide how many load cycles to count for this type of loading. The problem is that we do not know what happens when we measure a minimal force in between two peaks above 4kN. Will this cause only a single movement or multiple movements? A much more difficult problem is to estimate how many times this type of loading occurs. This is very weather dependant, as seen in the DOE results.

However, before investigating on these problems, it is interesting to make the calculation the other way around: how many movements do we need during a durability cycle to have a reduction of the pretension force of 50%? By simply inversing equation 12, we find that we need 93199 movements each durability cycle to have a reduction of 50% of the pretension force. Even for a Ford Fiesta ST 1.6 GTDI, this number of movements is not plausible.

The assumptions made at the beginning of this chapter are not valid for this kind of estimations. Out of my experience, I believe that there are two assumptions that are probably

not valid: we cannot assume the pretension force to be constant and the duration and amplitude of the displacement will have an influence on the loss of pretension force.

The ultrasonic measurements have proven the declining evolution of the pretension force. It seems logic that a bolted connection with less pretension force is easier to move, i.e. a displacement between the roll restrictor and the gearbox at a lower roll restrictor force.

Since the relative displacement between the roll restrictor and the gearbox causes non-rotational loosening, it seems logic that a movement of 20 micrometre will reduce less the pretension force than a movement of 200 micrometre. But also the speed of the displacement will have an influence on the embedding effect. Think of cutting or grinding machinery: each manipulation (drilling, reaming, grinding…) has an optimal speed. It seems logic that the embedding of a bolt head into the coating of the material will also be more pronounced at certain speeds. This kind of tribology problem cannot be studied on a test vehicle at the test track but should be performed in a detailed laboratory study where we can control each influential parameter.

5.3 Conclusion

The assumptions made in the beginning of this chapter are not valid. To make a proper estimation of the evolution of the pretension force during durability tests, there are two options.

The first option is to measure the evolution of the pretension force during a few days of the durability test and determine the two logarithmic constants. With the obtained logarithmic expression, one can then estimate the future evolution of the pretension force. [17] This type of testing requires however the use of an ultrasonic load probe and calibrated machined bolts with ultrasonic sensors. At Ford Lommel Proving Ground, we do not have such an ultrasonic load probe and neither do we have the equipment to calibrate or machine such bolts.

The second option is to perform a detailed investigation on the tribology of the bolts. These tests need to be performed in a laboratory under controlled circumstances, not at the test track.

With the currently obtained information, we are not able to predict the loosening effect of the roll restrictor bolts of different engines.

Chapter 6: Possible solutions

In this chapter, we will try to find possible solutions that reduce the embedding effect. Since we know that embedding, and in a later stage rotational loosening, are both caused by the relative movement between the roll restrictor and the gearbox or subframe. We will measure this displacement together with the axial force acting on the roll restrictor and drive the Chatterbumps event with not immediately clutching before the Chatterbumps braking. Tests in the past have shown that this will increase the roll restrictor forces with a factor 2. The aim of the higher forces is to find the level at which the hysteresis, or the non-linearity between the displacement and the force, occurs.

We will first measure the displacement and force with the bolts torqued at nominal torque. These results will act as a reference for the other measurements. Secondly, we will measure the effect of possible solutions: a torque increase, three types of washers, medium strength threadlocker (Loctite 243) and finally the effect of removing the paint on the roll restrictor bracket.

6.1 Reference measurement

Since the test car available for these measurements is a Ford Fiesta with a 100hp 170Nm 1.0 GTDI engine, we cannot simply take the measurements in chapter 3 as a reference. The standard event procedure, Chatterbumps braking, is slightly adapted: we vary the clutching time during the braking. If one presses the clutch before starting to brake on the Chatterbumps, the forces on the roll restrictor will be limited to approximately 6kN. This is the normal Chatterbumps braking according to the prescribed procedure by Ford. When we press the clutch whilst braking, or even just before stand still, the full inertia of the engine is exposed to the fast varying wheel velocity which results in much higher loads on the roll restrictor.

The car was loaded according to the DTL load scheme and all tests were performed on a dry track.

In the following graph, we can spot a hysteresis above loads of approximately 4kN, which corresponds very well to the test results seen in chapter 3.

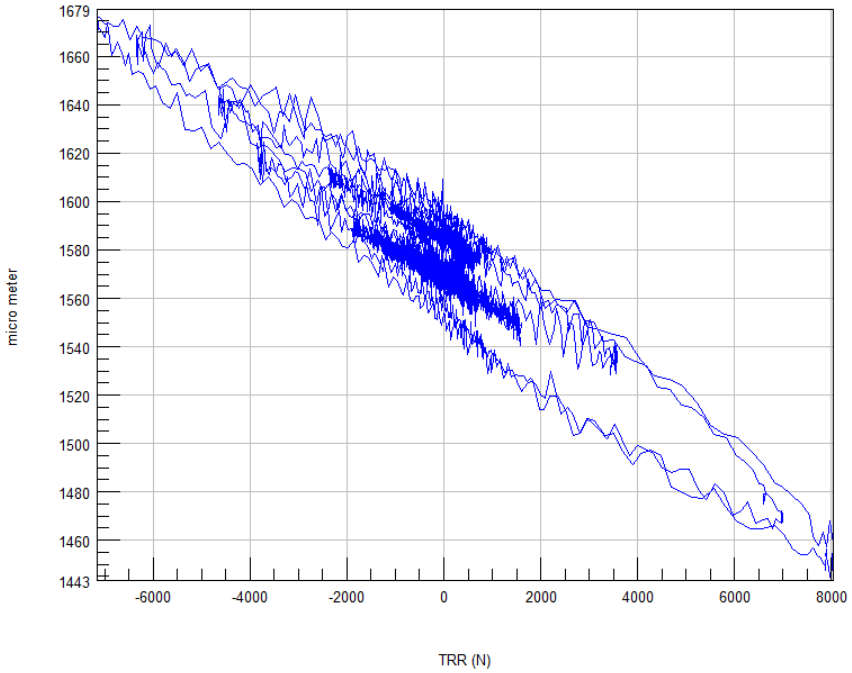

Figure 28: Displacement versus the roll restrictor force with the bolts at nominal torque

When the loads are increased, the situation becomes dramatically.

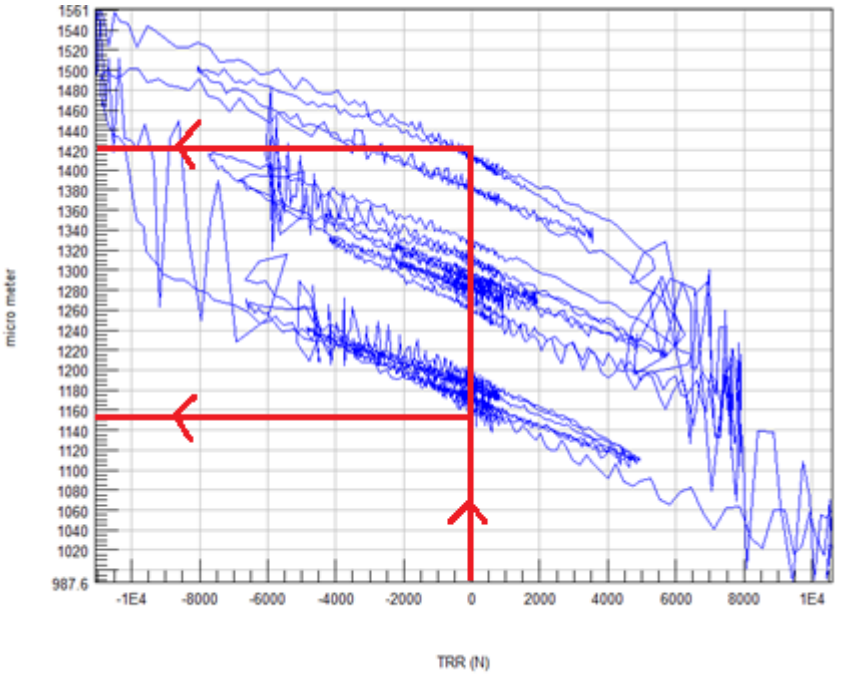

Figure 29: Displacement versus the roll restrictor force with the bolts at nominal torque, high loads

Note that the maximum force of 11.120kN (absolute value) is really exotic for this car with only 170Nm of engine torque and an output of 100hp. When we look back to the measurements of the roll restrictor forces on a Ford Fiesta ST in wet conditions, 13.7kN (measured for the DOE analysis in Chapter 3.2) can be achieved when the event is driven according to the correct test procedure.

6.2 Torque increase of the bolts

A first possible solution is to increase the torque of the bolts. We torqued the bolts of the roll restrictor to the maximum allowable torque. This does not require any new hardware, but you always need to take an uncertainty of the torque measurement into account. When we implement a torque increase in mass production, the maximum and minimum torque also increases. This new maximum torque may then be out of the specifications of the gearbox, subframe or bolts. Nevertheless, it might be interesting to evaluate the effect of this change.

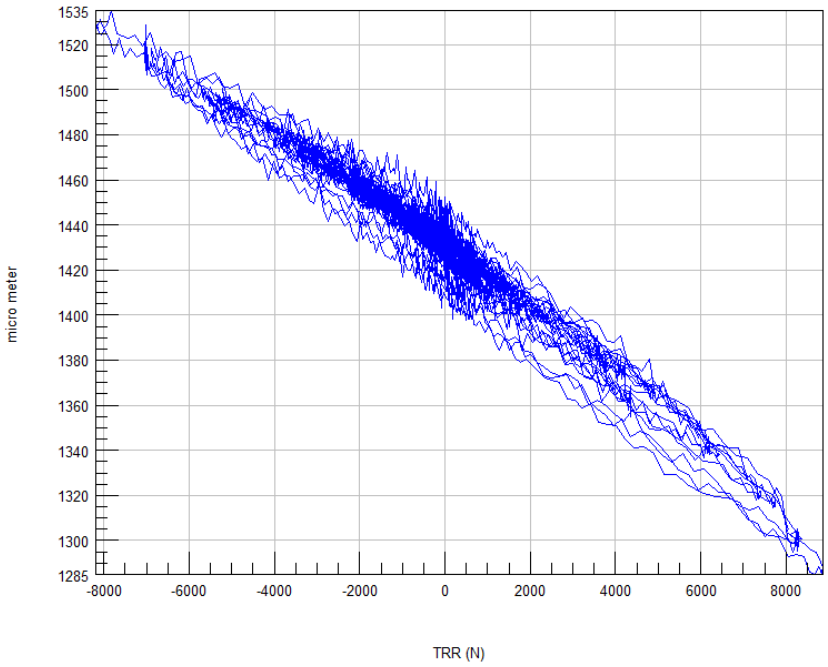

Figure 30: Displacement versus the roll restrictor force with the bolts at maximum torque

Figure 30 shows almost no signs of movement between the roll restrictor bracket and the gearbox, even though the forces reach over 8kN. This torque increase would thus reduce the embedding effect in a high degree for powertrains such as the 1.6 Sigma engine or the 1.0 GTDI Fox engine. The rigid joint would nearly always be guaranteed. When we increase the forces on the roll restrictor, the hysteresis appears again. This can be observed in Figure 31.

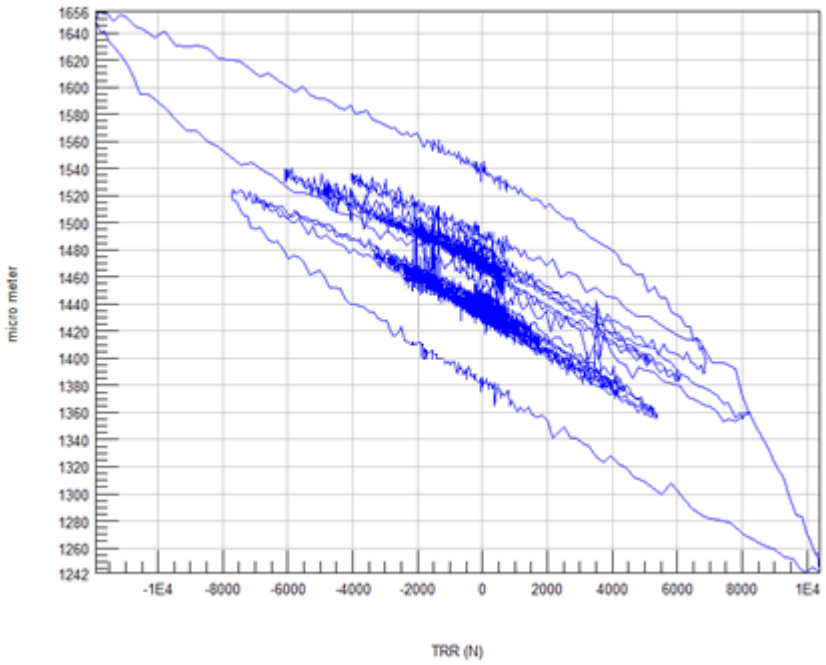

Figure 31: Displacement versus the roll restrictor force with the bolts at maximum torque, high loads

When the loads exceed 8kN, we can spot again the hysteresis. However, at this higher torque we have only 160µm hysteresis instead of 280µm at nominal torque. This is a reduction of 43%, but it is not straight forward to predict the influence on the embedding effect or the loss of pretension force. If it is technically possible to increase the torque without new design of the gearbox or subframe, this torque increase could reduce the embedding effect and might be interesting to try out on a Ford Fiesta ST in a complete durability test. If it is not possible to increase the torque of the bolts (the female thread is tapped into the Aluminium gearbox casing), these results might be interesting for future design of the roll restrictor, gearbox or subframe.

6.3 Washers

The second proposed solution consists of a washer between the head of the bolt and the clamped component. We will try out three types of washers.

Figure 32: From left to right: spring washer DIN 128, wave washer DIN 137A, M10 flat washer DIN 1440

The first washer we will use is a normal flat washer M10 DIN 1440. Secondly, we will try out a wave washer M10 DIN 137A and finally a spring washer DIN 128.

6.3.1 Flat washer

A flat washer has the advantage of a more even spreading of the pretension force on the component. The effect of this property on the hysteresis can be observed in Figure 33.

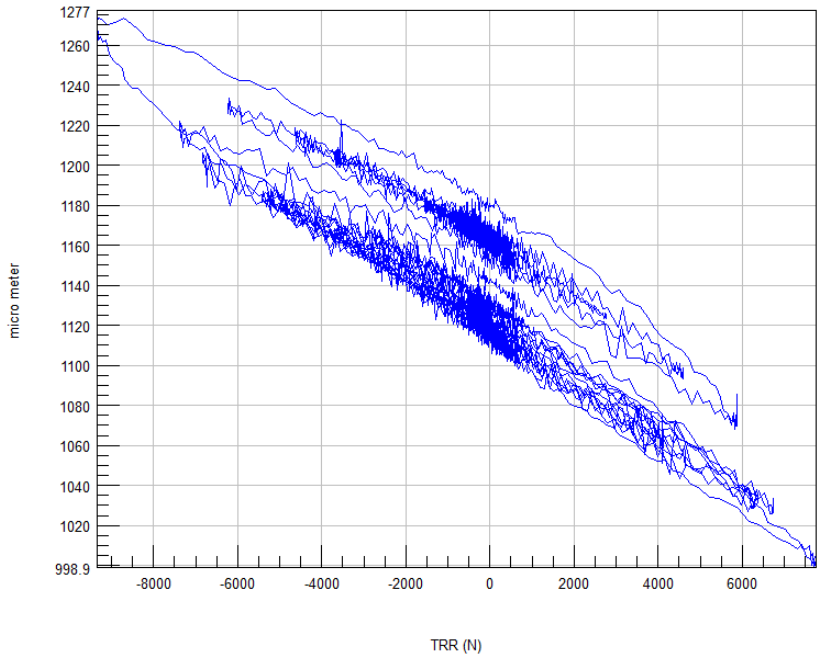

Figure 33: Hysteresis with a flat washer

The hysteresis is very limited for forces below 7kN compared to the reference measurement. At 9.380kN however, one can spot a permanent movement of the component relative to the gearbox. So we can conclude that this washer will reduce the embedding effect, but not as good as a torque increase. For the Ford Fiesta ST, this type of washer will diminish the embedding problem, however without providing us with a durable solution.

6.3.2 Wave washer

A wave washer will give us the spreading of the pretension force on the component and due to the bended construction of the washer, it will also act as a spring between the component and the head of the bolt.

Note that the wave washer is only 1mm thick, whereas the other two tested washers are 2.5mm (DIN1440) and 2.85mm (DIN128) thick. So the spreading of the forces of a wave washer will not be as efficient as the other two types.

The effect on the hysteresis of this type of washer is shown below.

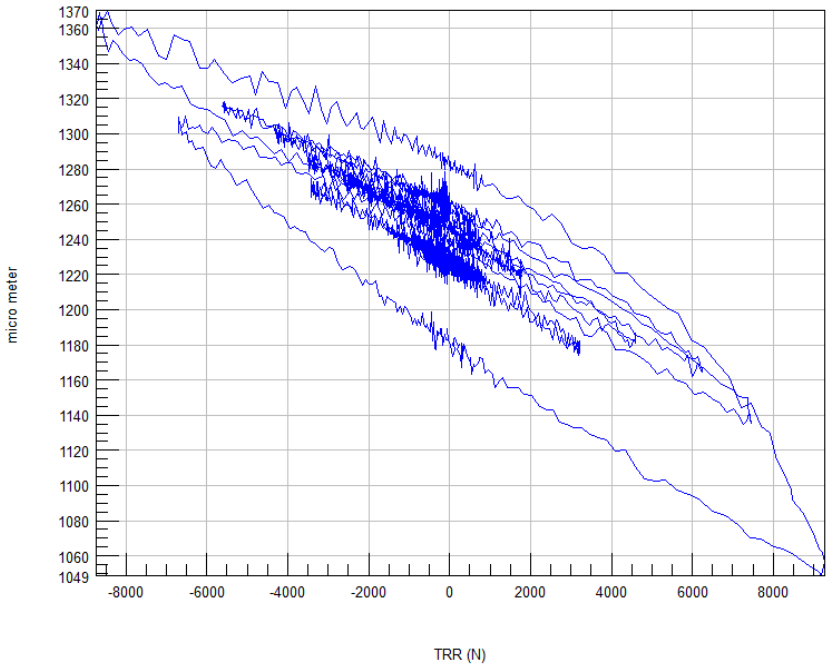

Figure 34: Hysteresis with a wave washer

The results of this washer are very poor. Even at low loads of about 5kN, the component can move. When we compare this result to the first reference measurement, it is hard to say that this wave washer makes any difference.

6.3.3 Spring washer

A spring washer combines the spreading of the pretension force and the effect of a spring between the clamped component and the bolt head, with the property of preventing the bolt to rotate in the loosening direction. This may influence the loosening effect described by Junker. How this washer affects the non-rotational loosening effect is clarified with Figure 35.

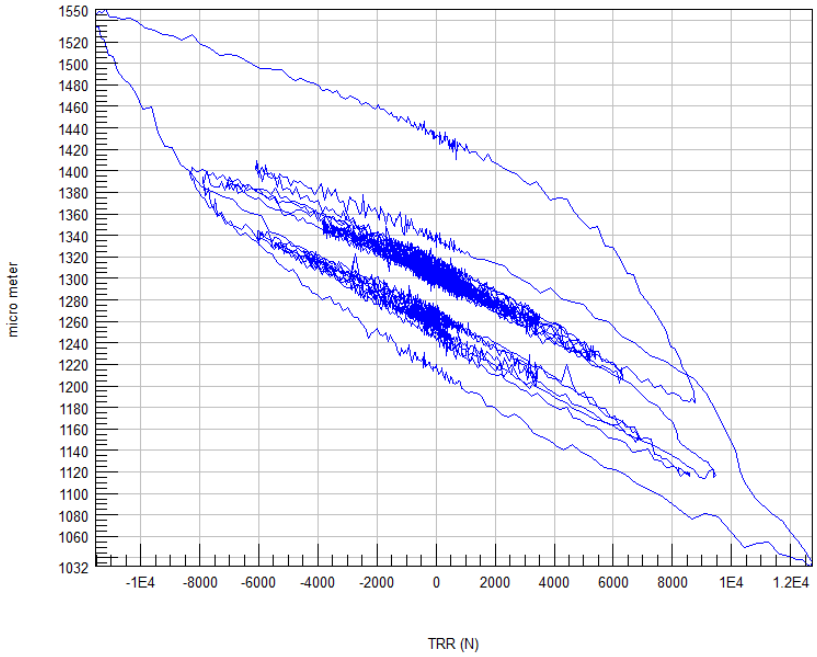

Figure 35: Hysteresis with a spring washer

The repeatability of the Chatterbumps event is mostly very poor, which makes it hard to reproduce the same loads on the roll restrictor, to render these tests comparable. To compare this graph with all the previous measurements, one should only look at the hysteresis without the large displacement that occurs at 12kN. We then see that the hysteresis only occurs above 8kN. Which means that the spring washer is slightly better than the flat washer. When we look at the graph for loads below 8kN, the hysteresis of 30µm is very similar to the hysteresis in the first measurement of the torque increase.

When we observe the hysteresis that occurs as a result of the 12.613kN load, we see that the hysteresis is 220µm. Comparing this result with the 160µm movement, measured when the torque was increased, we can conclude that the spring washer has a slightly inferior effect to a torque increase. It is thus not a solution for the Ford Fiesta ST.

6.4 Medium strength threadlocker

Threadlocker is a special type of anaerobe glue which will increase the friction on the thread surface after the bolt is torqued to the final torque. This will prevent rotational loosening, but should have no effect on the movement between the roll restrictor and the gearbox. We were not able to use the same type of threadlocker used on bolts for mass production. This type of threadlocker is glued in a more solid state on the bolts before they are assembled. We used a liquid threadlocker with medium strength: Loctite 243. One could also use Loctite 270 high strength threadlocker, but this could cause problems when loosening the bolts. The effect of the threadlocker is examined in Figure 36.

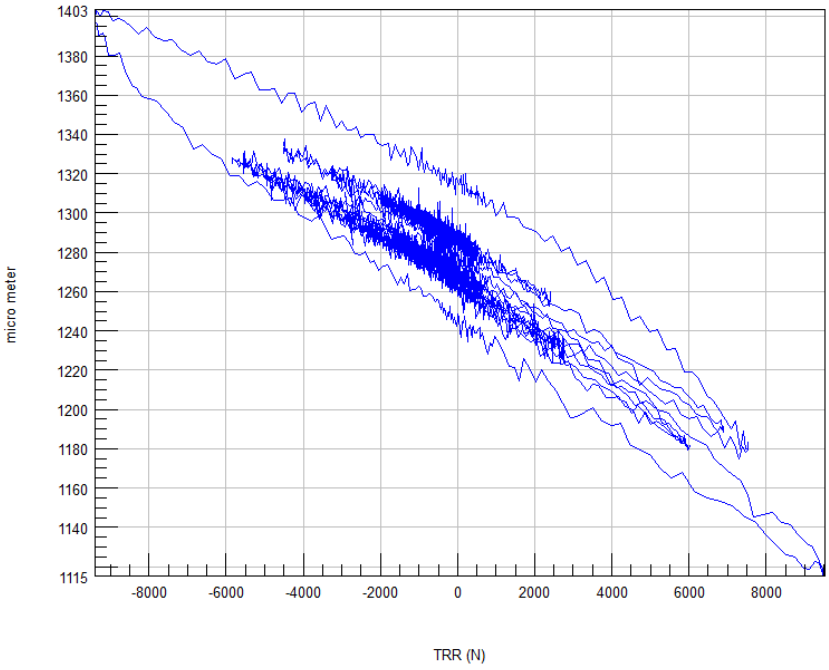

Figure 36: Hysteresis with a threadlocker

We can spot a hysteresis at only 4kN, which is exactly the same as the reference results. Threadlocker against the movement between the roll restrictor and the gearbox, which causes non-rotational loosening, is without effect.

6.5 Removing the paint

When we performed tests on the long term, it was possible to see with the naked eye that the paint of the subframe and the roll restrictor bracket was severely damaged on the contact surface of the bolt head. So when we remove all the paint on this contact surface, there is no more possible loss of clamp length, and thus pretension force, due to the paint getting away from the contact zone.

It should be interesting to know the influence of the paint of the roll restrictor bracket on the movement of the component. In this final experiment, We removed all the paint on the front and back side of the roll restrictor bracket near the holes. We used a pneumatic steel wire brush to do so. Also the surface round the female thread on the gearbox was brushed.

Figure 37 shows the surface finish of the roll restrictor bracket.

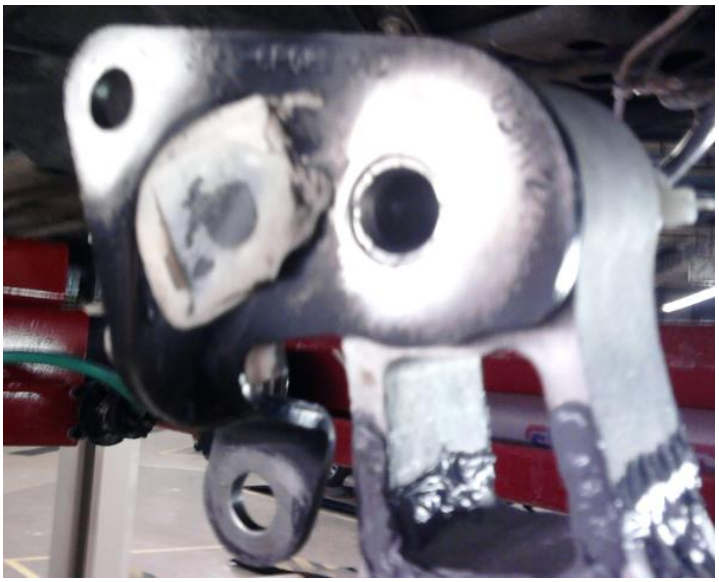

Figure 37: Wire brushed roll restrictor bracket

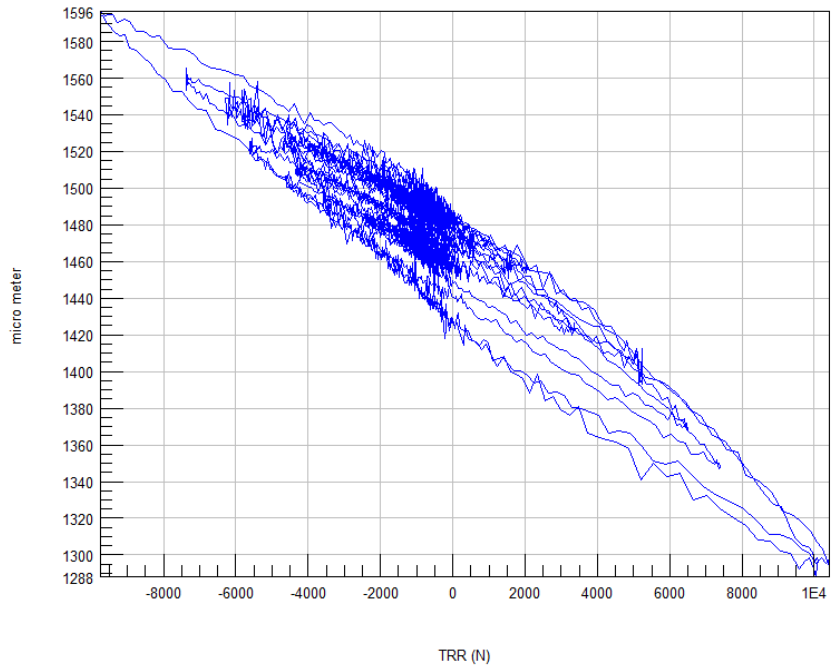

Figure 38: Hysteresis with no paint on the roll restrictor bracket

We are still able to spot a hysteresis of 70µm when 10.490kN loads are applied. If we compare this to the 280µm hysteresis at 11kN measured in our reference, we can conclude that removing the paint is by far the most efficient way to reduce the relative movement of the roll restrictor on the gearbox. This has a great potential to be the best solution for all Ford Fiesta powertrains, even for the 180hp 240Nm ST version, since the roll restrictor force of this car almost never exceeds this value during a durability test (see measurements Chapter 3.2).

The drawback of this solution is the corrosion problem. We should be able to paint the full roll restrictor bracket, except the contact surface with the bolt head and the gearbox. This can be achieved by placing plastic rings in the holes that cover the contact area before painting the

component. However, these plastic ring should only be removed just before assembly to avoid corrosion appearing during the transport of the component.

Another solution is to remove the coating at the contact surface with a self-centering grinder or a surface cutter or reamer. A picture of a surface reamer can be found in Appendix Figure B 27. When one develops a special tool with three surface reamers positioned in front of the holes in the roll restrictor bracket. The component can be brought into contact with those three surface reamers in one movement, like some kind of bench drill. A concept drawing of such machine is shown in Appendix Figure B 28**Fout! Verwijzingsbron niet gevonden.**. This would not result in corrosion problems, since the coating is removed just before assembly, but it adds a cycle time in the order of 10 seconds per engine mount. However, when there is no more coating left on the contact surface, the three step torqueing procedure is no longer necessary, so the time gain there could compensate the time loss by removing the coating. This process can be performed at the assembly line itself or in preassembly.

6.6 Conclusions

The results of all tested possible solutions are resumed in the following table.

Table 10: Overview results

Possible solution tested	Movement above	Hysteresis
Reference	4kN	280µm at 11kN load
Torqued at maximum torque	8kN	160µm at 11kN load
Flat washer	7kN	
Wave washer	No effect compared to reference	
Spring washer	8kN	220µm at 12kN load
Threadlocker (Loctite 243)	No effect compared to reference	
Removing the paint	Almost no movement	70µm at 10,5kN load

The most remarkable result comes from the test in which we removed the paint of the roll restrictor bracket. The bracket will hardly move, even at loads of 10kN. The embedding effect will not take place, neither the rotational loosening effect. Care must be taken to prevent the component against corrosion.

It might be interesting to try out the use of different anti-corrosion paintings. E-coating is a standard protection for automotive components, but it creates a large scatter on the force/torque relation. These two negative contributions might be reduced when another type of coating is applied. When one looks for a different coating, a harder and/or thinner coating should be preferred. Most of these thinner and harder coatings, such as electroplating, are more expensive than the used E-coating.

Conclusions

The loosening of the roll restrictor bolts of Ford passenger cars is a combination of rotational and non-rotational loosening. Both failure mechanisms are triggered by a small displacement between the roll restrictor and the gearbox.

The non-rotational movement can be measured with ultrasonic sensors and a load probe. The evolution of the clamp load is linear with the number of durability cycles when it is plotted in a log-log graph. This can be used to predict the occurrence of a failure, but the obtained results are only valid for one engine type.

Rotational movement happens in a later stage of the failure. When the bolts have lost 25% of their initial torque, the bolts start to rotate when high loads are applied on the component. The rotational loosening leads to a very fast failure of the connection.

A design of experiments analysis showed that the loads on the transmission roll restrictor are mainly dominated by weather and engine torque. One can use the found transfer function to make a first order approximation of the roll restrictor forces for engines with a torque between 155 and 240Nm. The design of experiments analysis also showed that the test mass installed in the car (DTL or MDL) does not have a significant influence on the roll restrictor forces.

Care must be taken when the on-torque of a bolt is measured. When one notices the occurrence of the stick-on effect during a measurement, a possible overestimation of 30% should be taken into account. It is thus advisable to extend the Ford system requirement that allows a torque reduction of 50% of the minimal torque after a full durability test: when technicians measure the on-torque after a full durability test and the stick-on effect is observed, the remaining torque should be 71.4% (=50%/0.7) to guaranty with certainty the same remaining pretension force.

A solution for the loosening problem should eliminate the movement between the component and the gearbox. This movement can be measured with a capacitive displacement sensor and strain gauges on the roll restrictor. The relative displacement between the roll restrictor and the gearbox can be observed by hysteresis when we plot the displacement as a function of the roll restrictor force. We have used the capacitive sensor and the strain gauges on the roll restrictor to compare the performance of a few possible solutions.

A spring washer or a torque increase reduce the embedding effect. Other washers or the use of threadlocker do not result in a significant difference. A removal of the e-coating on the contact surface however, eliminates almost every possible movement between the component and the gearbox. This can be implemented in mass production by placing a special tool in a subassembly line. This subassembly costs extra time, but this might be recovered by using a single torqueing procedure instead of the three step torqueing procedure.

One can choose not to coat the contact surface in the first place. But during transport of the component, this surface should be protected in another way against corrosion.

For future testing at Ford Lommel Proving Ground, it might be interesting to test with the same procedure how different kinds of coatings on the component influence the relative motion. One should search for an anti-corrosion coating that provides enough protection and can be as thin and hard as possible. Some coatings might resist better against the embedding effect as others. It might be interesting to investigate the influence of coating related parameters: thickness, hardness… A design of experiments analysis could help us choosing the right protective coating.

From a theoretical point of view, a laboratory study of the tribology between the bolt head and clamped component could give us more information about the influence of the speed and magnitude of the relative displacement on the embedding effect. When one also investigates the influence of the declining pretension force on the roll restrictor force at which a relative displacement is possible, a more accurate modelling of the embedding effect of different engines should be possible. From a practical point of view however, the model obtained will always be a rough estimation. Tribology problems are very complex and depend very much on parameters we can never fully control during production: since most Ford passenger cars are produced in different countries, there are different suppliers that produce parts that are not equal in terms of tribology aspects. From my experience in car production, a change to another supplier of coatings, materials or bolts happens very often. All these influences will result in a bigger uncertainty on the result of the obtained model.

Bibliography

[1] E. Scharlee, Body and chassis durability, slide presentation, vehicle attribute program product development Europe, 22 April 2008.

[2] H. Wittel, D. Muhs, D. Jannasch en J. Vossiek, Roloff/Matek Machinenelemente, vol. 19, Vieweg + Teubner, 2009, pp. 217-264.

[3] ASM International Handbook Committee, Fatigue and Fracture, vol. 19, S. R. Lampman, Red., The materials information society, 1996, pp. 287-288.

[4] S. Nassar, B. S. Munn en X. Yang, „Effect of threaded fastener condition on low cycle fatigue failure in metric bolt under transverse loadings," *SAE Technical Paper,* nr. 2008-01-0700, pp. 1-9, January 2008.

[5] S. Toshiyuki, H. Yamanaka, M. Ishimura en Y. Shoji, „Experimental evaluation of screw thread loosening in bolted joints with some parts and analytical approach of loosening mechanism of the joints under repeated transverse loadings," *SAE Technical Paper,* nr. 2006-01-0988, pp. 1-13, April 2006.

[6] S. Hashimura, „Influences of various factors of bolt tightening on loosening-fatigue failure under transvers vibration," *SAE Technical Paper,* nr. 2007-01-0807, pp. 1-11, April 2007.

[7] S. Hashimura en Y. Kurakaka, „A study to predict fatigue limits of bolted joints under transverse vibration," *SAE Technical Paper,* nr. 2010-01-0964, pp. 1-12, December 2010.

[8] G. H. Junker, „New criteria for self-loosening of fasteners under vibration," *SAE Technical Paper,* nr. 690055, pp. 1-24, January 1969.

[9] R. Friede en J. Lange, „Loss of preload in bolted connections due to embedding and self loosening," *SDSS' Rio 2010 Stability and ductility of steel structures,* pp. 1-8, September 2010.

[10] P. Bouche, Seminar Strain Gauges, Faculty Club Leuven, 2011, pp. 1-32.

[11] D. K. Lambert, "Capacitive proximity sensor," 20 04 2004. [Online]. Available: http://www.freepatentsonline.com/6724324.html. [Accessed 28 02 2013].

[12] A. McDougall, "PI in Control," 2010. [Online]. Available: http://pc-control.co.uk/Capacitive.htm. [Accessed 28 02 2013].

[13] Robert Bosch gmbh, “Capacitec proximity sensor system,” 2013. [Online]. Available: http://www.bosch.us/content/language1/html/7748.htm. [Accessed 12 02 2013].

[14] P. J. Jianbiao, Minitab tutorial for Design and Analysis of Experiments, Minitab, 2007, pp. 1-32.

[15] Ford Motor Company, Six Sigma Black Belt, 10.3, vol. 2, open source six sigma, 2011, pp. 504-577.

[16] G. Hartmann, „Potentials and Limitations of Ultrasonic Clamp load Testing,” *SAE Technical Paper*, nr. 2007-01-1668, pp. 1-6, 2007.

[17] S. Hareyama, R. Takada, T. Shimodaira, K. Tamura, A. Hoshi en M. Nakashima, „A Proposal for the Absolute Estimation Method on Self-loosening of Bolted Joints during Off-road Vehicle Operation,” *SAE Technical Paper*, pp. 1-7, May 2011.

Appendices

Appendix 1: Figures

List of appendix figures

Appendix Figure B 1: Cobblestones slalom event

Appendix Figure B 2: Traction control event

Appendix Figure B 3: Chatterbumps event

Appendix Figure B 4: Chuckholes lane

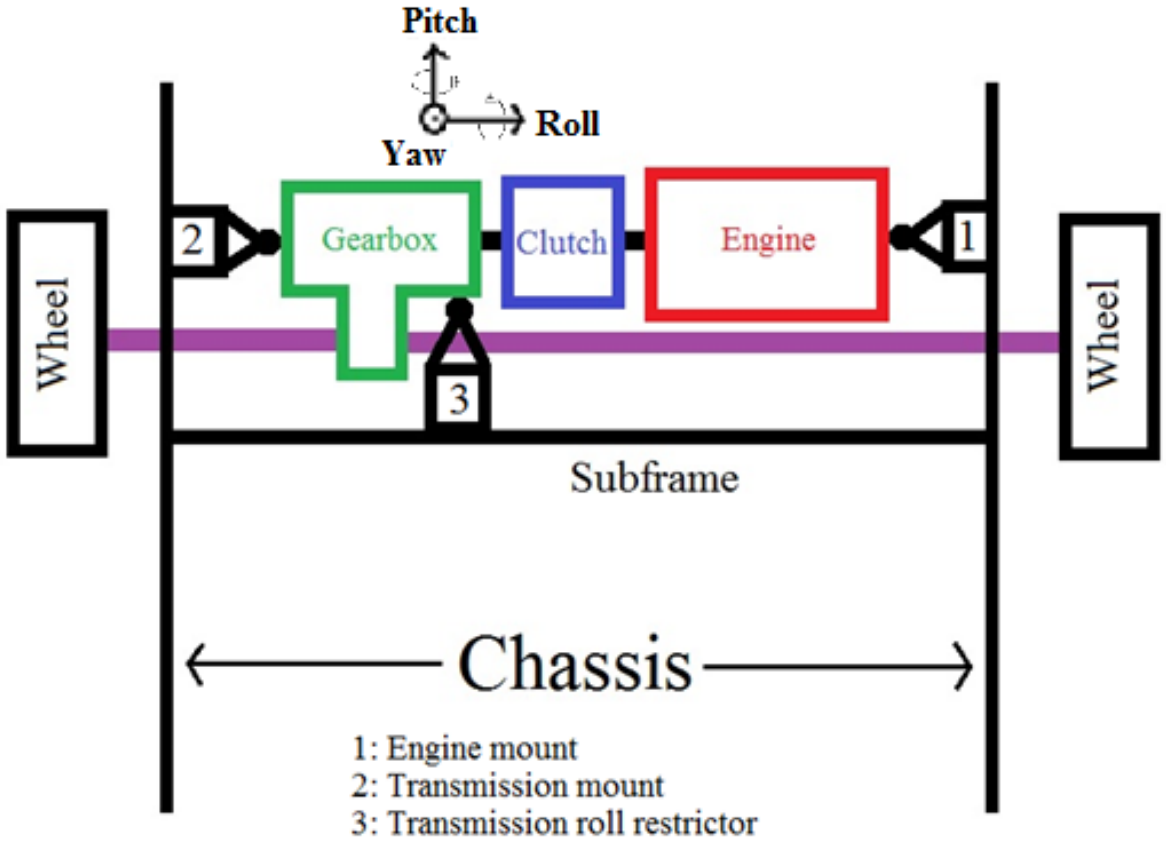

Appendix Figure B 5: Powertrain layout of a Ford Fiesta, top view

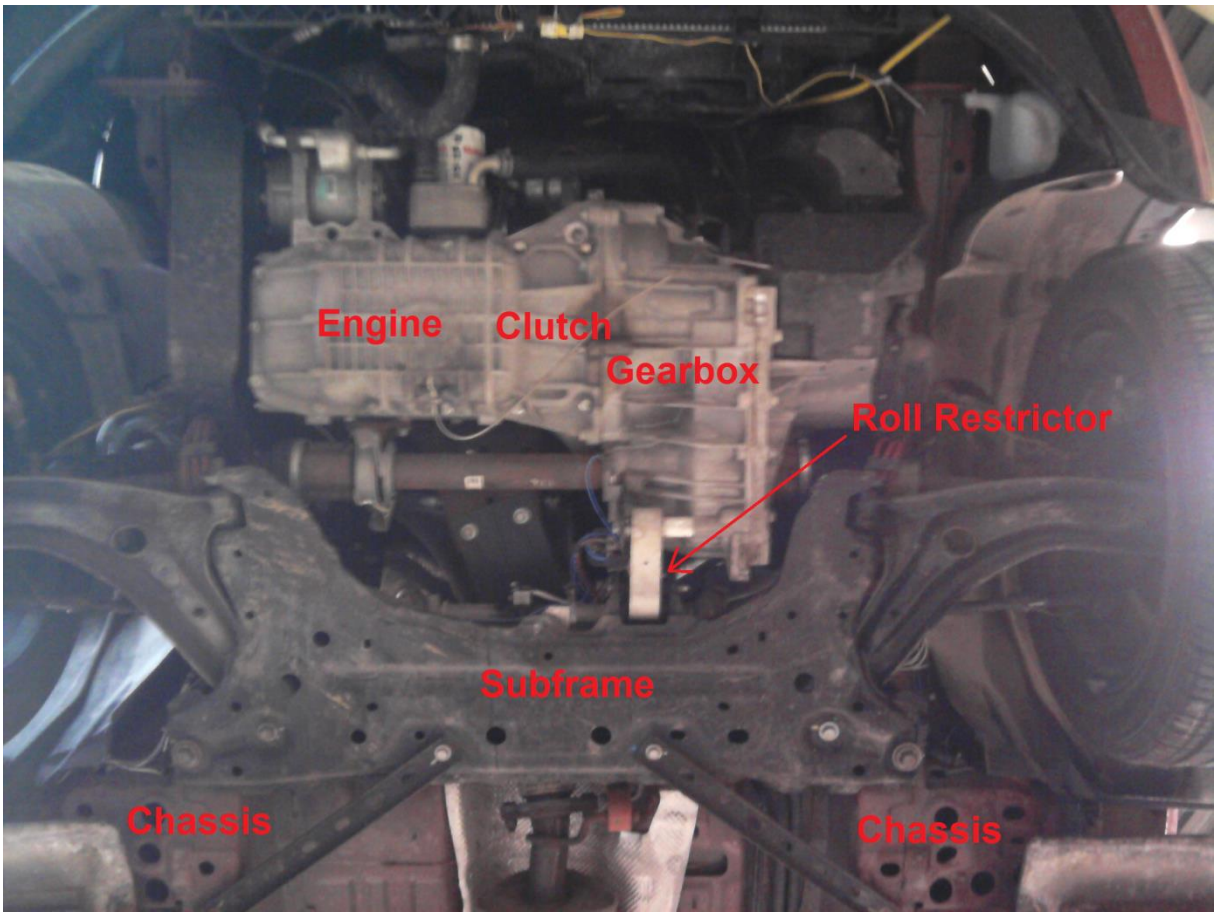

Appendix Figure B 6: Powertrain of a Ford Fiesta, bottom view

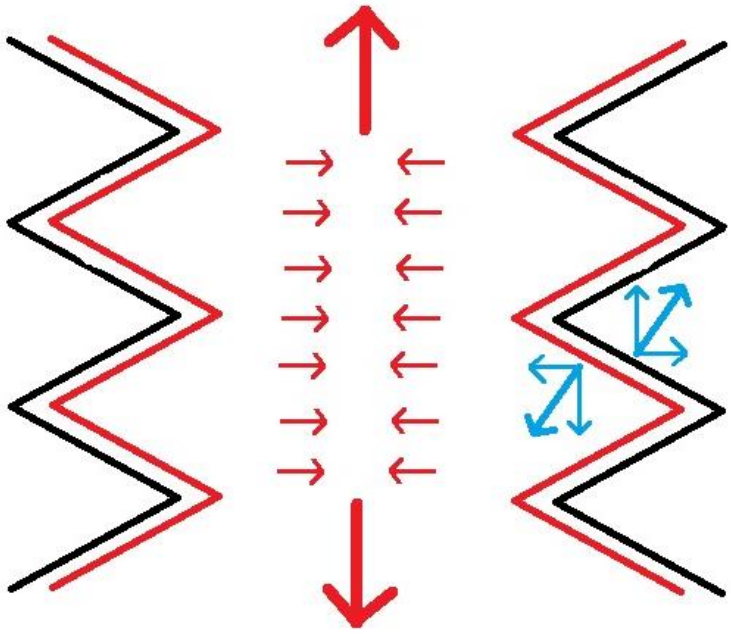

Appendix Figure B 7: Poisson shrinkage of a bolt and widening of the female thread

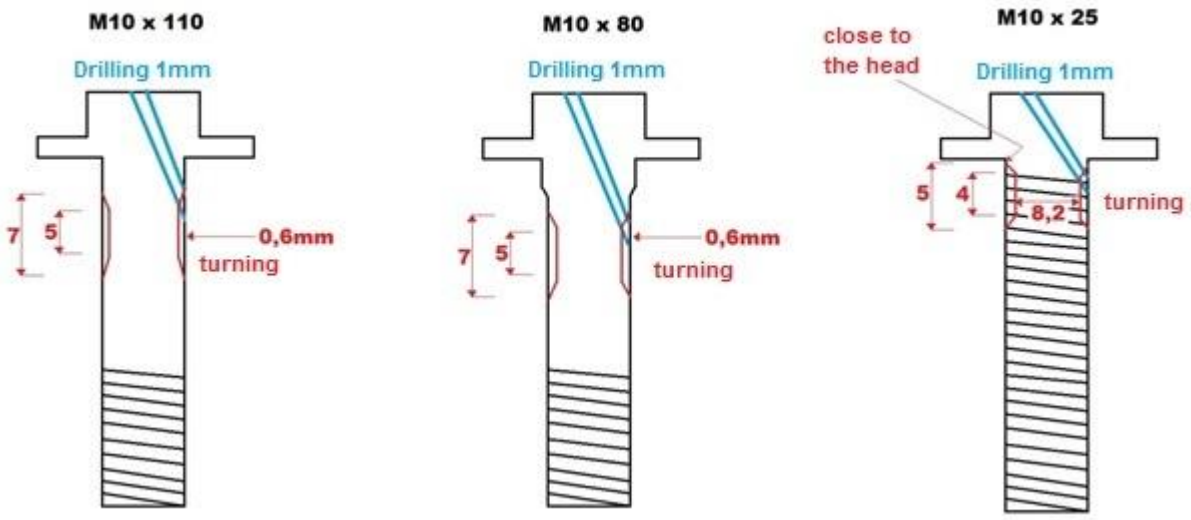

Appendix Figure B 8: Machining the roll restrictor bolts to make it possible to glue strain gauges

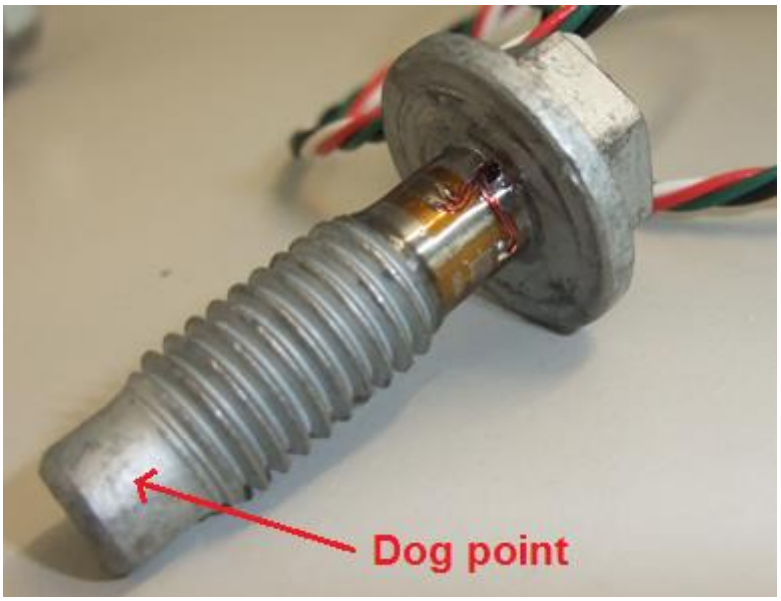

Appendix Figure B 9: W500233 (M10x25) instrumented with a pseudo half bridge

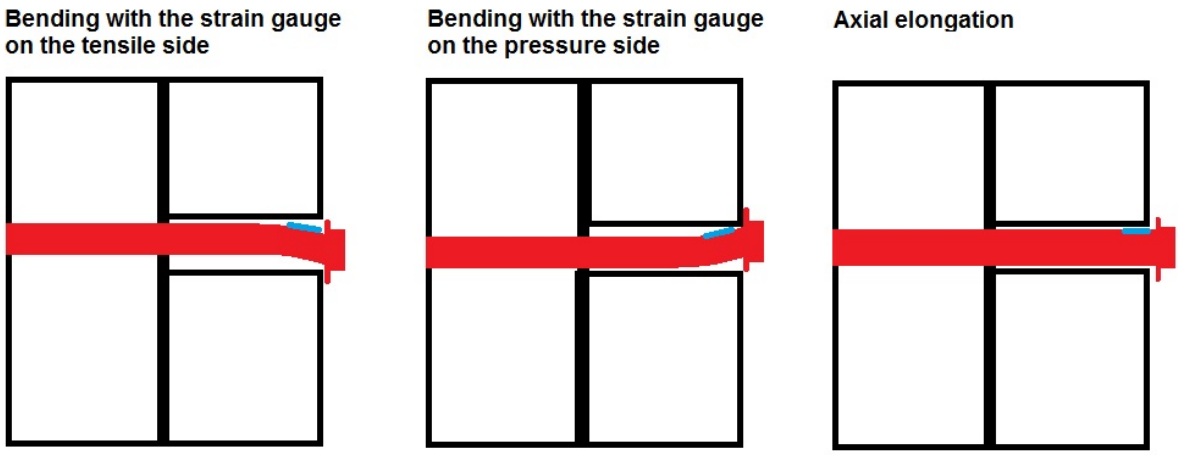

Appendix Figure B 10: Different cases that will be indistinguishable with the pseudo half bridge

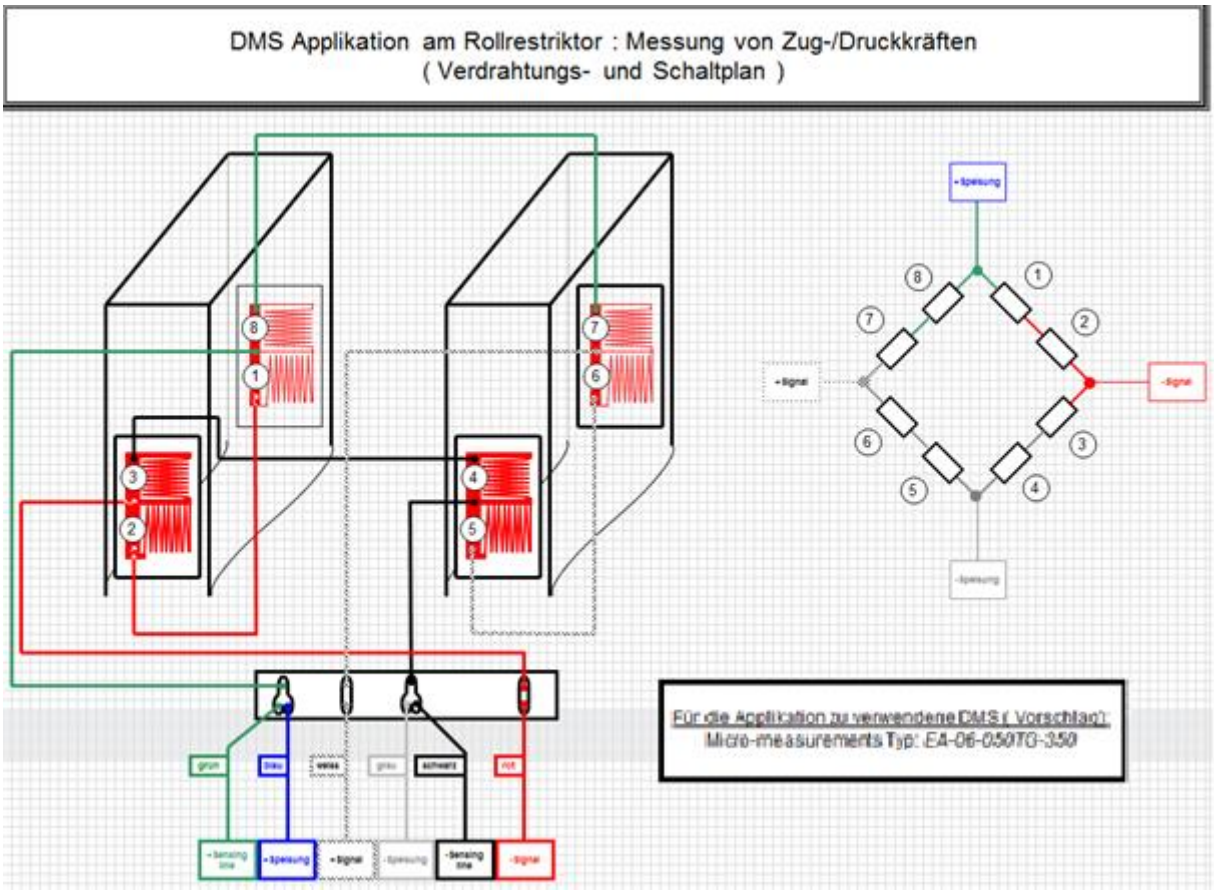

Appendix Figure B 11: Standard scheme for instrumenting a roll restrictor

Appendix Figure B 12: SLS 095 sliding resistance

Source: http://www.yongho-e.com/PDF/penny/lvdt/sls.pdf

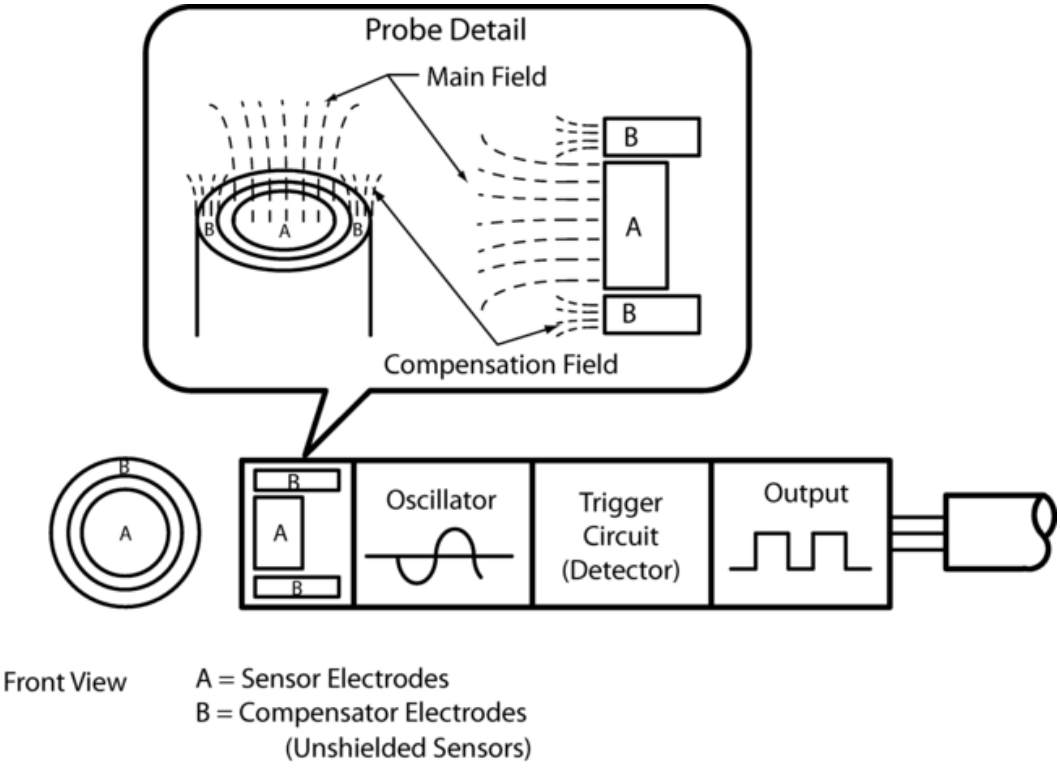

Appendix Figure B 13: Principle of capacitive sensing

Source: http://www.ab.com/en/epub/catalogs/12772/6543185/12041221/12041231/Capacitive-Proximity-Sensing.html

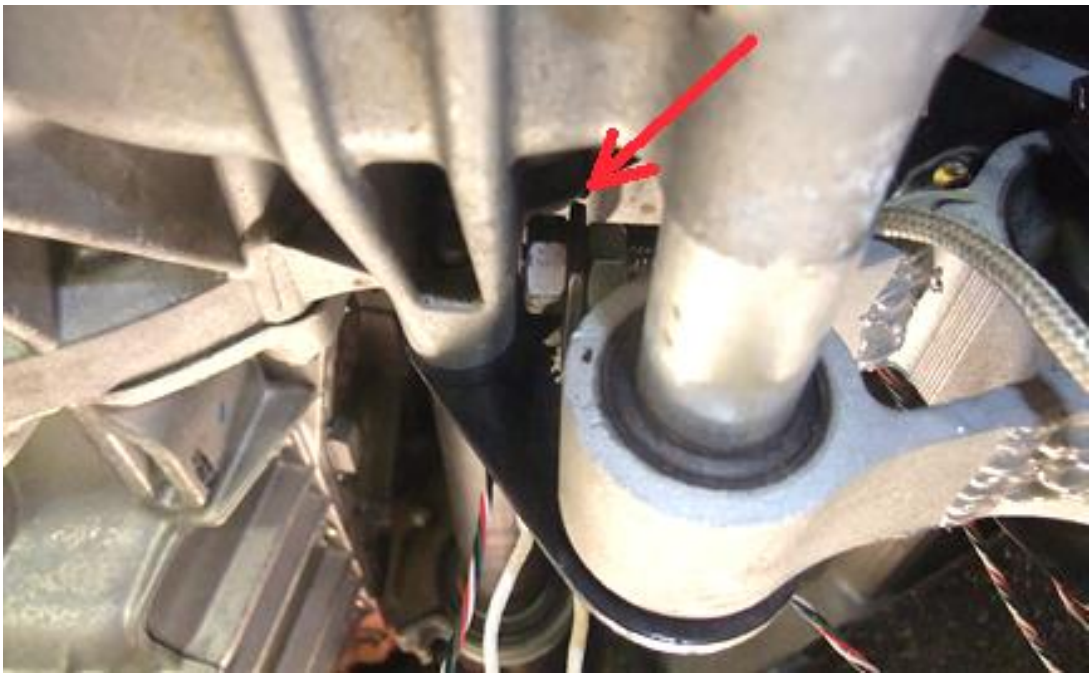

Appendix Figure B 14: Capacitive sensor at the back of the roll restrictor bracket on the gearbox side

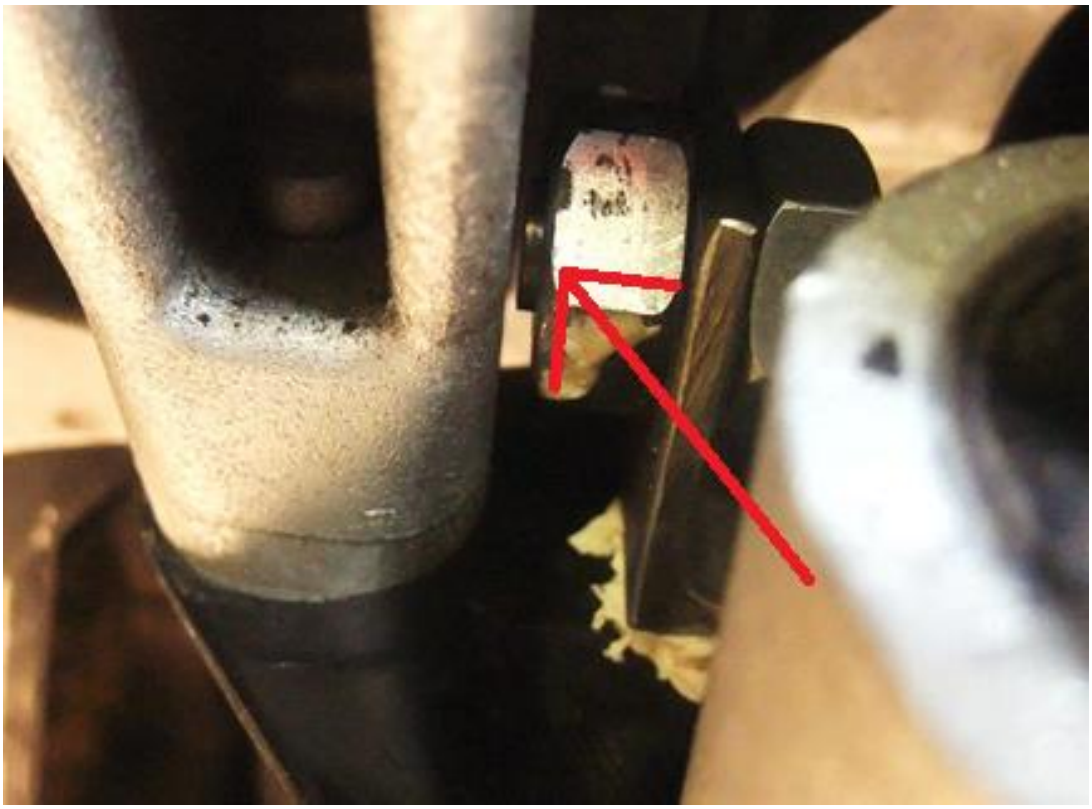

Appendix Figure B 15: Close-up of the capacitive sensor

Appendix Figure B 16: Dewe-43 V data acquisition system

Source: http://www.dewetron.com.sg/uploads/7/7/1/6/7716986/1307800228.png

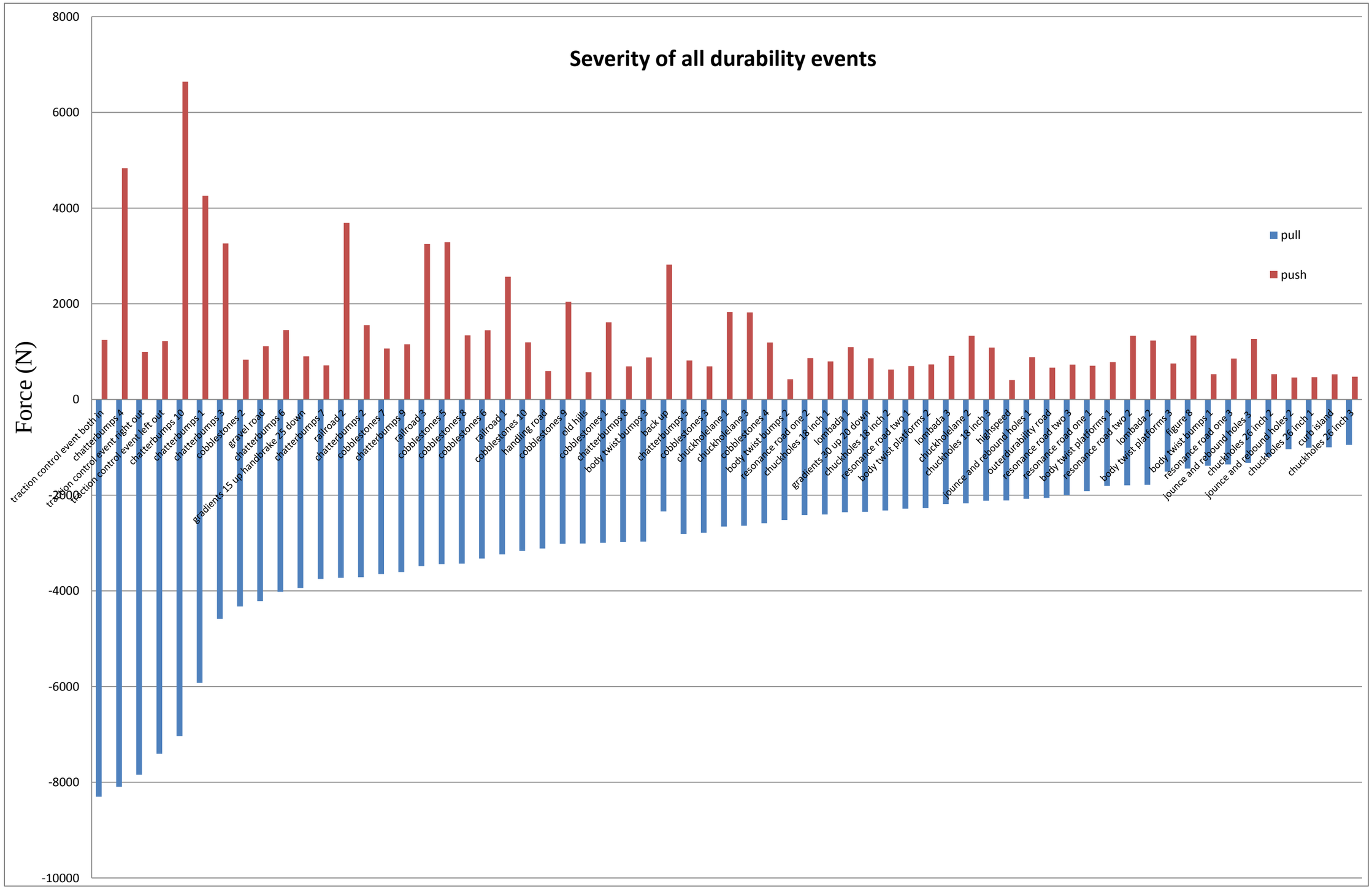

Appendix Figure B 17: Comparison of all durability events in terms of roll restrictor forces

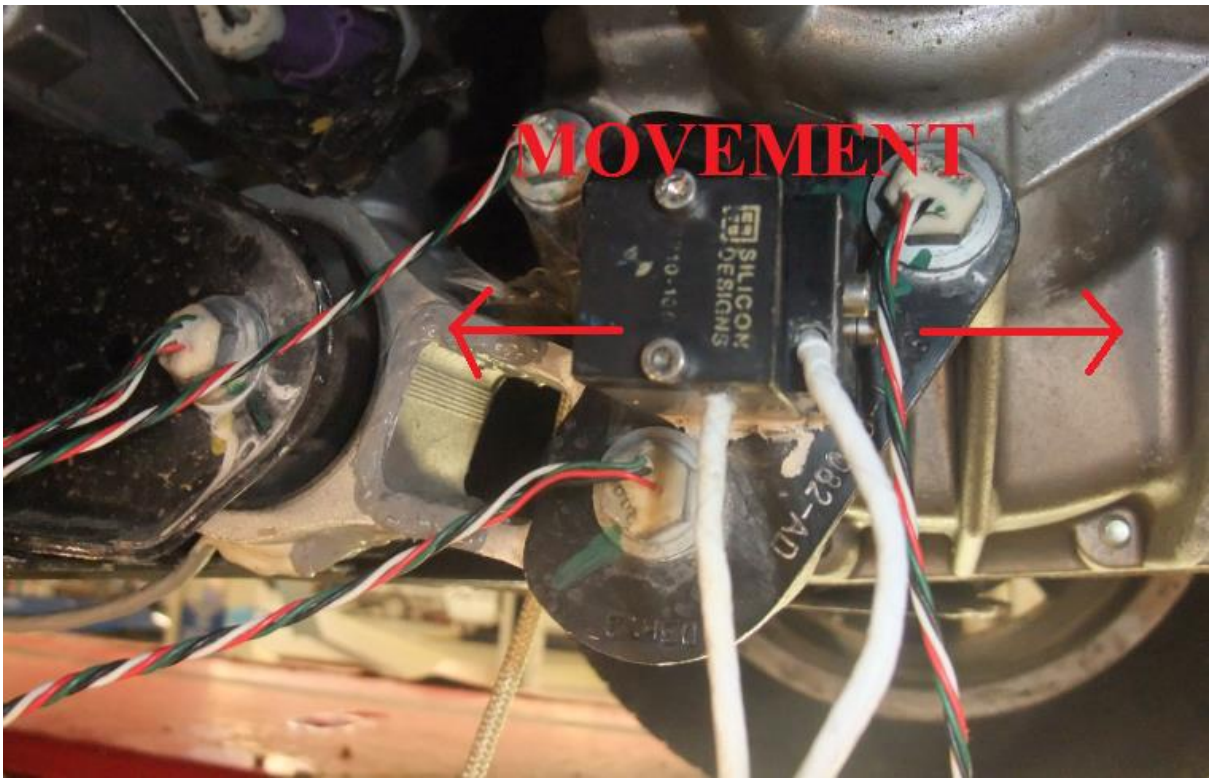

Appendix Figure B 18: Measured movement of the instrumented roll restrictor

Appendix Figure B 19: On the left the load cell readout for calibration, on the right the LP3000

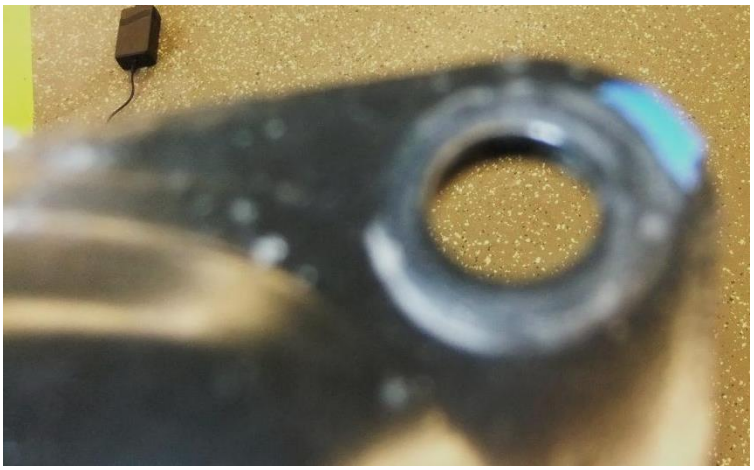

Appendix Figure B 20: Roll restrictor bracket coating damaged by the head of bolt W500233

Appendix Figure B 21: Roll restrictor bracket coating damaged by movement between the component and the gearbox, reverse side of the figure above

Appendix Figure B 22: Bush on the subframe side of the roll restrictor

Appendix Figure B 23: From left to right: bolt 1 torqued at 15,2Nm, after 25 passages, after 40 passages

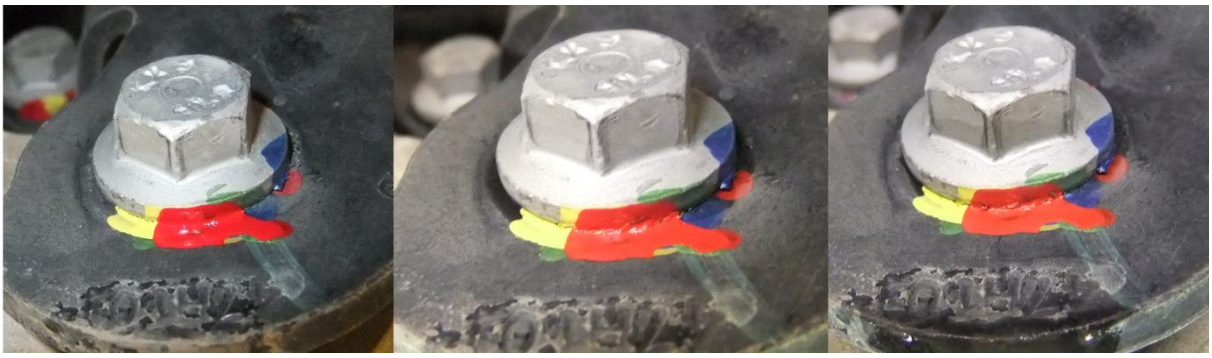

Appendix Figure B 24: From left to right: bolt 2 torqued at 7,6Nm, after 25 passages, after 40 passages

Appendix Figure B 25: From left to right: bolt 3 torqued at 8,2Nm, after 25 passages, after 40 passages

Appendix Figure B 26: From left to right: bolt 4 torqued at 8,6Nm, after 25 passages, after 40 passages

Appendix Figure B 27: Surface reamer

Source: http://image.made-in-china.com/2f0j00ksSaJRTFfYoO/Impregnated-Diamond-Core-Bit-Surface-Set-Reaming-Shell-Diamond-Casing-Shoe-Bit-Core-Barrel-and-Overshot.jpg

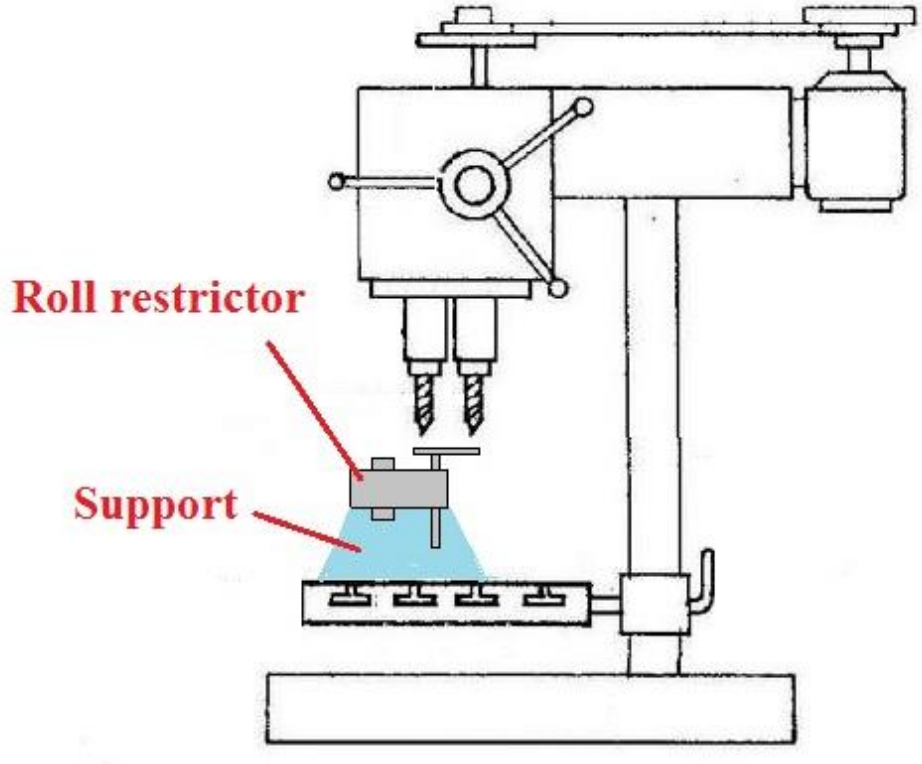

Appendix Figure B 28: Concept drawing of a multispindle surface reamer

Source: http://taranath.files.wordpress.com/2010/12/f51txg0funowjgu-medium.jpg

Appendix 2: Calibration data and other technical information

Strain gauges used on the bolts

VISHAY PRECISION GROUP

062TV

Micro-Measurements

General Purpose Strain Gages - Shear/Torque Pattern

GAGE PATTERN DATA

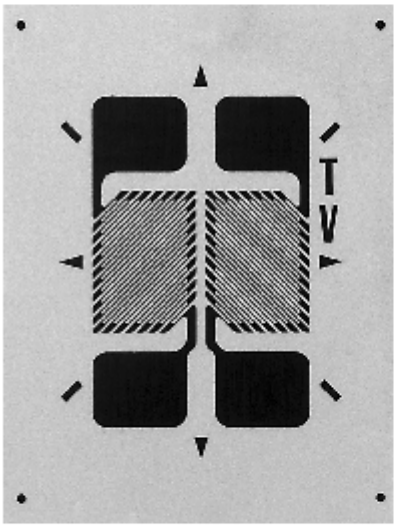

actual size

GAGE DESIGNATION See Note 1, 3	RESISTANCE (OHMS) See Note 2	OPTIONS AVAILABLE See Note 3
EA-XX-062TV-350 **SA-XX-062TV-350** **SK-XX-062TV-500**	350 ± 0.2% 350 ± 0.4% 500 ± 0.4%	E, L, LE

DESCRIPTION

Two-element 90° torque gage.

GAGE DIMENSIONS Legend: ES = Each Section, S = Section (S1 = Sec 1), CP = Complete Pattern, M = Matrix. inch / millimeter

Gage Length	Overall Length	Grid Width	Overall Width	Matrix Length	Matrix Width
0.062 ES	0.175 CP	0.055 ES	0.115 CP	0.27	0.21
1.57 ES	4.45 CP	1.40 ES	2.92 CP	6.9	5.3

GAGE SERIES DATA See Gage Series data sheet for complete specifications.

Series	Description	Strain Range	Temperature Range
EA	Constantan foil in combination with a tough, flexible, polyimide backing.	±3%	–100° to +350°F [–75° to +175°C]
SA	Fully encapsulated constantan gages with solder dots.	±2%	–100° to +400°F [–75° to +205°C]
SK	Fully encapsulated K-alloy gages with solder dots.	±1.5%	–452° to +450°F [–269° to +230°C]

Note 1: Insert desired S-T-C number in spaces marked XX.

Note 2: Tolerance is increased when Option W, E, SE, LE, or P is specified.

Note 3: Products with designations and options shown in bold are not RoHS compliant.

Strain gauges used on the roll restrictor

125AC

Micro-Measurements

VISHAY PRECISION GROUP

General Purpose Strain Gages - Linear Pattern

GAGE PATTERN DATA

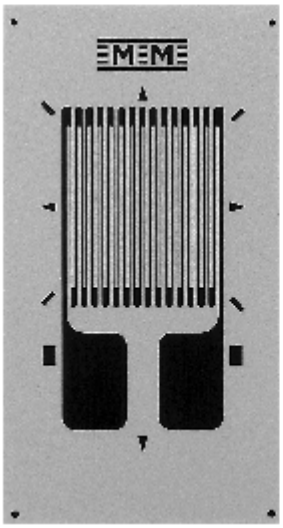

actual size

GAGE DESIGNATION See Note 1, 3	RESISTANCE (OHMS) See Note 2	OPTIONS AVAILABLE See Note 3
EA-XX-125AC-350	350 ± 0.15%	W, E, L, LE, P
ED-DY-125AC-10C	1000 ± 0.3%	E, L*, LE*
EK-XX-125AC-10C	1000 ± 0.15%	W, SE
S2K-XX-125AC-10C	1000 ± 0.3%	
WA-XX-125AC-350	350 ± 0.3%	W*
WK-XX-125AC-10C	1000 ± 0.3%	W*
EP-08-125AC-350	350 ± 0.15%	
SA-XX-125AC-350	350 ± 0.3%	
SK-XX-125AC-10C	1000 ± 0.3%	
SD-DY-125AC-10C	1000 ± 0.6%	
WD-DY-125AC-10C	1000 ± 0.6%	

DESCRIPTION

Widely used general-purpose gage with high-resistance grid. See also 125AD, 125UN, and 125UW patterns. EK-Series gages are supplied with duplex copper pads (DP) when optional feature W or SE is not specified.

GAGE DIMENSIONS Legend: ES = Each Section, S = Section (S1 = Sec 1), CP = Complete Pattern, M = Matrix. inch / millimeter

Gage Length	Overall Length	Grid Width	Overall Width	Matrix Length	Matrix Width
0.125	0.250	0.125	0.125	0.40	0.22
3.18	6.35	3.18	3.18	10.2	5.6

GAGE SERIES DATA

See Gage Series data sheet for complete specifications.

Series	Description	Strain Range	Temperature Range
EA	Constantan foil in combination with a tough, flexible, polyimide backing.	±5%	–100° to +350°F [–75° to +175°C]
ED	Isoelastic foil in combination with tough, flexible polyimide film.	±2%	–320° to +400°F [–195° to +205°C]
EK	K-alloy foil in combination with a tough, flexible polyimide backing.	±1.5%	–320° to +350°F [–195° to +175°C]
S2K	K-alloy foil with laminated thick, high-performance polyimide backing.	±1.5%	–100° to +250°F [–75° to +120°C]
WA	Fully encapsulated constantan gages with high-endurance leadwires.	±2%	–100° to +400°F [–75° to +205°C]
WK	Fully encapsulated K-alloy gages with high-endurance leadwires.	±1.5%	–452° to +550°F [–269° to +290°C]
EP	Annealed constantan foil with tough, high-elongation polyimide backing.	±20%	–100° to +400°F [–75° to +205°C]
SA	Fully encapsulated constantan gages with solder dots.	±2%	–100° to +400°F [–75° to +205°C]
SK	Fully encapsulated K-alloy gages with solder dots.	±1.5%	–452° to +450°F [–269° to +230°C]
SD	Equivalent to WD Series, but with solder dots instead of leadwires.	±1.5%	–320° to +400°F [–195° to +205°C]
WD	Fully encapsulated isoelastic gages with high-endurance leadwires.	±1.5%	–320° to +500°F [–195° to +260°C]

Note 1: Insert desired S-T-C number in spaces marked XX.

Note 2: Tolerance is increased when Option W, E, SE, LE, or P is specified.

Note 3: Products with designations and options shown in bold are not RoHS compliant.

*Options available but not normally recommended. See Optional Features data sheet for details.

Calibration of the transmission roll restrictor

Instrumentation Lommel

Date: 16 - nov - 2012 15:13

Calibration Report No.: 700999_1_70525_79449_F2L

Object of Calibration

Equipment ID	700999
Equipment Description	TESTTRANSDUCER
Manufacturer	none
Type	
Serial Nr.	
Rated Range	0 to 15000 (N)
Remark	

Was calibrated against the following equipment, which itself is traceable to National Standards.

Calibrating Equipment

Description	Equipment Id	Type	Serial No.
KALIBRATIETOESTEL TEST	584002	112S.20KN	06.903235

Other Instruments Used

Description	Equipment Id	Type	Serial
TEST 1 AXIAAL 20KN UKBANK	210005	P3U1.20KN	06.90236

Extra Information

Channel Number	1
Output Description	Stuurstang 15KN Trek

Measuring Conditions

Calibration Procedure	INS-20b
Calibrated Range	0 to 15000 (N)
Number Of Cycles	3
Number Of Calibration Steps	10

Environmental Conditions

Temperature (°C)	20	(+/- 2)
Barometer (mbar)	1013	(+/- 5)
Humidity (%)	34	(+/- 10)

Results of Calibration

Sensitivity (Elec. unit / Eng. unit)	-0.000051034	mV/V / N	(Best Fit)
Sensitivity (Eng. unit / Elec. unit)	-19594.7	N / mV/V	
Offset	0.29372	mV/V	
Max. Non-Linearity (%FS)	0.6356 %		
Max. Hysteresis (%FS)	-0.7161 %		
Total uncertainty * (%FS)	1.1 %		
Calibration Excitation Voltage	(None)	Volt	

The Calibration of the above instrument was carried out by RAERDEN on 15-Nov-2012 07:41:38

* The Total uncertainty indicated is the "root sum square" of the Max. Non-Linearity and the Max. Hysteresis which may be maximum 30% of the required measurement precision (VDI/2616/5, 7.4)

Instrumentation Lommel

Date: 16 - nov - 2012 15:13

Calibration Report No.: 700999_1_70525_79449_F2L

Measured Values: (Average of 3 cycles)

UP			DOWN			HYSTERESIS
Set Value N	Meas. Value mV/V	Non Linearity	Set Value N	Meas. Value mV/V	Non Linearity	Hysteresis
0	0.0000	0.0000	0	0.0000	0.0000	0.0000
1500	- 0.0764	0.0184	1500	0.0733	0.4233	0.4089
3000	- 0.1525	0.0834	3000	- 0.1477	0.6973	- 0.6139
4500	- 0.2267	0.1176	4500	- 0.2232	0.8356	- 0.7180
6000	- 0.3055	0.1135	6000	0.2998	0.8238	- 0.7133
7500	- 0.3822	0.0667	7500	- 0.3769	0.7618	- 0.6950
9000	- 0.4594	- 0.0181	9000	- 0.4546	0.6115	- 0.6296
10500	- 0.5369	- 0.1354	10500	0.5329	0.3852	- 0.5206
12000	- 0.6142	- 0.2371	12000	- 0.6115	0.1135	- 0.3566
13500	- 0.6922	- 0.4151	13500	- 0.6905	- 0.1857	- 0.2195
15000	0.7700	0.5776	15000	0.7700	- 0.5268	0.0092

Datasheet Accelerometer

SILICON DESIGNS, INC.
Advanced Accelerometer Solutions

Model 2210
Analog Accelerometer Module

- Capacitive Micromachined
- Nitrogen Damped
- ±4V Differential Output or 0.5V to 4.5V Single Ended Output
- Fully Calibrated
- Low Power Consumption
- -40 to +85°C Operation
- +9 to +32V DC Power
- Simple Four Wire Connection
- Low Impedance Outputs Will Drive Up To 15 Meters of Cable
- Responds to DC and AC Acceleration
- Non Standard g Ranges Available
- Rugged Anodized Aluminum Module
- Low Noise
- Serialized for Traceability

Available G-Ranges

Full Scale Acceleration	Model Number
± 2 g	2210-002
± 5 g	2210-005
± 10 g	2210-010
± 25 g	2210-025
± 50 g	2210-050
±100 g	2210-100
±200 g	2210-200
±400 g	2210-400

DESCRIPTION

The model 2210 accelerometer module combines an integrated model 1210L accelerometer with high drive, low impedance buffering for measuring acceleration in commercial/industrial environments. It is tailored for zero to medium frequency instrumentation applications. The anodized aluminum case is epoxy sealed and is easily mounted via two #4 (or M3) screws. On-board regulation is provided to minimize the effects of supply voltage variation. It is relatively insensitive to temperature changes and gradients. The cable's shield is electrically connected to the case while the ground (GND) wire is isolated from the case. An optional initial calibration sheet (2210-CAL) and periodic calibration checking are also available.

OPERATION

The model 2210 accelerometer module produces two analog voltage outputs, which vary with acceleration as shown in the graph on the next page. The sensitive axis is perpendicular to the bottom of the package, with positive acceleration defined as a force pushing on the bottom of the package. The signal outputs are fully differential about a common mode voltage of approximately 2.5 volts. The output scale factor is independent from the supply voltage of +9 to +32 volts. At zero acceleration the output differential voltage is nominally 0 volts DC; at ±full scale acceleration the output differential voltage is ±4 volts DC respectively.

APPLICATIONS

- Vibration Monitoring
- Vibration Analysis
- Machine Control
- Modal Analysis
- Robotics
- Crash Testing
- Instrumentation

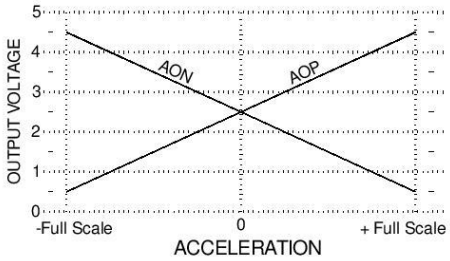

SIGNAL DESCRIPTIONS

Vs and GND (Power): Red and Black wires respectively. Power (+9 to +32 Volts DC) and ground.

AOP and AON (Output): Green and White wires respectively. Analog output voltages proportional to acceleration; AOP voltage increases (AON decreases) with positive acceleration. At zero acceleration both outputs are nominally equal to 2.5 volts. The device experiences positive (+1g) acceleration with its lid facing up in the Earth's gravitational field. Either output can be used individually or the two outputs can be used differentially. (See output response plot below)

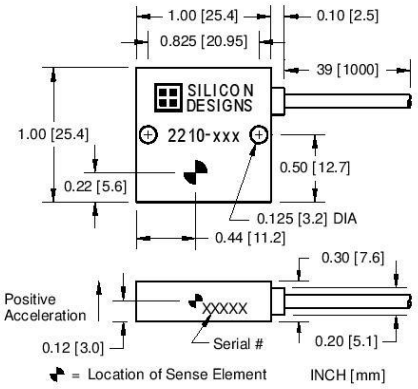

PERFORMANCE - By Model: V_S=+9 to +32VDC, T_C=25°C									
MODEL NUMBER	**2210-002**	**2210-005**	**2210-010**	**2210-025**	**2210-050**	**2210-100**	**2210-200**	**2210-400**	**UNITS**
Input Range	±2	±5	±10	±25	±50	±100	±200	±400	g
Frequency Response (Nominal, 3 dB)	0 - 300	0 - 400	0 - 600	0 - 1000	0 - 1500	0 - 2000	0 - 2500	0 - 3000	Hz
Sensitivity, Differential [1]	2000	800	400	160	80	40	20	10	mV/g
Output Noise, Differential (RMS, typical)	13	32	63	158	316	632	1265	2530	µg/(root Hz)
Max. Mechanical Shock (0.1 ms)	2000								g

PERFORMANCE - All Models: Unless otherwise specified, Vs=+9 to +32VDC, T_C=25°C, Differential Mode.					
PARAMETER		**MIN**	**TYP**	**MAX**	**UNITS**
Cross Axis Sensitivity			2	3	%
Bias Calibration Error	-002		2	4	% of span
	-005 thru -400		2	3	
Bias Temperature Shift (T_C= -40 to +80°C)	-002 & -005		100	300	(ppm of span)/°C
	-010 thru -400		50	200	
Scale Factor Calibration Error [2]			2	3	%
Scale Factor Temperature Shift (T_C= -40 to +80°C)			+300		ppm/°C
Non-Linearity (-90 to +90% of Full Scale) [2]	-002 thru -100		0.5	1.0	% of span
	-200		0.7	1.5	
	-400		1.0	2.0	
Power Supply Rejection Ratio		50	>65		dB
Output Impedance			1		Ω
Output Common Mode Voltage			2.45		VDC
Operating Voltage		9		32	VDC
Operating Current (AOP & AON open)			12	14	mA DC
Mass (not including cable)			10		grams
Cable Mass			25		grams/meter

Note 1: Single ended sensitivity is half of values shown.

Note 2: 100g versions and above are tested from -65g to +65g.

DIFFERENTIAL vs. SINGLE ENDED OPERATION

The model 2210 accelerometer will provide its best performance when you connect it to your instrumentation in a differential configuration using both the **AOP and AON output** signals. But a differential connection may not always be possible. In such cases, it is perfectly fine to connect the accelerometer to your instrumentation in single ended mode by connecting AOP and GND to your instrumentation and leaving **AON** disconnected. Keep in mind however, that for a single-ended connection, the signal to noise ratio is reduced by half, the signal is more susceptible to external noise pickup, and the accelerometer's output will vary directly with any change in the +2.5V reference that you provide.

CABLE SPECIFICATIONS & LENGTH CONSIDERATIONS

The cable consists of four 28 AWG (7x36) tin plated copper wires with Teflon FEP insulation surrounded by a 40 AWG tin plated copper braided shield. The shield jacket is Teflon FEP with a nominal outer diameter of 0.096". Cable lengths of up to 15 meters (50 feet) can be added to the standard 1 meter cable without the need to test for output instability. For lengths longer than 15 meters, we recommend you check each individual installation for oscillation by tapping the accelerometer and watching the differential output for oscillation in the 20kHz to 50kHz region. If no oscillation is present then the cable length being used is OK. From the standpoint of output current drive and slew rate limitations, the model 2210 is capable of driving over 600 meters (2000 feet) of its cable type but at some length between 15 and 600 meters, each device will likely begin to exhibit oscillation.

Datasheet of the capacitive distance sensor

Capacitec

HPT-150 Threaded Probe

Temperature Ranges A and E

Specifications

Temperature Ranges:

Temperature Range A
Low: 32º F [0º C]
High: 302º F [150º C]
Temperature Range E
Low: -100º F [-73º C]
High: 400º F [205º C]

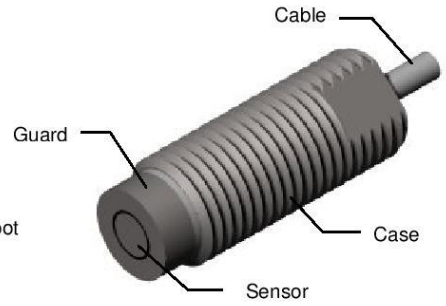

Linear Range: 0.100 inches [2.54 millimeters] with a 5 foot [1.52 meters] long Capacitec L2 cable. For cables longer than 5ft consult factory.

Maximum Range: 0.150 inches [3.81 millimeters]

Calibration:
- A 20 point archived calibration record of voltage output versus nominal displacement is provided standard with every probe.
- Several NIST traceable calibrations are available.

Material: Case, guard, and sensor are 303 stainless steel

Driven Guard: The guard element is driven with an electronic voltage of 2V to 20V peak to peak. The guard must not be grounded.

Dip Coating: "-D" epoxy dip coatings are optional to prevent accidental earth grounding or shorting of the elements.

Mounting:
- Probe is designed to be mounted into a 3/8-24 UNF-2B threaded hole. A "Q" (0.332 inch diameter) tap drill must be used to drill the hole.
- Distance to target is adjusted by rotating the probe.
- An optional nut may be used to lock the probe in place.

Cable:
- Coaxial Capacitec L2 or L3 cable is standard.
- Probe must be calibrated with the cable type and length selected.
- Cable must not be cut or spliced.

Probe Lengths: There are 3 standard probe lengths, and 6 non-standard probe lengths. See drawing for dimensions.

US Email: sales@capacitec.com
EU Email: eurosales@capacitec.com
Web: www.capacitec.com

Capacitec

HPT- 150 Threaded Probe
Part Number Reference Guide

HPT – 150 X - X - XX - XX - X

PROBE LENGTH	OPERATING TEMPERATURE	CABLE TYPE	CABLE LENGTH	CONNECTOR TYPE
A - .500" (12.70)	A - 32 to 302°F (0 to 150°C)	L2 - .093" coax (2.36)	5 - 5' Standard (1524)	M – 10-32 Microdot (Not compatible with I2 or N cable)
B - .625" (15.88)	E - 100 to 400°F (-73 to 205°C)	L3 - .063" coax (1.60)	X - Other in ft.	B – BNC
C - .750" (19.05)	V - 100 to 1600°F (-73 to 371°C)	I2 - .125" coax (3.18)		MCX – MCX (Not compatible with I2 or N cable)
D - .850" (21.59)	S - 100 to 1832°F (-73 to 1000°C)	T – High Temp .063" coax (1.60)		
E - 1.000" (25.40)		N – High Temp .140" coax (3.56)	(DIMENSIONS) IN MILLIMETERS	
F - 1.250" (31.75)				
G - 1.500" (38.10)				
H - 1.750" (44.45)				
I 2.000" (50.80)				

EXAMPLE: HPT-150E-A-L3-5-B

HPT-150E
A TEMPERATURE RANGE

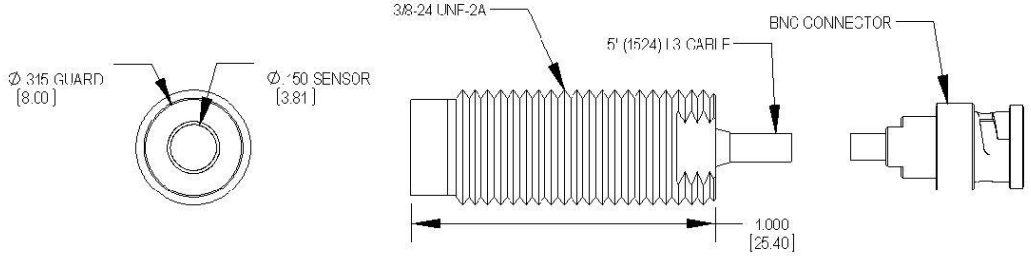

US Email: sales@capacitec.com
EU Email: eurosales@capacitec.com
Web: www.capacitec.com

Capacitec

HPT-150
Standard Threaded Probes
Temperature Ranges A and E
Lengths A, E, and I

DIMENSIONS ARE NOMINAL VALUES

CUSTOM LENGTH OPTIONS	
OPTION	LENGTH
B	.625 [15.88]
C	.750 [19.05]
D	.875 [22.23]
F	1.250 [31.75]
G	1.500 [38.10]
H	1.750 [44.45]

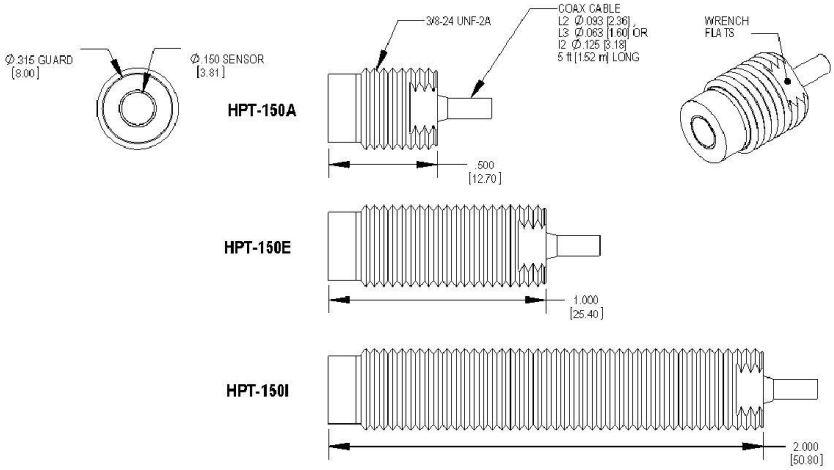

TEMPERATURE RANGE				
OPTION	RANGE (°F)		RANGE (°C)	
	LOW	HIGH	LOW	HIGH
A	32 °	302 °	0 °	150 °
E	-100 °	400 °	-73 °	205 °

US Email: sales@capacitec.com
EU Email: eurosales@capacitec.com
Web: www.capacitec.com

Calibration of the capacitive sensor

Instrumentation Lommel

Date: 03 - dec - 2012 15:55

Calibration Report No.: 144006_1_71009_79857_F2L

Object of Calibration

Equipment ID	144006
Equipment Description	VERPLAATSINGSOPNEMER THOMATRONIK (CAPACITIEF)
Manufacturer	CAPACITEC
Type	HPT-150E-V-N2-80 - 2.5
Serial No.	150-8990
Rated Range	.875 to 1.875 (mm)
Remark	

Was calibrated against the following equipment, which itself is traceable to National Standards.

Calibrating Equipment

Description	Equipment Id	Type	Serial No.
DATA ACQUISITION/SWITCH UNIT HP34970A	580002	34970A	US37C02835
CAPACITEC CALIBRATION STAND	144600	CS 10 9538 1MR	08920

Other Instruments Used

Description	Equipment Id	Type	Serial
Extra Used Equipment	Extra Used Equipment	Versterker Lpg.Nr. = 144107	

Extra Information

Channel Number	1
Output Description	capacitec 0.875 - 1.875 mm

Measuring Conditions

Calibration Procedure	INS-211b
Calibrated Range	.875 to 1.875 (mm)
Number Of Cycles	1
Number Of Calibration Steps	6

Environmental Conditions

Temperature (°C)	22	(+/- 2)
Barometer (mbar)	998	(+/- 5)
Humidity (%)	33	(+/- 10)

Results of Calibration

Sensitivity (Elec. unit / Eng. Unit)	4.0005994	VDC / mm	(Best Fit)
Sensitivity (Eng. unit / Elec. unit)	0.25	mm / VDC	
Offset	0.0	VDC	
Max. Non-Linearity (%FS)	0.4196 %		
Max. Hysteresis (%FS)	UNKNOWN		
Total uncertainty * (%FS)	0.42 %		
Calibration Excitation Voltage	(None)	Volt	

The Calibration of the above instrument was carried out by RAEREDEN on 03-Dec-2012 03:46:08

** The Total uncertainty indicated is the "root sum square" of the Max. Non-Linearity and the Max. Hysteresis which may be maximum 30% of the required measurement precision (FAP03-15, 7.6)*

Instrumentation Lommel

Date: 03 - dec - 2012 15:55

Calibration Report No.: 144006_1_71909_79857_F2L

Measured Values: (Average of 1 cycles)

UP		
Set Value mm	Meas. Value VDC	Non Linearity
.875	3.4923	- 0.2049
1	3.9964	- 0.1295
1.125	4.5129	0.2045
1.25	5.0176	0.4196
1.375	5.5123	0.2857
1.5	5.9912	- 0.2416
1.625	6.4868	- 0.3530
1.75	6.9943	- 0.1681
1.875	7.5071	0.1488

Datasheet sliding resistance

Hybrid Technology LINEAR SENSORS

SLS 095 is an entirely new range of miniature linear position sensors designed to provide maximum performance benefits within an extremely compact body diameter of 9.5mm. Using the proven benefits of Hybrid Track Technology and including a number of unique design features, the SLS 095 is ideally suited to volume OEM manufacturers, where high performance and reliability with competitive pricing and rapid despatch has paramount importance.

- Competitively priced
- Simple to install
- Long operating life
- Superior reliability
- Rapid despatch

Hybrid Track

The hybrid track comprises a high resistivity conductive plastic film bonded to a precision wire-wound element. The conductive plastic film is wiped by a precious metal contact. The technology provides infinite resolution and a very long life (since the majority of the current still flows in the wire, the carbon content of the conductive plastic film is low, and the film is therefore very hard). Track linearity is very good, temperature coefficient of resistance is low and predictable and resistance stability with change in humidity is excellent.

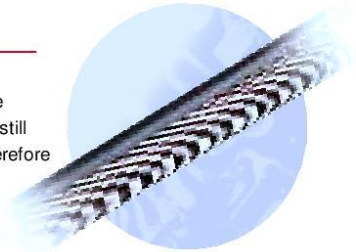

High integrity reduces design cost

Hybrid track technology sensors used in a control system allow simple, low current electronics to be used, while the low hysteresis, low electrical noise and the self-compensating effect for track wear allow the system designer to achieve improved control system accuracy and long term integrity without increasing design costs. The technology also enables quick, easy installation.

Total reliability

Hybrid track technology provides a highly reliable solution for absolute position sensing problems. The self-cleaning, long life contact design and stable, predictable output of the hybrid track improves service life and reduces the need for regular maintenance or re-calibration of the control system.

NO MAINTENANCE

HYBRID TECHNOLOGY LINEAR SENSORS

Rapid Despatch

SLS 095

Features	Benefits
Short body to stroke length	Reduced installation space
Sealing to IP66 and corrosion resistant rod end bearings	Operation in hostile environments
Cable integrally moulded	Excellent strain relief with secure sealing
Minimum size and weight	Ideal for robotics and small mechanisms
Rapid despatch of any option	Eliminates customer inventory
CE approved	Confidence in EMC performance
Interchangeable with Penny+Giles HLP 095 sensors	Increased performance with a significant cost saving

CE

EMC
The products detailed in this document have been tested to the requirements of EN50081-1 (Emissions) and EN50082-2 (Immunity).

Circuit Recommendation
Hybrid track potentiometers feature a high wiper contact resistance, therefore operational checks should be carried out only in the voltage divider mode. Hybrid track potentiometers should be used only as voltage dividers, with a minimum wiper circuit impedance of 100 x track resistance or 0.5MΩ (whichever is greater). Operation with wiper circuits of lower impedance will degrade the output smoothness and affect the linearity.
For variable resistor applications Penny & Giles wirewound potentiometers should be used. Please ask for technical literature.

SLS 095

PERFORMANCE

Electrical stroke E	**mm**	***10***	***20***	***30***	***40***	***50***	***75***	***100***
Resistance ±10%	**kΩ**	0.4	0.8	1.2	1.6	2.0	3.0	4.0
Independent linearity	**±%**	0.5	0.35	0.25	0.25	0.25	0.15	0.15
Power dissipation at 20˚C	**W**	0.2	0.4	0.6	0.8	1.0	1.5	2.0
Applied voltage maximum	**Vdc**	8.9	17.9	26	40	44	67	74
Resolution		Virtually infinite						
Hysteresis (repeatability)		Less than 0.01mm						
Operational temperature	**°C**	–30 to +100						
Output smoothness		To MIL-R-39023 grade C 0.1%						
Insulation resistance		Greater than 100MΩ at 500V d.c.						
Operating mode		Voltage divider only - see Circuit Recommendations on page 2						
Wiper circuit impedance		Minimum of 100 x track resistance or 0.5MΩ (whichever is greater)						
Operating force maximum								
sealed	**gf**	300 in horizontal plane						
unsealed	**gf**	100 in horizontal plane						
Life at 250mm per second		Typically greater than 100 million operations (50 x 10^6 cycles) at 25mm stroke length						
Dither life		200 million operations (100 x 10^6 cycles) at ±0.5mm, 60Hz						
Shaft seal life		20 million operations (10 x 10^6 cycles)						
Shaft velocity maximum	**m/s**	2.5						
Vibration		RTCA 160D 10Hz to 2kHz (random) @ 4.12g (rms) - all axes						
Shock		40g 6mS half sine						

OPTIONS

Integral shaft seal - IP 66
Designed to accept integral shaft seal to give IP66 rating

Mounting
Can be supplied with rod end bearings or a plain body for use with body clamps or flange mounting kit.

AVAILABILITY

All configurations can be supplied within 5 days from the factory.

ORDERING CODES

SLS 095/...../...../...../.....

Electrical stroke
Resistance
Sealing 50 = IP50, 66 = IP66
Mounting option R = Rod Ends
P = Plain

Mounting kits (order separately)
Body clamp kit - SA200841
Flange kit - SA200842

DIMENSIONS AND MOUNTING OPTIONS

ROD END BEARING MOUNTING SLS 095

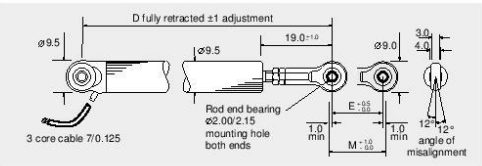

PLAIN BODY MOUNTING SLS 095

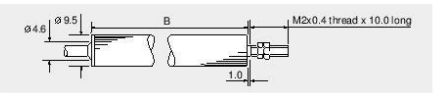

MOUNTING OPTIONS

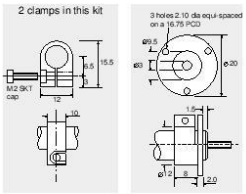

Body clamp
SA200841

Flange mounting
SA200842

Note: Drawings not to scale

Electrical stroke E	**mm**	***10***	***20***	***30***	***40***	***50***	***75***	***100***
Mechanical stroke M	**mm**	***12.5***	***22.5***	***32.5***	***42.5***	***52.5***	***77.5***	***102.5***
Body length B	**mm**	45.5	55.5	65.5	75.5	85.5	110.5	135.5
Between centres D		70	80	90	100	110	135	160
Weight approximate (Mounting option R)	**g**	11	13	14.5	16	17.5	21.5	25.5

ELECTRICAL CONNECTIONS

3 core cable: PUR sheathed 0.3m long with PTFE insulated 7/0.125 cores.

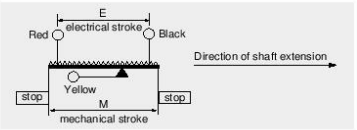

Available from Penny+Giles

A wide range of instrumentation for measurement and control solutions in industrial and aerospace applications. Please ask for more details.

Penny+Giles quality systems meet the requirements of ISO9001, the Civil Aviation Authority and numerous customer's certification standards.

Quality is at the heart of all our systems ensuring the reliability of our products from initial design to final despatch.

Registered No. 924881

■ VRVTs ■ LVDTs - *industrial/ aerospace* ■ Hybrid Linear Potentiometers
■ Solenoids ■ Rotary Potentiometers ■ Joystick Controllers ■ In-Cylinder Transducers

Contact Worldwide

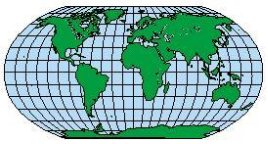

WEB SITE
www.pennyandgiles.com

UNITED KINGDOM
Penny+Giles Controls Ltd
15 Airfield Road
Christchurch
Dorset BH23 3TJ
Telephone: +44 (0) 1202 409409
Fax: +44 (0) 1202 409410
Email: xsales@pennyandgiles.com

USA
Penny+Giles Controls Inc
919 N Plum Grove Road
Suite A and B
Schaumburg IL 60173-4760
Telephone: +1 847 995 0840
Fax: +1 847 995 0838
Email: us.sales@pennyandgiles.com

GERMANY
Penny+Giles
Straussenlettenstr. 7b
85053 Ingolstadt
Telephone: +49 (0) 841 61000
Fax: +49 (0) 841 61300
Email: info@penny-giles.de

Penny+Giles products are in service with these industries throughout the world.

Aerospace
Automotive
Construction
Defence
Leisure
Marine
Material handling
Mining
Motorsport
Off-highway
Petrochemical
Plastics and Rubber
Power generation
Process control
Transportation
Timber and Forestry

Penny+Giles
A Curtiss-Wright Company

Doc Ref: SLS095/03/02

Datasheet Data acquisition system

Automotive
Energy & Power Analysis
Aerospace & Defense
Transportation
General Test & Measurement

DEWE-43
Universal Data Acquisition Instrument

When connected to the high speed USB 2.0 interface of any computer the DEWE-43 becomes a powerful measurement instrument for analog, digital, counter and CAN-bus data capture.

Eight simultaneous analog inputs sample data at up to 204.8 kS/s and in combination with DEWETRON Modular Smart Interface modules (MSI) a wide range of sensors are supported

- *Voltage*
- *Pressure*
- *Temperature*
- *Position*
- *Torque*
- *Velocity*
- *Acceleration*
- *Force*
- *Sound*
- *RPM*
- *Frequency*
- *And more*

The included DEWESoft application software adds powerful measurement and analysis capability, turning the DEWE-43 into a dedicated recorder, scope or FFT analyzer.

Key Features

- *Best price/performance ratio*
- *Connects to any computer via USB interface*
- *8 simultaneous sampled analog inputs*
- *24-bit resolution, up to 204.8 kS/s per channel*
- *8 counter inputs or 24 digital inputs*
- *2 high speed CAN interfaces*
- *CPAD2 expansion for static signals*
- *DEWESoft instrument software included*

The DEWE-43 is a perfect fit for

- *Mobile applications*
- *Field-service*
- *Maintenance*
- *Debug and diagnostic tasks*

PORTABLE INSTRUMENTS DEWE-43

Re-inventing Data Acquisition

worldwide
DEWETRON
www.dewetron.us

Connectivity

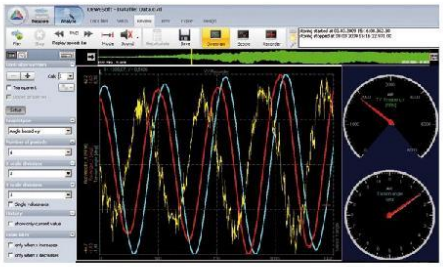

Analog

There are eight analog inputs, each has its own sigma-delta A/D converter and is sampled at up to 204.8 kS/s at 24-bit resolution. Anti-aliasing filters are included for each channel and all are our "universal" type, which can handle full bridges and voltages up to ±10 V natively and support our tiny Modular Smart Interfaces (MSI). MSIs are able to convert any of the analog inputs to a different input type, including IEPE accelerometer / microphone, ±200 V, RTDs, thermocouples and charge.

Counter / Digital input

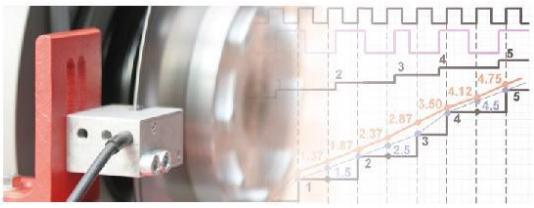

The DEWE-43 offers eight Lemo sockets where each can either be used as one counter input or as three digital inputs – this is a software selection and can be set individually for each socket.

Thanks to the special DEWETRON technology, they are acquired absolutely synchronously to the analog channels. DEWETRON counters are able to perform

- *Basic counting*
- *Gated counting*
- *Up/down counting*
- *Two pulse edge separation*
- *Frequency measurement*
- *Pulse width measurement*
- *Period time measurement*
- *Duty cycle*

CAN

The two high speed CAN interfaces are able to acquire data from vehicle CAN – or vehicle OBDII interface – as well as from any sensor outputting CAN data. Additionally DEWETRON CPAD2 modules can be connected to the CAN interface for adding slow channels like temperature.

DEWESoft - Data Acquisition Software

The powerful and very easy to use data acquisition software DEWESoft turns the DEWE-43 into a complete measurement instrument.

Synchronous data acquisition of different sources, data export to almost any analysis software as well a the powerful online mathematics and filtering are just a few key features.

- *Easy-to-use*
- *Synchronous data acquisition of different sources*
- *Data export to almost any analysis package*
- *Powerful online mathematics and filtering*
- *Extensions for special applications*
- *Networkable operation with synchronization*
- *DCOM programmable extensibility*

The standard version of the DEWE-43 includes the basic version DEWESoft-SE and is sufficient for many applications. For measurement tasks like Order Tracking, Human Body Vibration, FRF, Rotational & Torsional Vibration or Sound Level measurement there is an extended DEWE-43-DSA version available which includes the powerful DEWESoft-DSA software. DEWE-43-DSA additionally offers a faster sampling rate of 204.8 kS/s per channel (standard DEWE-43 has 51.2 kS/s per channel).

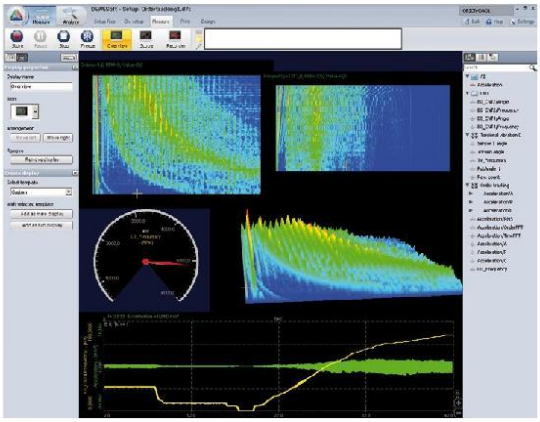

SPECIFICATIONS		DEWE-43-DSA	DEWE-43
ANALOG INPUT			
Number of channels		8 (simultaneously sampled)	
Measured values		Voltage, full bridge (IEPE, charge, thermocouple and RTD with MSI adapters)	
Resolution		24-bit	
Type of A_{DC}		Sigma-Delta	
Sampling rate		204.8 kS/s	
-3 dB bandwidth		76 kHz @ 204.8 kS/s	
Input Ranges	Voltage	±0.01 V, ±0.1 V, ±1 V, ±10 V	
	Voltage via MSI-BR-V200	up to ±200 V	
	Full bridge	±10 mV/V, ±100 mV/V, ±1000 mV/V	
	Half or quarter bridge	With external bridge completion	
	IEPE via MSI-BR-ACC	±0.1 V, ±1 V, ±10 V	
	Thermocouple via MSI-BR-TH-x	Full range of thermocouple type (isolated thermocouple only)	
	Pt100, Pt200, Pt500, Pt1000, Pt2000 and resistance via MSI-BR-RTD	-200°C to 1000°C and 0 to 6.5 kOhm	
AMPLIFIER CHARACTERISTICS			
Accuracy		±0.1 % of range, ±0.5 mV	
Input impedance		10 MΩ||33 pF (common mode), 20 MΩ||47 pF (differential mode)	
CMRR		>80 dB	
Sensor supply voltage		±5 V 0.1 % @ 50 mA, 12 V @ 100 mA per channel (total max. 5W)	
Voltage mode coupling		DC	
Overvoltage protection		±70 V	
DYNAMIC CHARACTERISTICS			
Signal to noise @ fs<1000 Hz		< 100 dB	
Crosstalk		< 100 dB	
COUNTER/DIGITAL INPUTS			
Number of channels		8 counters or 24 digital inputs (per software each counter can be selected to be 3x digital input)	
Counter modes		Event counting, encoder input, period, pulsewidth, duty cycle, frequency measurement	
Resolution		32-bit	
Time base		102.4 MHz	
Signal levels		TTL/CMOS	
Input voltage protection		30 V	
CAN INPUTS			
Number of channels		2	
Specification		CAN 2.0B, up to 1 MBaud	
Physical layer		High speed	

ENVIRONMENTAL		
Operating temperature	0 to 50°C	
Storage temperature	-20 to 70°C	
Relative humidity	95 % non condensing @ 60°C	
PROCESSING		
System	Requires PC based system with DEWESoft software	
Interface	USB 2.0	
POWER REQUIREMENTS		
Supply voltage	6 to 36 V_{DC}	
Supply overvoltage protection	80 V	
Negative input voltage protection	-30 V	
Typical power consumption	Typ. 5 W (max. 11 W at full sensor supply load)	
PHYSICAL		
Dimensions (L x W x H)	223 x 78 x 45 mm (8.78 x 3.08 x 1.77 inch)	
Weight	0.72 kg	

SOFTWARE		
Displays	Recorder, Scope, FFT, 3D Waterfall FFT, Octave, ...	
Triggers	Edge, Filtered Edge, Window, Pulsewidth, Slope, FFT, ...	
Online standard mathematics	Formula editor, FIR-, IIR-, FFT-filter, basic statistics, reference curve	
Online special mathematics	DEWE-43-DSA: Human Body Vibration, Order Tracking, Rotational & Torsional Vibration, Sound Level, Frequency Response Function	-

Applications

Recorder

Synchronous recording of different signals

- Voltage
- Pressure
- Temperature
- Position
- Torque
- Velocity
- Acceleration
- Force
- Sound
- RPM
- Frequency
- And more

Order Tracking

- Dedicated re-sampling method for sharp order separation
- Measurement in time domain to keep all benefits
- 2D, 3D waterfall in order or frequency domain
- Amplitude, phase extraction
- Recalculation in post processing
- Phase synchronous RPM input with 12.5 ns resolution
- EASY TO SETUP

Torsional and Rotational Vibration

- Time domain measurement
- Angle based view
- Additional to all other functions (analog, CAN, GPS, video, ...)
- Configurable display
- Direct sensor connection
- 80 MHz time base
- High resolution ±0.03rpm ±2 mdeg@12000 rpm

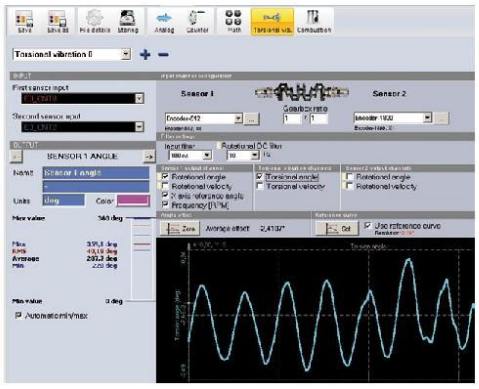

Balancing

- User interface which guides through all steps
- Order tracking based balancing method
- Single or dual plane
- Multiple balancing for two directions saves time
- 2D graph for plane view
- RPM channel with color indicator (RPM range)
- Alarm output if velocity exceeds predefined value
- Displays tacho probe time signal to set trigger
- Vector polar plots of 1st order of all runs (initial, trail, ...)
- Weight splitting
- Acceleration, velocity, displacement in recorder
- Time domain measurement

The shown applications are only a few examples, many more can be covered using the DEWE-43 instrument.

DEWETRON, INC. • 10 High Street, Ste K • Wakefield • RI • 02879 • USA
Tel +1 (401) 284-3750 • Fax +1 (401) 284-3755 • sales@dewmerica.com

worldwide DEWETRON

Datasheet Load Probe LP3000B

Stand 03/2007

Standard Measuring Unit **LP 3000B**

The battery powered standard measurement device for fixed measurement places.

PC-supported ultrasonic measurement system with logical menu navigation for the clamp load measurement of bolted joint connections.

Order number: 401.10002 (CPU = 800 MHz)
Order number: 401.10003 (CPU = 1600 MHz)

Available only as a Set LP3000B 800/1600, see pricelist.

Ultrasonic Module
Pulse-Echo ultrasonic operating time in real time

Impulse voltage:	*5 V Peak at 50 Ω*
Measurement cable:	*Coax cable 50 Ω*
Resolution:	*100 pico seconds/s*
Pulse recurrence:	*384 Hz*
Scan rate:	*up to 160 Hz*
Display speed:	*up to 50 Hz*

PC:	*JRex-PM, 3.5"*
Display:	*6.5" TFT transflective VGA Display*
*CPU:**	*Intel® Celeron® M 800 MHz / 1600 MHz*
RAM:	*512 MB*
*Memory:**	*2 GB CF Memory*
*Connections:**	*VGA, LAN 10/100, 2 x USB 2.0, RS 232*
Power pack:	*Input 100-240 V ~ 50-60 Hz, 1 A*
Battery:	*2 x Lithiumpolymer, 11.1 V / 3.2 Ah*
Battery durability:	*approx. 2,5 hrs. with 2 batteries***
Dimensions:	*W: 263, H: 70, L: 230 mm*
Weight:	*3.21 kg (incl. batteries)*
Temp. operating range:	*0°C up to +40°C*
Operating system:	*Windows® XP Pro*
Software:	*LoadProbe 3000B*

* dependent on the current model
** batteries can be changed during operation process!

The mentioned values are based on the manufacturer's specification. Technical changes reserved.

Intellifast GmbH
Am Neuen Rheinhafen 10 · 67346 Speyer · Germany
Phone: +49 (0) 6232 9195 0 · Fax: +49 (0) 6232 9195 19
www.intellifast.de · info@intellifast.de
A member of AMG Advanced Metallurgical Group, N.V.

intellifast
INTELLIGENT FASTENER TECHNOLOGIES

1. Kalibrierverfahren
calibration procedure

Der Kalibriergegenstand wird in Reihe mit einem von der PTB kalibrierten Referenznormal in einer Kraft-BNME aufgebaut und in gleicher Kraftrichtung belastet. Die Kalibrierung beruht auf dem vergleich der Messwerte. Sie erfolgt nach der Richtlinie DAkkS-DKD-R 3-3 (2010-01) unter Berücksichtigung ISO 376 (Ausgabe 2005-02).

The device under test is mounted to the force calibration facility in line with a refrence standard calibrated by the PTB. The load is applied on the device under test and the ref. standard in the same direction. The calibration is based on the comparison of the measurement results and is executed according to DAkkS-DKD-R 3-3 (2010-01), in consideration of ISO 376 (issue 2005-02).

2. Kalibriereinrichtung
calibration facility

Bezeichnung *calibration standard*	200 kN Kraft - BNME; akkreditierter Messbereich: 0,2 kN bis 200 kN
Anschlussmessunsicherheit *best measurement capability*	0,1 % vom Messwert

2.1 Angaben zum Bezugsnormal
reference standard

Aufnehmer *transducer*	Kraftaufnehmer	Messbereich *range*	200 kN
SnNr. *serial number*	75585	Identifizierung *identification*	0581 PTB 07
Typ *typ*	Z4S5		

2.2 Angaben zum Anpasser
amplifier data

Typ *typ*	ML30B	Filter *filter*	20 Hz Bessel
SerienNr. *serial number*	#818830027	Speisespannung *voltage supply*	5 V
Hersteller *manufacture*	HBM	Messkanal *channel*	Slot-1
Identifizierung *identification*	ML30B-01		
Anschluss *connection*	AP01 / Sub-D 6-Leiter		

3. Angaben zur Kalibrierung
calibration conditions

Umgebungstemperatur *ambient temperature*	(21,5 ± 1) °C	Umgebungsluftdruckdruck *atmospheric pressure*	(1009 ± 0,5) mbar
Umgebungsfeuchte	(44 ± 5) %		

4. Angaben zur Kalibrieranordnung
calibration arrangement

4.1 Gegenstand
object

Aufnehmer *transducer*	Z/D-Kraftaufnehmer	Messbereich *range*	100 kN
SnNr. *serial number*	1146692	Identifizierung *identification*	***
Typ *typ*	41	Nullsignal *zero signal*	-0,00968 mV/V

4.2 Kabelanschluss
cable data

Länge (fest verbunden) *length*	5 m	Ausführung *version*	6-Leiter
Verlängerung *extension*	Ford - 0,5 m		

4.3 Angaben zum Anpasser
amplifier data

Typ *typ*	ML30B	Filter *filter*	20 Hz Bessel
SerienNr. *serial number*	#882521048	Kalibriersignal *calibration signal*	***
Hersteller *manufacture*	HBM	Speisespannung *voltage supply*	5 V
Identifizierung *identification*	ML30B-02	Ziffernschritt *numeral step*	0,000001 mV/V
Anschluss *connection*	AP01 / Sub-D 6-Leiter	Schwankungsbreite *fluctuation range*	0,000010 mV/V
Messkanal *channel*	Slot-2		

4.4 Angaben weitere Geräte
additional devices

Typ *typ*	***	Filter *filter*	***
SerienNr. *serial number*	***	Kalibriersignal *calibration signal*	***
Hersteller *manufacture*	***	Speisespannung *voltage supply*	***
Identifizierung *identification*	***	Ziffernschritt *numeral step*	***
Anschluss *connection*	***	Schwankungsbreite *fluctuation range*	***
Messkanal *channel*	***		

4.5 Angaben zu Einspannteilen
mounting accessories

Pos.1 *pos.-1*	Ford Druckstück	Pos.-4 *pos.-4*	***
Pos.-2 *pos.-2*	***	Pos.-5 *pos.-5*	***
Pos.-3 *pos.-3*	***	Pos.-6 *pos.-6*	***

5. Angaben zum Kalibrierablauf
calibration sequence data

Kalibrierablauf *calibration sequence*	ISO-376 *sequence ISO-376*	(nach DIN EN ISO 376 (Ausgabe Feb.05) *(acc. to DIN EN ISO 376 (issue feb. 05)*	
Einbaustellungen *mounting position*	0° - 120° - 240°		
Anzahl Vorbelastungen *preload*	5		
Anzahl Messreihen (MR) *measuring runs (mr)*			
aufwärts *increasing*	4	abwärts *decreasing*	2
Anzahl Messpunkte / MR *steps / mr*	10		

5.1 Angabe zum Messunsicherheitsbeitrag bei reduzierten Kalibrierablauf
uncertainty data for reduced calibration sequences

Quelle der MU-Beiträge *source of uncertainty data*			
Fall *case*	***	t-Faktor *t-factor*	***

6. Angaben zur Messunsicherheit

uncertainty data

Angegeben ist die erweiterte Messunsicherheit, die sich aus der Standardmessunsicherheit durch Multiplikation mit dem Erweiterungsfaktor *k=2* ergibt. Sie wurde gemäß DAkkS-DKD-R 3-3 (2010-01) ermittelt. Der Wert der Messgröße liegt mit einer Wahrscheinlichkeit von 95% im zugeordneten Werteintervall.
Die Kalibrierung gilt von 10% bis 100% des Nennbereiches des jeweilig eingesetzten Kraftbezugsnormals.

The stated uncertainty is the extended uncertainty, which is calculated as the standard uncertainty multiplied with the extension factor k=2 referring to the guideline DAkkS-DKD-R 3-3 (2010-01).
The value of the measurand lies with a probability of 95 % within the interval given by the uncertainty value.
The area of validity of the calibration lies between 10% to 100% of the use reference-standard

7. zusätzliche Bemerkungen / Anmerkungen

additional comments

-

8. Messergebnisse

measurement results

8.1 Angezeigte Messwerte und Auswertung in ***Richtung Druck,*** Ausgabe der Werte erfolgt in ***mV/V***
readings and results for load direction tension *values in*

8.2 Die Messergebnisse sind in den nachfolgenden Tabellen wiedergegeben. Die angezeigten Werte sind jeweils um die Nullanzeige reduziert.
mesuarement results are shown in the table below. Listed values are correted by their offset.

Tabelle-1 Angezeigte Werte bei Vorbelastung
table-1 *readings for preload*

	0 Grad	*120 Grad*	*240 Grad*
Nullanzeige / *zero* :	0,000000	0,000000	0,000000
Anzeige bei Höchstkraft / *at max.calibration force* :	-2,253785	-2,253906	-2,253906
Restanzeige / *zero deviation* :	-0,000005	0,000054	0,000054

Tabelle-2 Angezeigte Messwerte
table-2 *readings*

Kraft *force*	unveränderte Position *unchanged position*		verschiedene Positionen *rotated position*			
in kN	*R1*	*R2*	*R3*	*R4'*	*R5*	*R6'*
0	0,000000	0,000000	0,000000	0,000000	0,000000	0,000000
10	-0,224151	-0,224225	-0,224220	-0,224273	-0,224564	-0,224544
20	-0,449355	-0,449322	-0,449327	-0,449468	-0,449666	-0,449976
30	-0,674346	-0,674354	-0,674370	-0,675244	-0,674888	-0,675992
40	-0,899536	-0,899670	-0,899569	-0,901357	-0,900182	-0,901957
50	-1,125074	-1,125100	-1,125072	-1,127499	-1,125752	-1,128242
60	-1,350729	-1,350779	-1,350631	-1,353165	-1,351347	-1,353949
70	-1,576351	-1,576402	-1,576293	-1,578490	-1,577099	-1,579511
80	-1,802133	-1,802147	-1,801986	-1,803980	-1,802921	-1,804951
90	-2,027913	-2,027924	-2,027796	-2,029358	-2,028798	-2,030406
100	-2,253767	-2,253856	-2,253559	-2,254708	-2,254606	-2,255864

Tabelle-3 Rel. Restanzeige bezogen auf die Kalibrierhöchstkraft
table-3 *zero deviation relative to max. calibration force*

Nach Vorbelastung
after preload

Einbaustellung / *mounting pos.* :	*0 Grad*	*120 Grad*	*240 Grad*
	in %	*in %*	*in %*
Nullpunkt-Änd. / *zero deviation* :	0,002	0,002	0,002

Nach Messreihen
after measuring

Messreihe / *measurement run* :	*R1*	*R2*	*R3 / R4'*	*R5 / R6'*
	in %	*in %*	*in %*	*in %*
Nullpunkt-Änd. / *zero deviation* :	0,003	0,000	0,003	0,001

Tabelle-4 Arithmetische Mittelwerte, rel. Spannweiten, rel. Umkehrspanne, Unsicherheiten

table-4 average values, rel. ranges, rel. hysteresis, uncertainties

Kraft *force*	unveränderte Position *unchanged position*		verschiedene Positionen *rotated position*					
						kubisch / *cubic*		
	Bester Schätzw. *average val.* $\bar{x}_{wr}$	Rel. Wiederh.pr. *repeatab.* b'	Bester Schätzw. *average val.* $\bar{x}_r$	Rel. Vergl.präz. *reproduc.* b	Rel. Umkehrsp. *hysteresis* v	ausgegl. Mittelw. *interp.value* X_a	Rel. Appr.abw. *interp.err.* f_c	Messun-sicherheit *uncertainty* W
in kN	*in mV/V*	*in %*	*in mV/V*	*in %*	*in %*	*in mV/V*	*in %*	*in %*
0	0,000000		0,000000			0,000000		
10	-0,224188	0,033	-0,224311	0,184	0,008	-0,224542	-0,103	0,18
20	-0,449339	0,007	-0,449449	0,076	0,050	-0,449379	0,016	0,12
30	-0,674350	0,001	-0,674535	0,080	0,147	-0,674471	0,009	0,15
40	-0,899603	0,015	-0,899762	0,072	0,198	-0,899780	-0,002	0,17
50	-1,125087	0,002	-1,125299	0,060	0,218	-1,125265	0,003	0,17
60	-1,350754	0,004	-1,350902	0,053	0,190	-1,350887	0,001	0,16
70	-1,576377	0,003	-1,576581	0,051	0,146	-1,576606	-0,002	0,14
80	-1,802140	0,001	-1,802347	0,052	0,112	-1,802383	-0,002	0,13
90	-2,027919	0,001	-2,028169	0,049	0,078	-2,028178	0,000	0,12
100	-2,253812	0,004	-2,253977	0,046		-2,253952	0,001	0,11

	unveränderte Position *unchanged position*		verschiedene Positionen *rotated position*				
					linear / *linear*		
	-	-	-	-	ausgegl. Mittelw. *interp.value* X_a	Rel. Appr.abw. *interp.err.* f_c	Unsicherh. interval *uncertainty* W'
in kN	-	-	-	-	*in mV/V*	*in %*	*in %*
0	-	-	-	-	0,000000		
10	-	-	-	-	-0,225262	-0,422	0,59
20	-	-	-	-	-0,450524	-0,239	0,36
30	-	-	-	-	-0,675786	-0,185	0,33
40	-	-	-	-	-0,901048	-0,143	0,31
50	-	-	-	-	-1,126310	-0,090	0,26
60	-	-	-	-	-1,351573	-0,050	0,21
70	-	-	-	-	-1,576835	-0,016	0,16
80	-	-	-	-	-1,802097	0,014	0,14
90	-	-	-	-	-2,027359	0,040	0,16
100	-	-	-	-	-2,252621	0,060	0,17

Tabelle-5 Ausgeglichene Mittelwerte in Abhängigkeit von der Kraft

table-5 interpolation equation

Kraft in kN	0,0	1,0	2,0	3,0	4,0
10,0	-0,224542	-0,247013	-0,269487	-0,291964	-0,314444
15,0	-0,336926	-0,359411	-0,381899	-0,404390	-0,426883
20,0	-0,449379	-0,471877	-0,494378	-0,516882	-0,539387
25,0	-0,561896	-0,584406	-0,606919	-0,629434	-0,651952
30,0	-0,674471	-0,696993	-0,719517	-0,742043	-0,764571
35,0	-0,787101	-0,809633	-0,832167	-0,854703	-0,877240
40,0	-0,899780	-0,922321	-0,944864	-0,967409	-0,989955
45,0	-1,012503	-1,035052	-1,057603	-1,080156	-1,102709
50,0	-1,125265	-1,147821	-1,170379	-1,192939	-1,215499
55,0	-1,238061	-1,260624	-1,283188	-1,305753	-1,328319
60,0	-1,350887	-1,373455	-1,396024	-1,418594	-1,441165
65,0	-1,463736	-1,486309	-1,508882	-1,531456	-1,554031
70,0	-1,576606	-1,599181	-1,621758	-1,644335	-1,666912
75,0	-1,689489	-1,712068	-1,734646	-1,757225	-1,779804
80,0	-1,802383	-1,824962	-1,847542	-1,870121	-1,892701
85,0	-1,915281	-1,937860	-1,960440	-1,983019	-2,005599
90,0	-2,028178	-2,050757	-2,073336	-2,095914	-2,118492
95,0	-2,141070	-2,163648	-2,186224	-2,208801	-2,231377
100,0	-2,253952				

Tabelle-6 Interpolationsgleichungen / Klassifizierung

table-6 interpolation equation

Die Interpolationsgleichung wurde nach der Methode der kleinsten Fehlerquadrate aus den Mittelwerten in verschiedenen Einbaulagen ermittelt.

The interpolation equation was calculated using the least squares method and is based on the average values in rotated mounting positions.

Y3 = A * X + B * X^2 + C * X^3 **(x in kN)**

Y1 = EW * X **(y in mV/V)**

kubisch / *cubic*

A = -0,022438 **B = -0,00000167** **C = 0,0000000066**

linear / *linear*

EW = -0,022526 selbstbestimmte Spezifikatinsgrenze (Standard.): **0,62 % v. EW**

6.1 Klassifizierung

rating

Kraftbereich / *range*		Geräteklasse
ab 10% bis 100%	ab 10 kN bis 100 kN	2
ab 20% bis 100%	ab 20 kN bis 100 kN	2
ab 30% bis 100%	ab 30 kN bis 100 kN	2
ab 40% bis 100%	ab 40 kN bis 100 kN	2
ab 50% bis 100%	ab 50 kN bis 100 kN	2

Technical data of the Ford 1.6 Ti-VCT Sigma engine

PERSINFORMATIE

Ford Duratec 1.6 Ti-VCT

Four cylinders, 16 valves, two fully variable camshafts

In their pursuit of improving the automobile, developers have traditionally had their eye on ever stronger engines. Ever since internal combustion engines began powering vehicles nearly 120 years ago, generations of engineers have considered larger valves with longer opening durations as the "yellow brick road" towards their dreams of greater engine performance.

The internal combustion engine's 120 year development has been marked by this quest for additional power. Engineers mostly focused their attention on longer valve duration and increased overlap to achieve this. Racing engines were often the prototypes for later production engines. The traditional dominance of pure power increases has only taken a back seat to other developments in recent decades as exhaust technology and its numerous implications began to drive engine development. Racing technology has also by and large ceased to provide the model for production series development. Only now is the focus of vehicle engineers shifting back to power train technology emphasising driving dynamics and hence driving pleasure. Greater flexibility in valve timing promises to deliver a higher quality engine that is more fun to drive, without compromising on low exhaust emissions and good fuel economy.

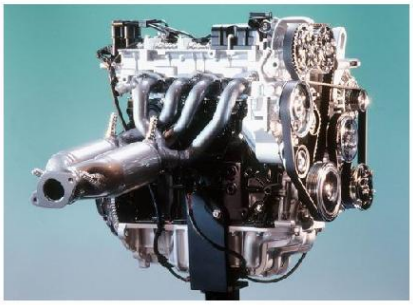

The Ford Duratec Ti-VCT engine uses a double-flow catalytic converter. All of the mechanical components of this modern variable cam timing system are located inside the wheels driving the double overhead camshaft.

At Ford, the road towards this type of progress is being paved by a new technology: fully variable valve timing, or Ti-VCT which is the engineers' abbreviation for "Twin independent Variable Cam Timing." Ti-VCT uses two camshafts controlled by continuously variable actuators. This is a second-generation system with hydraulic variation of the camshafts in the direction of rotation, helping change the duration of the valves' opening relative to the piston position.
A number of similar variable valve timing mechanisms have been used in past engine systems. These systems typically only offered a choice between two timing options: "early" or "late" – that is a choice between two positions of the camshafts.

Unlike previous systems, the hydraulically actuated positions of the camshafts are not limited to just "early" or "late". The Ford Duratec Ti-VCT system is map-controlled according to the required engine load; in other words according to the relationship between the position of accelerator pedal and engine speed. The system's ability to respond to a wide range of situations is a supported by measurement of 2000 parameters in various program maps, all of which have been carefully and continuously refined by Ford engineers during the course of the development project.

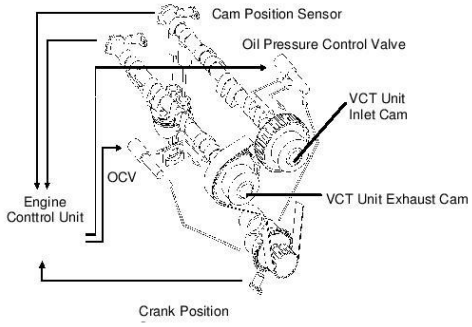

The characteristic trait of the Ford Duratec Ti-VCT system is its fully variable control of both camshafts, driven by the parameters

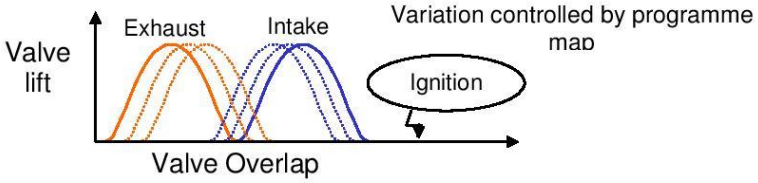

The novelty of Ford's approach is the application of this complex independent twin cam technology to a fuel-efficient 1.6-litre petrol engine. This engine had already undergone optimisation to achieve excellent fuel economy and low emissions of untreated exhaust gas. Fitting this unit with a map-controlled variable camshaft timing system significantly expands the engine's potential. The power delivered by Ford Duratec 1.6 L Ti-VCT has been increased by a respectable 15 hp over the original from 100 to 115 hp. Remarkable, as well, is the engine's peak torque development of 155 Nm. Impressive as these figures are, these power improvements were not the primary motivation for the new developments.

Variable control of both camshafts is performed by two vane-type rotors inside the wheels driving the camshafts. This control is based on a precisely defined programme map and powered exclusively by the engine's

The fact that the Duratec 1.6-litre DOHC engine develops its high torque levels across an unusually wide range of engine speeds is a true breakthrough. This can be seen in the fact that while the engine develops its peak torque of 155 Nm already at 4000 rpm, it already comes very close to doing so at 2000 rpm. For a naturally aspirated engine, the torque curve shows exceptional, plateau-like characteristics, rising quickly and then levelling out across a wide range of engine speeds in a way normally found only in more complex, turbo-charged engines.

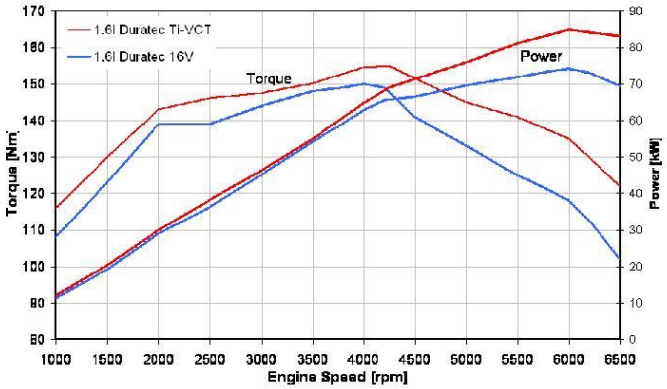

Ford Duratec 1.6 Ti-VCT shows an impressive torque curve over a wide range of engine speeds.

Engine Performance Indicator: Specific Mean Pressure

Specific mean pressure, p_{me}, is a particularly good factor for describing the performance of modern engines. It is determined by dividing maximum torque (expressed in Newton metres) by engine size (expressed in litres) and multiplying the quotient by the non-variable factor of 0.1279 ($p_{me} = Md_{max} / V_h$ x 0.1279). The result of this calculation represents the mean combustion pressure inside the cylinder in bar. Regardless of the size of the engine, this value provides a measure for the quality of the engine's torque. The Ford Duratec 1.6L **Ti-VCT**'s p_{me} of 12.4 bar is exceptionally high for a naturally aspirated engine. Moreover, the fact that this value shows only minor variations across wide ranges of the engine speed band is further proof of the unit's high quality. This factor, in and of itself, marks Duratec **Ti-VCT** as an effective and efficient engine, offering high levels of agility across a wide range of engine speeds.

Technological Basis

In essence, the fully variable valve timing system used by Ford Duratec Ti-VCT only requires three different elements. Two hydraulic control elements, so-called phase actuators, are located inside the wheels driving the camshafts. The effects of oil pressure and spring action enable these elements to vary the camshafts, according to engine speed and load range.

Two hydraulic, four-to-three-way-type valves serve as control elements. These assist in either retarding or advancing the valve timing. The hydraulic connection between the oil circuit and the variable camshaft control system is provided by a newly designed bearing support for the camshafts. This construction contains the ducts for the hydraulic control elements in addition to the usual oil ducts supplying the camshaft bearings. In the Ford Duratec system, these are "driven" exclusively by the respective operating oil pressure of the engine.

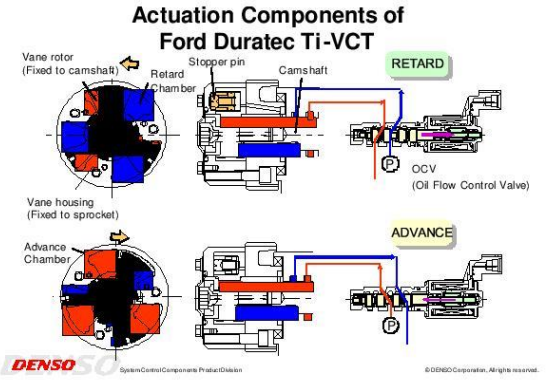

Two variable control elements drive the rotation of the vane-type phase actuator fixed to each camshaft. The variable control is performed, powered only by the operating oil pressure of the engine, distributed via two 4.3-way valves.

Basic Characteristics of Engineering Design

To understand better the way in which Ford's variable valve timing system works, it may be helpful to briefly review the conventionally known extremes of engine characteristics. Back in the nineteen-fifties and sixties, standard production engines typically used somewhat "restrained" valve timing, characterised by short duration and overlap. While this resulted in low engine output, it gave very stable idle speeds. This gives these old engines their characteristic feel of a lot of "muscle," always a surprise to someone driving one of these "oldies" for the first time today. A 1.6 litre engine of that time delivered 55 to 60 hp, then, was roughly half of that produced by a modern engine.

Engines dating back even further to the fifties even top this. They practically "pull the torque-rabbit out of their hat" at such low engine speeds that, by today's standards, comparing them with a locomotive may seem more appropriate than with an automobile. One of Ford's long term successes in those days was the legendary Model T, of which 16 million units were produced. The car developed 20 hp from 2890 cc of cubic capacity, delivered by the crankshaft (stroke: 101.5 mm, bore: 95 mm) with commensurate ease at roughly 1,800 rpm. This was enough, as the British auto magazine "Motor" observed in 1912, to accelerate the car from zero to 40 mph (65 kph) in roughly 40 seconds. The shortest gear of "Tin Lizzy's" planetary gear set had a speed range up to about 14 km/h and the

vehicle itself was suitable for "carrying two tons of hay or pulling a plough across a farmer's field." No doubt, the motto, "nothing beats cubic capacity," dates back to those days.

The other valve timing extreme is typically found in racing engines. These fully exploit the power potential of the engine by using maximum valve lift and uncompromisingly long opening duration. Today, the Fiesta Cup racing version of Ford Fiesta's 1.6-litre performance engine delivers approximately 200 hp. However, this uncompromising output of power is reflected clearly by the engine's sound, particularly at idle speed. At idle, the engine rumbles strongly, showing its lack of smoothness. This characteristic is due to the engine's enormous valve durations and lifts, which do not allow an even distribution of cylinder charges and combustion. The rumbling sound at idle is the result of a compromise in tuning the engine, which has been optimised with a clear emphasis on delivering maximum power at 8,500 rpm. The remainder of the engine speed range was simply of no concern to the race engineers.

Variable cam timing, as used by the Ford system, now aims to combine the advantages of both extremes, without producing the disadvantages of either.

The Ford Duratec 1.6-litre Ti-VCT's fully variable valve timing expands the scope of advantages in both directions, without compromising on refinement, smoothness, power or performance. At near idle speed and in the lower load ranges, valve timing is such that the intake valves open and close relatively late. Instead of the usual overlap, during which intake and exhaust valves remain open at the same time, Ford Duratec even uses underlap, which means that both valves of a combustion chamber remain closed for a very brief time span. This results in stable idle as well as low exhaust emissions.
Load is the first factor that drives valve timing. In case of high loads at low engine speeds - for example, while the car is being accelerated without the driver bothering to shift down in time - both camshafts will change towards higher overlap. Suitable controls, particularly of the exhaust camshaft, produce an appropriate flushing effect of the combustion chamber, and the exiting exhaust gas draws fresh gas into the combustion chamber behind it. The result is a particularly good development of torque while maintaining good fuel economy.

Control Strategies for Ford Duratec Ti-VCT

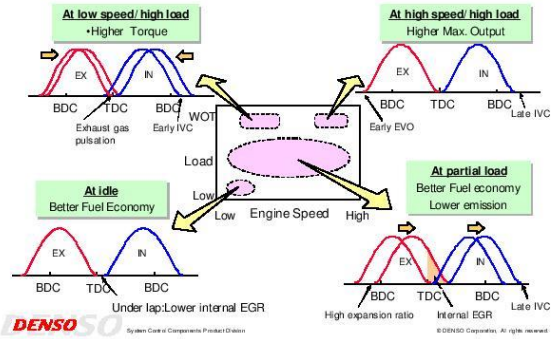

In the medium engine speed and load range, timing is optimised to produce higher overlap. At idle and high engine speeds, these valve positions are avoided. Such sophisticated

Particularly in the medium load range, both camshafts are gently retarded so that the valves open late. In this case, the engine management system carefully times the overlap so that it causes a certain amount of internal exhaust gas recirculation in the lower load range, which helps to reduce the nitrogen oxides in the exhaust gas typically generated under high loads.

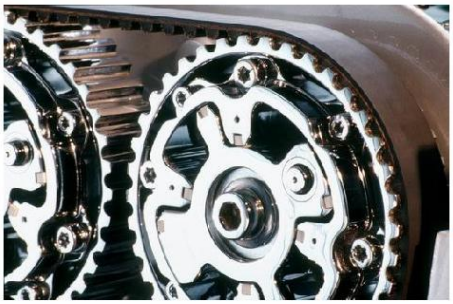

Many active valve timing systems previously used were only able to vary timing between early and late. With its Duratec Ti-VCT system, Ford is now using the first map-controlled variable cam timing system in smaller engines: high-tech for better fuel economy and higher torque.

Only as load and engine speed increase, is valve overlap gradually reduced. This is motivated by the physics of the pulsating gas column on the intake side. The intake system has been fine-tuned to produce a highly effective pulsating charge caused by the gas column vibrating heavily at high engine speeds. Without degrading the cylinder charge, it is thus possible to time the intake camshaft – similar to the process at idle – for late closing of the intake valve and minimum overlap, which minimises short circuiting between fresh gas and exhaust. Despite the fact that valve duration at 6,000 rpm is within the range of merely a few hundredths of a second, this allows the combustion chamber to be filled with a good charge nonetheless.

Ford Duratec Ti-VCT: Valve Timing Variation

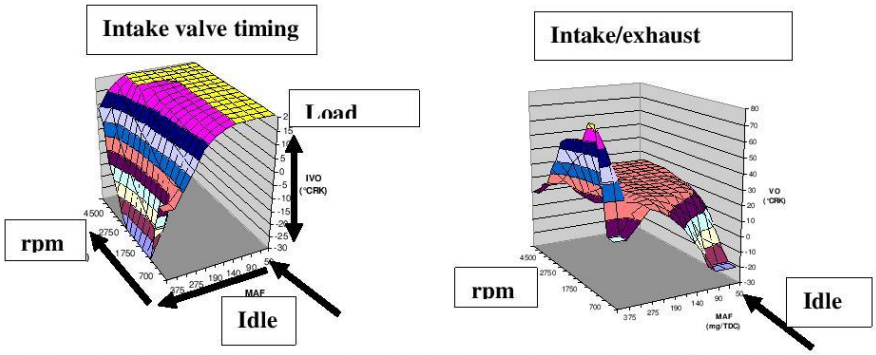

Characteristic of the timing map for the intake camshaft (left) is the fact that, starting at idle (lower right-hand corner), variable timing is passive up to just under 50 percent of the load (yellow field in diagram), then progressively moving towards advance, whereby extremely early intake opening occurs only in the lower engine speed range under full load. The right-hand diagram shows the overlap between both durations, characterised by an extensive range of

constant timing (orange field) at medium load and engine speed. Extremely large overlap occurs in the medium engine speed range and at full load, significant underlap only when the engine operates at near idle speeds.

Fuel Economy Improvement in the Medium Load Range

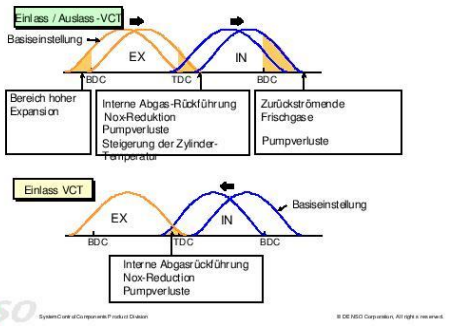

Ford Duratec Ti-VCT also allows fine control over effects which may degrade the cylinder charge. Exhaust gas recirculation caused by larger overlap reduces nitrogen-oxides and improves fuel economy.

In summary, the cylinder head of Ford Duratec **Ti-VCT** 1.6 L has been endowed with a few more capabilities than those possessed by engines with conventional valve timing. Despite staying below the peak values of power and torque typically delivered by engines with a greater cubic capacity, the improvements in available torque and power offered by Ford Duratec **Ti-VCT** 1.6 L make this modern engine highly attractive. The distribution of high torque levels across a wide range of engine speeds could make the driver feel that he or she is driving a car powered by a much larger engine. Together with its basic feel of considerable "muscle," the new Ford engine provides remarkably enhanced driving dynamics and, not to forget, about a five-percent improvement in fuel economy.

Postscript:
In the good old days of Ford's Model T such qualities were not even pie in the sky. It took almost another century before such highly sophisticated features related to valve timing appeared on the horizon.
In 1912, Ford's Model T had two tiny, lateral valves per cylinder positioned upside-down from today's perspective, each with a diameter of about 30 millimetres. Valve lift of 5 millimetres was minimal as well. Underlap, in other words, the phase during which both valves were firmly closed, was "one eighth of the rotation of the crankshaft", according to the garage manual published in 1912 – and this translates into 45 degrees to this day. As a piece of consolation: Fuel consumption was roughly 28.5 miles per gallon (10 litres per 100 km). When pulling a plough, however, according to sources from those days, consumption was a lot higher. A full tank (10 US. gallons, 38 litres) was said to roughly suffice for ploughing one hectare of land.

To compare, Ford's Model T, which was apparently suitable for farming, the valve diameter (30 mm) and lift (5 mm) resulted in an open valve surface of 3.5 cm² per cylinder, opened across a total angle window of 225 degrees each, measured at the crankshaft.
As a four-valve engine, Ford Duratec Ti-VCT naturally opens up more available valve space, although, with 1.6 litres of displacement, it is a much smaller engine than its ancestor with its proud 2.89 litres. Above the 79-mm bore in the Duratec Ti-VCT engine, approximately 20 centimetres of free valve space is available, which opens across a time window of about 232 degrees. This surface alone is six times as large as that of the old Model T. It is remarkable that, in addition to its six times larger valve space, the nominal speed of the modern engine has sextupled as well. Ford Duratec 1.6 Ti-VCT, in a manner of speaking, has evolved by a factor of six. The fact that this evolution does not make the engine feel merely like a hot racing machine is attributable – among other factors – to its map-controlled variable cam timing.

However, unlike its ancestor, the Ford Duratec engine is no longer fit for farming. But in our day and age, Ford Motor Company's product offering includes a large selection of much more suitable equipment for this purpose.

In the good old days of Ford's Model T, engineers had not yet invented maximum engine speed. Instead, the engine's large cubic capacity was fully exploited to develop torque: "Tin Lizzy" delivered impressive 20 hp at 1800 rpm from its 2.89-litre displacement, and the veteran's maximum torque of 110 Nm at 900 rpm was not to be sneezed at either.

Technical data of the Ford 1.6 GTDI engine used in the Fiesta ST

| TECHNICAL SPECIFICATIONS

FORD FIESTA ST SPECIFICATIONS

PEFORMANCE AND ECONOMY

			Fuel consumption l/100 km (mpg)			Performance		
Engine	Power (PS)	CO_2 (g/km)	Urban	Extra Urban	Combined	Max speed kph (mph)	0-100 kph 0-62 mph (sec)	50-100 kph 31-62 mph (sec)*
1.6 EcoBoost (6-sp manual)	182	138	7.9 (35.8)	4.8 (58.9)	5.9 (47.9)	220 (137)	6.9	6.4

* In 4th gear

WEIGHTS

Kerb weight (kg)#	Gross Vehicle Mass (kg)	Gross Train Mass (kg)	Max. Towable Mass (braked) (kg)	Max. Towable Mass (unbraked) (kg)
1163	1575	N/A	N/A	N/A

Represents the lightest kerbweight assuming driver at 75 kg, full fluid levels and 90% fuel levels, subject to manufacturing tolerances and options, etc., fitted.

Towing limits quoted represent the maximum towing ability of the vehicle at its Gross Vehicle Mass to restart on a 12 per cent gradient at sea level. The performance and economy of all models will be reduced when used for towing. Nose weight limit is a maximum of 50 kg on all models. Gross Train Mass includes trailer weight

DIMENSIONS

Dimensions (mm)	3-dr
Exterior	
Overall length	3975
Overall width with/without mirrors	1978/1709
Overall width with folded back mirrors	1787
Overall height	1456
Wheelbase	2489
Interior	
Front headroom	991
Front max legroom (lowest rearmost seating posn)	1111
Front shoulder room	1350

For news releases, related materials and high-resolution photos and video, visit www.media.ford.com.
Follow www.facebook.com/fordofeurope, www.twitter.com/FordEu or www.youtube.com/fordofeurope

Rear headroom	953
Rear legroom	823
Rear shoulder room	1300
Luggage capacity (litres)‡	
5-seat mode, laden to package tray (with mini spare)	276
5-seat mode, laden to package tray (with tyre repair kit)	290
2-seat mode, laden to roof (with mini spare)	960
2-seat mode, laden to roof (with tyre repair kit)	974
Fuel tank capacity (litres)	
Petrol	42

‡ Measured in accordance with ISO 3832. Dimensions may vary dependent on the model and equipment fitted.

STEERING

System	Electronic Power Assisted Steering (EPAS), rack-and-pinion, 2.32 turns lock-to-lock
Ratio	13.69:1
Turning circle (m)	11.2

WHEELS AND BRAKES

	Front	**Rear**
Braking	Hydraulically operated dual-circuit system with diagonal distribution. Vented front discs, solid rear discs. Electronic four-channel anti-lock braking system (ABS) with electronic brake-force distribution (EBD) and Emergency Brake Assist (EBA)	
Disc dimensions (mm)	278 x 23	253 x 10
Piston calliper dimensions (mm)	54	34
Wheels	7.5J x 17 light alloy metal 5-spoke	7.5J x 17 light alloy metal 5-spoke
Tyres	205/40 R17	205/40 R17

CHASSIS

Front	**Rear**
Independent suspension with McPherson struts supported by L-shaped lower wishbones connected to vehicle sub-frame. Separate load paths for spring and damper	Torsion beam suspension with progressive tracking control. Coil springs positioned under-floor with separate monotube shock absorbers
3-mode Electronic Stability Control (ESC) and enhanced Torque Vectoring Control (eTVC)	

ENGINE DATA

		1.6-litre EcoBoost (182PS)
Type		Inline four cylinder turbo petrol, transverse
Displacement	cm^3	1596
Bore	mm	79.0
Stroke	mm	81.4
Compression ratio		10.1:1

Max power	PS (kW)	182 (134)
	at rpm	5700
Max torque	Nm	240
	at rpm	1600-5000
Valve gear		DOHC with 4 valves per cylinder
Cylinders		4 in line
Cylinder head		Cast aluminium
Cylinder block		Cast aluminium
Camshaft drive		Timing belt
Crankshaft		Cast iron
Engine management		Bosch
Fuel injection		High pressure direct fuel injection system with 6 hole injectors
Emission level		Euro Stage 5
Turbocharger		Fixed geometry turbo with active wastegate and active compressor recirculation valve
Lubrication system		Pressure-fed with variable displacement pump and full flow oil filter
System capacity with filter	litres	4.1
Cooling system		Water pump with thermostat and valves, with thermal management system
System capacity	litres	5.5
Transmission		Durashift 6-speed (B6) manual
Gear ratios		
		6^{th} 0.690 5^{th} 0.821 4^{th} 1.032 3^{rd} 1.357 2^{nd} 2.048 1^{st} 3.727 Reverse 3.818 Final Drive 3.824

Note: All fuel consumption and CO_2 emissions figures in g/km are from officially approved tests in accordance with EC Directive 93/116/EC. Fuel economy figures quoted are based on the European Fuel Economy Directive EU 80/1268/EEC and will differ from fuel economy drive cycle results in other regions of the world.

Note: The data information in this press release reflects preliminary specifications and was correct at the time of going to print. However, Ford policy is one of continuous product improvement. The right is reserved to change these details at any time.

# # #

About Ford Motor Company
Ford Motor Company, a global automotive industry leader based in Dearborn, Mich., manufactures or distributes automobiles across six continents. With about 171,000 employees and about 65 plants worldwide, the company's automotive brands include Ford and Lincoln. The company provides financial services through Ford Motor Credit Company. For more information regarding Ford and its products worldwide, please visit http://corporate.ford.com.

***Ford of Europe** is responsible for producing, selling and servicing Ford brand vehicles in 50 individual markets and employs approximately 47,000 employees at its wholly owned facilities and approximately 69,000 people when joint ventures and unconsolidated businesses are included. In addition to Ford Motor Credit Company, Ford Europe operations include Ford Customer Service Division and 24 manufacturing facilities (15 wholly owned or consolidated joint venture facilities and nine unconsolidated joint venture facilities). The first Ford cars were shipped to Europe in 1903 – the same year Ford Motor Company was founded. European production started in 1911*

Contact: Finn Thomasen
Ford of Europe
+44 (0)126 840 1908
fthomas3@ford.com